Stimuli-Responsive Microtools for Biomedical and Defense Applications

by
Kate Elizabeth Laflin Malachowski

A dissertation submitted to The Johns Hopkins University in conformity with the requirements for the degree of Doctor of Philosophy

Baltimore, Maryland
December 2013

Abstract

We live in a 3D world which has embraced ever shrinking technologies, yet the techniques used to create these micro- and nanoscale technologies are inherently 2D. Self-assembly of 2D templates into 3D devices enables the creation of complex tools cheaply, efficiently, and in mass quantity. I utilize this technique to create stimuli-responsive microgrippers, which are shaped like hands with flexible joints and rigid phalanges and range in size from 10 μm to 4 mm. Intrinsic stress within the hinges provides all the energy necessary for gripping, and thus they require no wires or batteries for operation. Here, I demonstrate their use for both biomedical and defense applications. These microgrippers can be used as microsurgical tools, gripping onto tissue in response to body temperature and excising tissue from the gastrointestinal tract in both *in vivo* and *ex vivo* porcine models. A Monte Carlo model confirmed that these tiny tools has a higher probability of sampling tissue from a lesion as compared to the traditional biopsy foreceps. These grippers were scaled down to 10 μm and used to capture single cells for *in vitro* isolation, imaging, and assays. All-polymeric, porous, stimuli-responsive therapeutic grippers or "theragrippers" which swell and de-swell around body temperature were created for drug delivery applications. These theragrippers can be loaded with commercial drugs for biphasic, site-specific controlled release and were successfully demonstrated in an *in vitro* and an *in vivo* model. For defense applications, integrating microelectronics like RFID's onto the microgrippers creates tagging, tracking, and locating (TTL) devices capable of latching onto clothing, hair, and moving animal targets. This integrated design is enabled using high throughput solder-based self-assembly. This defense application, particularly reliant on covert, wireless technology, benefits from our novel photothermal actuation mechanism using low

power, handheld lasers. In addition to triggering microgripper closing, this actuation scheme also enables complex sequential folding pathways, a step towards programmable matter.

Advisor: David H. Gracias, Ph.D.
Readers: Hongang Cui, Ph.D., David H. Gracias, Ph.D., Peter Searson, Ph.D., Christopher Morris, Ph.D., Denis Wirtz, Ph.D.

Acknowledgements

Completing my PhD would not have been possible without the immense support I received from my family leading up to this point: my parents, who have encouraged me throughout my whole life and instilled in me curiosity, creativity, and a love of learning; my brother, whose friendly academic competition drove me to even greater heights; Jean and Dan, technical mentors who provided not only sage career advice but also made sure we didn't subsist only on takeout. And my brilliant husband who has always challenged me to be my best and think deeply, but also to take time for myself. Thank you for being my sounding board, my fellow innovator, my shoulder to cry on, and my cheerleader.

Much is owed to my lab mates, mentors, and friends within the department. Evin Gultepe, Rohan Fernandes, Noy Bassik, and Joyce Breger proved invaluable as leaders in the lab and mentors, helping me find my own way when I felt very lost. My peers in lab, Shivi Pandey, Mustapha Jamal, Teena James, Hyerin Kwag, ChangKyu Yoon, and Qianru Jin provided guidance, technical advice, or a much needed hot chocolate break. The undergraduate and Master's students I worked with, particularly Tanziyah Muqeem, Beril Polat and Nandini Muthsubramanian, provided lots of day-to-day help with experiments and were always enthusiastic about our projects. Several students in the ChemBE department and INBT provided much needed guidance and support. Charli Dawidczyk was a fantastic friend, gym buddy, journal club fellow, and rant listener. Allison Chambliss provided technical support for all things biological. Abasha Lewis gave me the idea to try Hopkins in the first place and spent an inordinate amount of time studying for the qualifying exam with me.

The educators in my life have contributed in a huge way to my success. Donna West, my 10^{th} grade chemistry teacher and 12^{th} grade environmental science teacher taught me to love

science in a way no one else ever has. Her creativity and enthusiasm for teaching have done a great service to her many students throughout the years. My professors from Virginia Tech deserve a huge amount of credit for preparing me and encouraging me to continue my education. In particular, David Cox and John Walz provided exceptional mentoring and support.

Northrop Grumman, the INBT, and the Army Research Laboratory provided me with financial support throughout my degree that made it possible for me to pursue my own projects and interests. The ChemBE and INBT department staff were invaluable sources of information on how to get through the JHU graduate system, and were a welcome support system.

My advisor and collaborator at the Army Lab, Chris Morris, has been an invaluable source of education, support, and mentoring. His day-to-day direction and leadership helped me navigate the toughest times in my degree and build my self-confidence.

Finally, my advisor, David Gracias, led me through a journey of discovery and maturation. His creativity fostered innovative and exciting projects which were a joy to work on. He kept reaching for bigger and better goals and pushed me along with him.

To my family

Table of Contents

List of Tables

List of Figures

1. Introduction

Miniaturization of devices has permeated nearly every aspect of our lives in the 21st century. Cell phones and personal computers, which rely on miniaturized transistors and integrated circuits, enable freedom of information unimaginable in the days of punch cards and room-sized computing machines. Miniaturized biomedical devices like the PillCam and laproscopic surgical equipment have made diagnosis and surgery minimally invasive, facilitating fast recovery times and improved quality of life for patients. Microtechnology in fields such as chemical and biological sensing, GPS and navigation, and photonics and optoelectronics has also revolutionized aspects of national defense.

Robotic pick-and-place, which has been utilized extensively in macro and mesoscale device assembly, is not suitable for building devices at the microscale and below due to the dominance of surface forces over gravity.[1] There are many methods of fabricating devices at these small size scales including traditional microfabrication and photolithography, 3D fabrication methods like micromachining, stereolithography, 3D printing, and self-assembly of 2D templates into 3D devices. Each of these methods has its own advantages and disadvantages in terms of cost, efficiency, yield, size scale, and material compatibility.

The actuation mechanisms which control the movement of microscale devices are just as wide-ranging. The best known of these schemes is electrical actuation used in microelectromechanical systems (MEMS), but there are many more including pneumatic, magnetic, optical, thermal, chemical, and even biological. As with fabrication methods, each actuation scheme has its own advantages and disadvantages, but for biomedical and defense applications, several traits are predominantly important.

Wireless or untethered actuation and control facilitate movement, particularly navigation through narrow conduits, and thus allow an operator to remove himself or herself from the device. For biomedical applications, untethered locomotion and actuation enable microsurgical tools to navigate the body without hindrance. Drug delivery, surgery, and medical imaging would all benefit from ease of access and navigation in hard-to-reach areas of the body. For defense applications, wireless control can keep soldiers out of harm's way. Just as unmanned air vehicles (UAV) attempt to remove pilots from danger while still performing necessary reconnaissance, wireless robotics and devices could in the same way protect soldiers.

Low power and novel energy sources are also important for these devices. Electrical actuation schemes almost always derive power from wires, batteries, or wirelessly through antennas. However, on the microscale, both on-board batteries and antennas are impractical because of their size limitations. Novel devices which gather power from chemicals, lasers, or their surroundings are becoming more popular on small scales.

This work details novel microscale tools which are untethered and responsive to their surrounding environment. These tools require no batteries or antennas for energy. Here, we demonstrate these tools in several biomedical applications as surgical and drug delivery devices. Because they are tetherless and stimuli-responsive, they can easily navigate the conduits of the body and perform their given task at a prescribed time. We also utilize these tools in defense applications, primarily for covert reconnaissance. Here, the wireless nature of the tools allows them to attach to a target of interest and carry with them a payload such as a transponder tag. The Department of Defense has specifically

spoken of the need for significantly smaller devices which are both low cost and low power for reconnaissance activities. No device currently used is small enough to pass the "naked man test", wherein a tracking device is small enough to escape detection on a naked body. The tools described in this work fulfill all of these needs because of their small size, wireless actuation, and novel low power schemes, eliminating the need for a massive antenna or battery.

1.1 Microfabrication methods for 3D device creation

Traditional microfabrication techniques, particularly photolithography, are primarily used to create microscale devices. These methods excel at creating 2D integrated circuits that have revolutionized electronics. They have also been used extensively in the development of MEMS. However, these methods are limited in their ability to create 3D devices because they are inherently 2D, created in single layers on a flat substrate. Several methods have since been developed to overcome this limitation: multi-layer photolithography, direct-write techniques, 3D printing, and self-assembly are some of the most popular.

3D structures can be formed from the serial patterning of multiple 2D layers. These patterns can either be fabricated using surface micromachining[2, 3] or built up by wafer stacking or bonding to create a 3D structure **(Figure 1.1 a-c)**.[4, 5] The lithographic technique known as LIGA utilizes photolithography and electrodeposition to create 3D masters which can be repeatedly used with molding or embossing to replicate the master.[6] However, developing the master is serial and expensive, but once fabricated, this process is highly efficient.

Several microfabrication techniques eliminate the need for a photomask to define patterning. Stereolithography is a serial process in which multiple layers of photocurable material are sequentially deposited and cured using a beam of ultraviolet (UV) light. Excess, uncured resin is eventually removed, leaving a well defined 3D part.[7] A similar technique known as multiphoton absorption (MPA) or multiphoton polymerization (MPP) uses a focused laser beam to photocrosslink a liquid acrylic resin into 3D objects.[8] This technique, as in LIGA, can be used to create a master structure, which can be replicated with soft lithography to increase yield.[9]

3D printing has recently become a popular method of small scale fabrication, but success depends on the quality of the printer. Sun et al. printed lithium ion microbatteries with alternating anode and cathode inks printed with 30 μm resolution and high aspect ratios **(Figure 1.1 d)**.[10] Manoor et al. recently demonstrated the concurrent printing of silicone, metal nanoparticles, and a cell laden hydrogel to create a "bionic ear" **(Figure 1.1 e)**.[11] By patterning microelectronics into a 3D cell scaffold, they have created a biological device capable of sensing electromagnetic signals.

Nature can also provide guidance on the fabrication of microscale devices. From salt crystals, to proteins in our body, to the folds in our brain, nature uses self-assembly to build 3D devices. Self-assembly creates an ordered, complex structure from many individual disordered pieces, and is highly efficient and robust. Viruses, for example, utilize interactions between proteins to assemble into specific conformations ideal for infecting a host **(Figure 1.1 f)**.[12, 13] Researchers can harness the power of self-assembly to create 3D devices and structures from natural molecules or synthetic building blocks.

For example, DNA has been used to create 3D nanoscale devices which can change conformation on demand **(Figure 1.1 g)**.[14]

1.2 Microscale self-folding actuation mechanisms*

The actuation of microscale devices is as wide-ranging as the fabrication methods. Mechanical actuation at small size scales is primarily effected using pneumatic, hydraulic, or electrical actuation. These actuation schemes are well-developed, offering fast response times, high precision, reliability, and programmability. However, these methods typically require the use of a tether or a wire through which gas, liquid, or electricity flows. Tethered actuation presents a significant challenge at small size scales and constrains the operation of miniaturized devices to planar substrates. After such devices are released from the substrates on which they are fabricated, tethering restricts device maneuverability, especially in coiled or hard-to-reach places—such as those encountered within the human body or microfluidic channels in lab-on-a-chip devices. Wireless electrical devices provide an attractive solution to eliminate external wiring; however, wireless energy coupling to antennas, especially in the widely utilized GHz frequency (1 GHz = 30 cm) range, becomes increasingly inefficient as the antenna size decreases. Several alternative actuation schemes – thermal, magnetic, optical, and chemical actuation – are becoming increasingly popular as wireless, small scale actuation methods. These methods have facilitated the devices discussed in this thesis.

1.2.1 Electrical actuation

The rapid development of the field of MEMS in the 1990's produced a variety of electromechanical actuators using planar multilayer patterning techniques. MEMS devices provide unprecedented reconfigurablility, rapid responsivity, programmability,

and reliability. These attributes allow a high degree of versatility in a range of engineering applications, and allow conversion of electrical signals into mechanical forces and vice versa. Digital micromirror displays (DMD) **(Figure 1.2 a)** employ electromechanical actuation to rotate microscale mirrors mounted on torsional hinges, which can deflect the mirrors by ±10°, thereby enabling digitization of the display.[15] The size of each micromirror can be as small as 13 μm, resulting in a high resolution display (1280 by 720 pixels), and the micromirror units have a lifetime of 100,000 hours (>10 years). These qualities make the DMD technology reliable for commercial applications, and as a result the technology is currently being employed by more than 30 major projector manufacturers. Another important application of electromechanical actuation is the integration of battery-powered gears and transmission systems on the microscale **(Figure 1.2 b),** which enable these microstructures to rotate with speeds as high as 250,000 rpm.[16] Electromechanical actuation has also been utilized in biomedical applications such as diagnostic tools and assays,[17] micropumps,[18, 19] and a variety of devices for drug delivery[20-22] and surgery.[23, 24] Electromechanical actuation using miniaturized electromagnetic coils or micromachined piezoelectric modules is finding extensive applications in probing cell mechanics.[25]

In addition to electromechanical actuation, electrochemical mechanisms are also often used to drive mechanical actuation, especially for applications within liquid media. For example, electrochemical actuation has been used to enable reconfigurable structures. These devices were fabricated with rigid panels and flexible hinges made with lithographically patterned polypyrrole/gold (PPy/Au) bilayers **(Figure 1.2 c)**. Polypyrrole is a conducting polymer that swells with the application of voltage due to ion permeation.

In a bilayer, this swelling causes a differential stress and therefore the electrical actuation of hinges in three-dimensional structures.[26]

1.2.2 Pneumatic Actuation

Pneumatic actuation utilizes the compression or expansion of a gas or liquid to produce mechanical actuation. Advantages of pneumatic actuation include high energy density, mechanical force, significant length displacements, reversibility and design flexibility.[27] This actuation strategy has been used in integrated microdevices, such as those which employ inflatable polymeric balloons as hinges **(Figure 1.3 a)**. When the polymeric balloons within these hinges are inflated, they cause integrated rigid panels to bend. This concept has been extended to create the "microhand", which uses series of balloon hinges connected with rigid silicon panels.[28] This microhand was reported to have a gripping force of approximately 5 mN per finger when actuated with 80 psi pneumatic pressure of air **(Figure 1.3 b)** and has been used to enable robotic surgery, particularly in ophthalmology. In surgery, it was demonstrated that the microhand could simulate retinal surgery during which it was able to manipulate and lift up the retina of pig eyes. In their studies, researchers demonstrated that this pneumatically actuated microhand was able to hold up to 1 g of test weights. Another noteworthy application of pneumatic actuation can be found in miniaturized valves. For example, researchers have developed polydimethylsiloxane (PDMS)-based micropumps which utilize compressed air to inflate a diaphragm to open and shut valves.[29] This device mimics peristaltic motion and prevents backflow. Significant limitations of pneumatic actuation are based on the need for plumbing to enable liquid or gas flow, limiting miniaturization and maneuverability.

1.2.3 Magnetic Actuation

Magnetic actuation is an attractive method to enable parallel actuation from afar. Magnetic actuation can be enabled in a tetherless manner using either permanent magnets or contactless electromagnetic coils. For example, micromachined flaps with electrodeposited permalloy have been actuated out of plane **(Figure 1.4 a)**.[30] However these flaps return to their original flat profile as soon as the magnetic field is turned off. This limitation can be overcome through the use of an innovative design which utilizes primary and secondary locking hinges **(Figure 1.4 b)**.[31]

1.2.4 Optical Actuation

Optical actuation schemes convert light energy to mechanical actuation by the optical alteration of the physical or chemical properties of thin photosensitive films. An attractive feature of optical actuation is that it can be realized from a distance via the use of optically transparent substrates and high powered light sources such as lasers. Additionally, the selectivity of actuation can also be tuned to different optical wavelengths or polarization angles.[32]

Many optomechanical actuators utilize liquid crystal networks (LCNs) with azobenzene moieties that contract and relax reversibly in response to light.[33] The large mechanical effect is due to the trans–cis isomerization of azobenzene with exposure to 365 nm light, causing a large contraction. This isomerization and the resulting mechanical deformation can be reversed by exposure to higher wavelengths of light or thermally in the dark.[34] Anisotropic optical actuation of LCNs or liquid crystal gels (LCGs) with azobenzene,[32, 35] in response to light of different wavelengths, has also been demonstrated. In these cases, the anisotropy was caused by alignment of the liquid

crystals during fabrication[35] **(Figure 1.5 a),** or by using polarized light for actuation **(Figure 1.5 b)**.[32] This kind of actuation is reversible with minimal fatigue over 250,000 cycles.[36] Similarly, Mamada et al. capitalized on photo-induced phase changes, and thus enabled mechanical actuation in polymer networks by copolymerizing a photosensitive component with N-isoproprylacrylamide (NIPAM). On irradiation with UV light, photosensitive constituents were ionized which generated an osmotic pressure within the gels and caused them to swell.[37] Other polymers have also been created with photoactive components which induce a phase, and thus volume change, when exposed to light.[38]

Carbon nanotubes have also been used to create micro-opticalmechanical systems (MOMS) as actuators.[39] Composite cantilevers of carbon nanotube films with SU-8 were created which responded to 808 nm light by bending; the degree of bending correlated with the intensity of the laser and was comparable to MEMS-based SU-8 cantilevers.

1.2.5 Thermal Actuation

Thermal actuation utilizes heat to expand or contract a material by altering its modulus, viscosity, or molecular arrangement. The most widespread use of this mode of actuation is with shape memory alloys (SMA) such as nitinol or various shape memory polymers. For example, researchers have been able to develop a microgripper based on shape memory properties of nickel/titanium/copper (Ni/Ti/Cu, **Figure 1.6 a**).[40, 41] Thin-films (5 μm) of Ni–Ti–Cu were deposited on the top and bottom surfaces of the microgrippers. As a result, jaws could be opened 110 μm when heated 30 °C above body temperature. The overall dimensions of this microgripper were 900 μm × 380 μm × 200 μm. Nitinol has also been used in self-expanding stents[42] due to its ability to be

thermally actuated at the temperature of the human body. Hence, nitinol stents self-expand on release from contact with a chilled saline solution filled catheter, and have found widespread clinical use.

Researchers have also created thermally actuated micro-cages **(Figure 1.6 b)** composed of SU-8/diamond-like carbon (DLC) bilayers, with sizes as small as 40 μm in diameter, which close upon heating to a temperature of approximately 150°C.[43] This approach uses the thermal expansion coefficient mismatch of the SU-8 and DLC layers, leading to thermal stress that folds the micro-cage from its flat conformation to its closed cage conformation. Thermal actuation was effected using an integrated, wired, electrical resistive heater, but conceivably could also be achieved in a wireless manner using convection or radiation modes of heat transfer. In the latter modes of heat transfer, however, it would be challenging to selectively heat and actuate a part of this microscale device without altering and potentially damaging other components within an integrated system.

1.2.6 Chemical Actuation

Chemicals can diffuse over large distances through a variety of media, offering the possibility for wireless actuation at a distance with high sensitivity. Moreover, due to the large variety of chemicals available through organic synthesis and the specificity of chemical interactions, highly selective actuation schemes can be created. Chemical actuation also offers the possibility for autonomous, environment-specific behaviors without the need for active control. Both naturally-occurring and synthetically fabricated chemical actuation mechanisms exist, with nature often providing the inspiration for the synthetic systems.

A well-known natural chemomechanical system is the trapping mechanism of Dionaea muscipula, commonly referred to as the Venus flytrap, which can be schematized into a simple gradient-driven reaction **(Figure 1.7 a)**. The most important anatomical structure of the flytrap includes two terminal lobes connected through the midrib. The lobes are fringed with hairs that act as mechanosensors.[44] Stimulation of the hairs induces an electrical signal directed to the midrib, opening aquaporins to change the turgor pressure of the base of the lobes. This dramatic change in osmotic potential creates the macroscopically observable closing process perpendicular to the midrib; the closing of the leaf itself is postulated to be dependent on the curvature.[45]

Such natural systems inspired studies aimed at developing synthetic polymers whose mechanical properties change upon exposure to chemicals.[46] Stimuli-responsive polymers were first described by Tanaka et al. when they observed the reversible collapse and expansion of polyacrylamide networks in acetone-water solutions.[47, 48] This reversible behavior is controlled by chemical synthesis with the incorporation of co-polymers to enable responses to a range of chemical cues like pH. These polymers were aptly dubbed “smart polymers” due to their ability to respond to environmental cues.[49-61] Since Tanaka's initial work, environmentally sensitive polymers have been demonstrated to actuate in response to changes in pH, temperature, ionic strength, UV/visible light, photosynthetic stimulation and magnetic/electrical fields. These polymers have found applications in drug[49, 51-53, 55-60, 62-67] and gene delivery,[58, 68, 69] microfluidics,[58, 59, 61, 70] chemical and biosensors,[58, 59, 61] and as actuators.[58, 71-74] For example, Beebe et al. have demonstrated a pH-sensitive hydrogel valve that controls the flow of fluid in a microfluidic device **(Figure 1.7 b)**.[70] The device was created by flowing acrylic acid

and 2-hydroxyethyl methacrylate, ethylene glycol dimethacrylate, and a photoinitiator through a microfluidic channel while photopolymerizing the hydrogel around polydimethylsiloxane (PDMS) posts. The thin layers of polymerized hydrogel which remain on the posts swell in high pH and contract in low pH in approximately eight seconds, thus directing flow though the device. The benefit of such a device is that the single hydrogel structure performs the role of both the pH sensor and the actuator.

Integration and patterning of stimuli-responsive materials are required for the fabrication of MCMS devices. As compared to bulk materials, thin-films are more amenable to the generation of multilayer chemomechanical actuators using planar, lithographic integration. Polymeric thin-films differ significantly from bulk polymers because of lateral confinement on a 2D substrate. Assuming no delamination, this lateral confinement limits their expansion or contraction due to the stringent boundary conditions. Adherent thin-films have been studied and characterized by Harmon et al. who noticed that surface-confined, 4 μm thick films of pNIPAM swelled only 15-fold compared to bulk free standing films that swelled 100-fold.[75] This lower swelling effect has been rationalized by the modified Flory–Rehner theory that examines one-dimensional swelling.[76] Despite their overall decreased swelling, constrained films demonstrate a larger linear volume change than the volume change of bulk polymer in the same direction. However, these confined thin-films produce mechanical stresses, causing them to occasionally delaminate from their substrate, which presents a challenge for their fabrication and integration into microfabricated devices.[77]

The challenge of integrating stimuli-responsive thin-film polymeric gel devices can be overcome by utilizing more accommodating microfabrication processes. Guan et

al. fabricated a hydrogel bilayer with differential swelling properties to create a self-folding microstructure, the smallest size of which was approximately 100 μm long, 20 μm wide, and 6 μm thick. They used soft lithography techniques to fabricate chitosan/poly-(PEGMA-co-PEGDMA) microstrips, which folded when placed in water.[71] The poly-(PEGMA-co-PEGDMA) layer swelled significantly in water, whereas the chitosan did not. Because the two layers were well adhered, the microstrips folded from the differential stress between the two layers. Building on this work, He et al. demonstrated that a similar self-folding hydrogel, ranging in size from 240 μm–4 mm, could be used as an oral drug delivery device **(Figure 1.7 c)**.[66] This device, fabricated using soft lithography techniques and microimprinting, was composed of a pH-sensitive swelling hydrogel and a pH-insensitive, non-swelling hydrogel. Together, they constituted a self-folding bilayer, and were coated with a drug-loaded, mucoadhesive third layer. The device successfully gripped onto the walls of a porcine small intestine filled with pH 6.5 buffer and provided a longer residence time (as compared with controls for the drug in the mucoadhesive layer) by maximizing its contact with the intestinal walls and minimizing its contact with the fluid flow through the intestines. Drug leakage into the intestine was significantly lower, and better transport of the model drugs across the intestinal epithelium was achieved using this device.

Our lab also created differentially swelling hydrogel bilayers that respond to changes in pH and ionic strength. Two hydrogels were paired, one that responded to pH and ionic strength changes with large volume changes (poly(n-isopropyl acrylamide-co-acrylic acid) or NIPAM-AAc), and one that responded with almost no volume change (polyethylene glycol diacrylate or PEGDA), to create a folding bilayer. Because the two

bilayers were well-adhered, when one swelled or contracted and the other remained flat, the bilayer curved. By combining rigid segments of SU-8 with these flexible hydrogel bilayer hinges using multilayer lithographic patterning, we created all-polymer actuators in the shape of a Venus flytrap which closed and opened in response to changes in pH and ionic strength **(Figure 1.7 d)**.[72] This work will be discussed in greater detail in Section 5.3 of this thesis.

1.2.7 Biological Actuation

The movement of cells can also drive actuation of devices. Cell-polymer hybrids, while still an emerging technology, show significant promise in the creation of biomedical devices. In several cases, muscle cells have been patterned on polymer substrates and controlled by electrical stimulation to create walking robots[78] and swimming jellyfish **(Figure 1.8 a)**.[79] In the latter case, neonatal rat cardiomyocytes were seeded onto a PDMS film which could mimic the contraction and release of jellyfish bodies. The electrically stimulated contraction of the cells provided the fast power stroke which contracts the device into a bell shape, where the PDMS layer allowed for the slow elastic recoil of the recovery stroke, restoring the original shape of the device. Both this and the walking cell-laden robot are reversible over many cycles. Without the need for outside electrical stimulation, cell traction has been used to assemble 3D polyhedra, a technique referred to as "cell origami" **(Figure 1.8 b)**.[80] Here, NIH/3T3 cells and bovine carotid artery endothelial cells were cultured onto paralyene microplates. The cell traction force naturally generated by the cells from actomyosin interactions and actin polymerization was able to pull the microplates together in the shape of various 3D polyhedra including tubes, cubes, and dodecahedra. The number of cells in each joint

controlled the folding angle. While the force from cell contraction and motility is significantly lower than that of several other actuation schemes, the inherent biocompatibility of this method is attractive. Additionally, the creation of cell-laden 3D structures has applicability in tissue engineering, medical devices, and basic biological research.

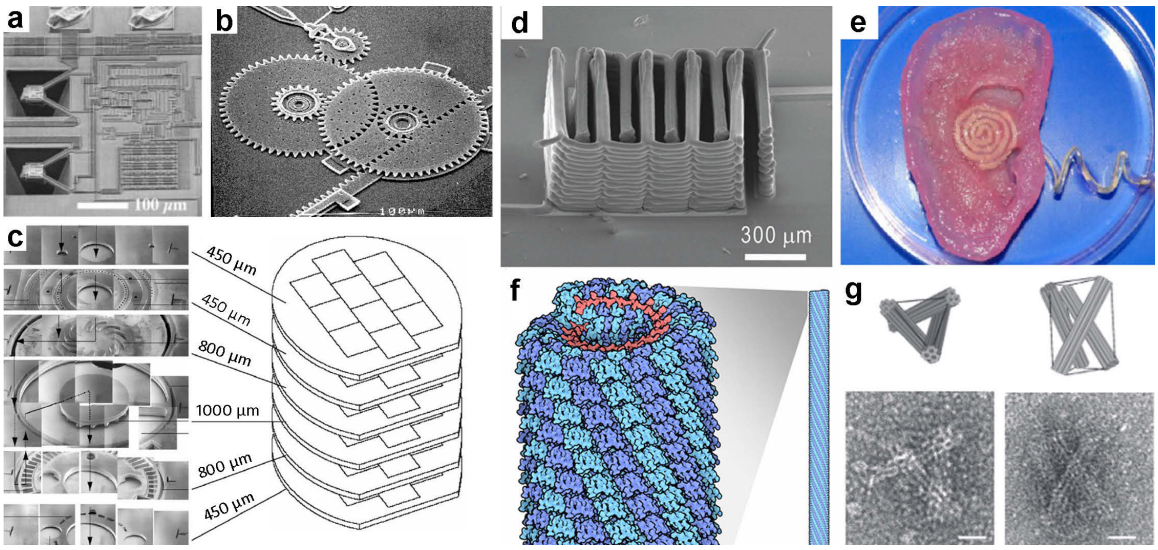

Figure 1.1. 3D Microfabrication techniques. (a) Silicon islands with circuitry formed from n-wells using selective TMAH etching for micromachining. Reprinted with permission from [3]. © 2011 IEEE. (b) Small and large meshed gears fabricated using multilayer microtransmission. Courtesy of Sandia National Laboratories, SUMMiT(TM) Technologies, www.mems.sandia.gov [81] (c) Combined optical images of a six-wafer micro-combustor, with a schematic of the stack. Reprinted from [4] Copyright 2003, with permission from Elsevier. Optical images originally appearing in [5] © 2011 IEEE. (d) 3D microbattery created by 3D printing alternating lines of anode and cathode inks with high aspect ratios. Reprinted with permission from [10]. Copyright © 2013 WILEY-VCH Verlag GmbH & Co. KGaA, Weinheim (e) Bionic ear formed by 3D printing of a cell-laden hydrogel with metallic nanoparticles. Reprinted with permission from [11]. Copyright 2013 American Chemical Society. (f) Viral self-assembly of a tobacco mosaic virus.[82] Image from the RCSB PDB September 2008 Molecule of the Month feature by David Goodsell (doi: 10.2210/rcsb_pdb/mom_2008_9). (g) DNA self-assembly into tensegrity prisms of different conformations. Reprinted with permission from Macmillan Publishers Ltd: Nature Nanotechnology [14], Copyright 2010.

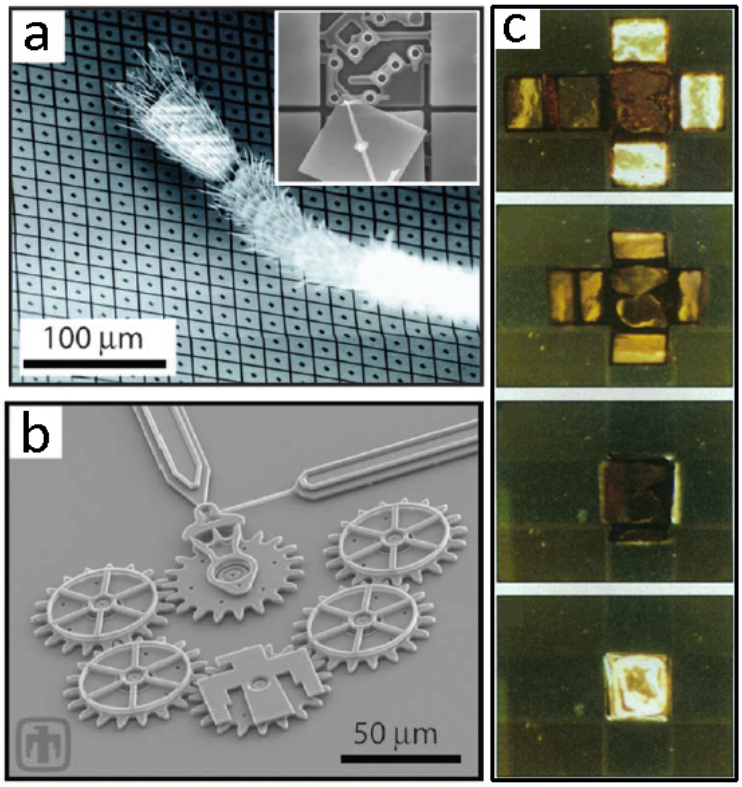

Figure 1.2. Microelectromechanical (MEMS) devices. a) Two pixels from a digital micromirror device (DMD) which can tilt due to electrostatic attraction produced by a voltage difference. Reprinted with permission from [15] Copyright Cambridge University Press. b) Example of MEMS microcomponents. Reproduced with permission. Copyright Sandia National Laboratories, SUMMiT (TM) Technologies. c) Photographs show a cruciform template actuated by hinges (PPy/Au) to compose a box closed around a grain of sand. From [26]. Reprinted with permission from AAAS.

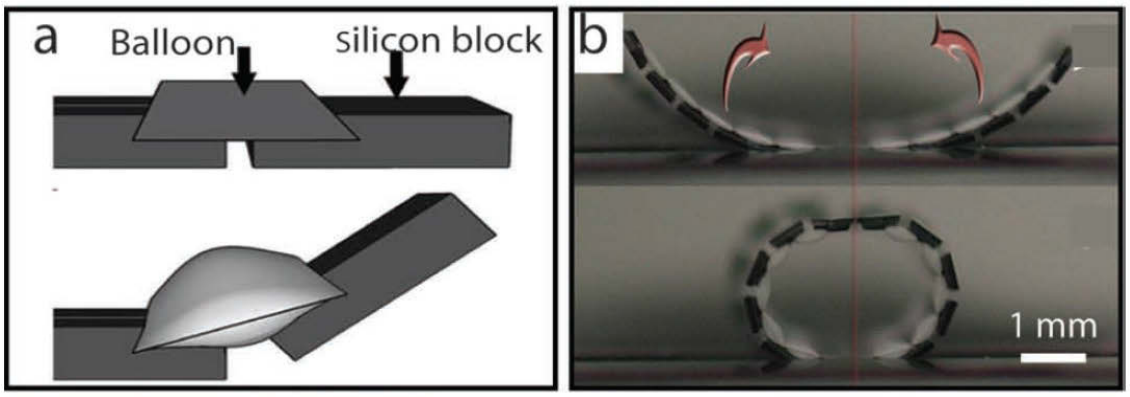

Figure 1.3. Examples of pneumatic actuation schemes. a) Operational principle of a pneumatically actuated microfinger. A parylene balloon is placed between two Si blocks. When compressed air is applied into the balloons, the attached Si phalanges make relative out-of-plane motion, making the microfinger curl. b) Side view of the actuation of the microhand, showing two opposing microfingers. A microfinger is articulated by six Si phalanges and joined by inflatable balloons. When the balloons inflate, the fingers are curved inwards and face themselves along the central axis (grey line). a,b) Reprinted with permission from Macmillan Publishers Ltd: Eye,[28] copyright 2009.

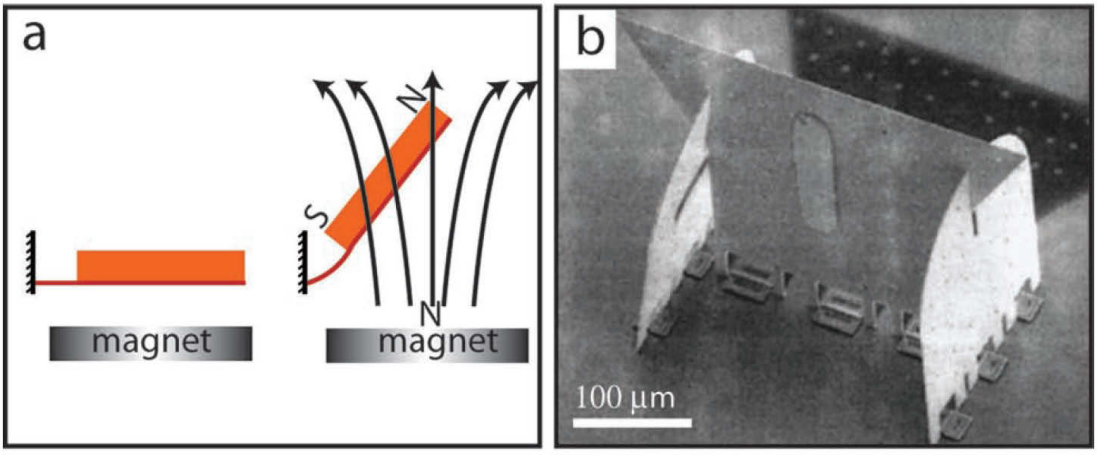

Figure 1.4. Examples of magnetic actuation schemes. a) Magnetic actuation of a unit actuator by an external electromagnet: rest position under zero external magnetic field and out-of-plane actuation under a non-zero magnetic field. Adapted with permission.[30] Copyright 1995, IEEE. b) Scanning electron microscopy (SEM) image of a 3D magnetically actuated device that uses three folding and interlocking flaps. Reproduced with permission.[31] Copyright 1999, IEEE.

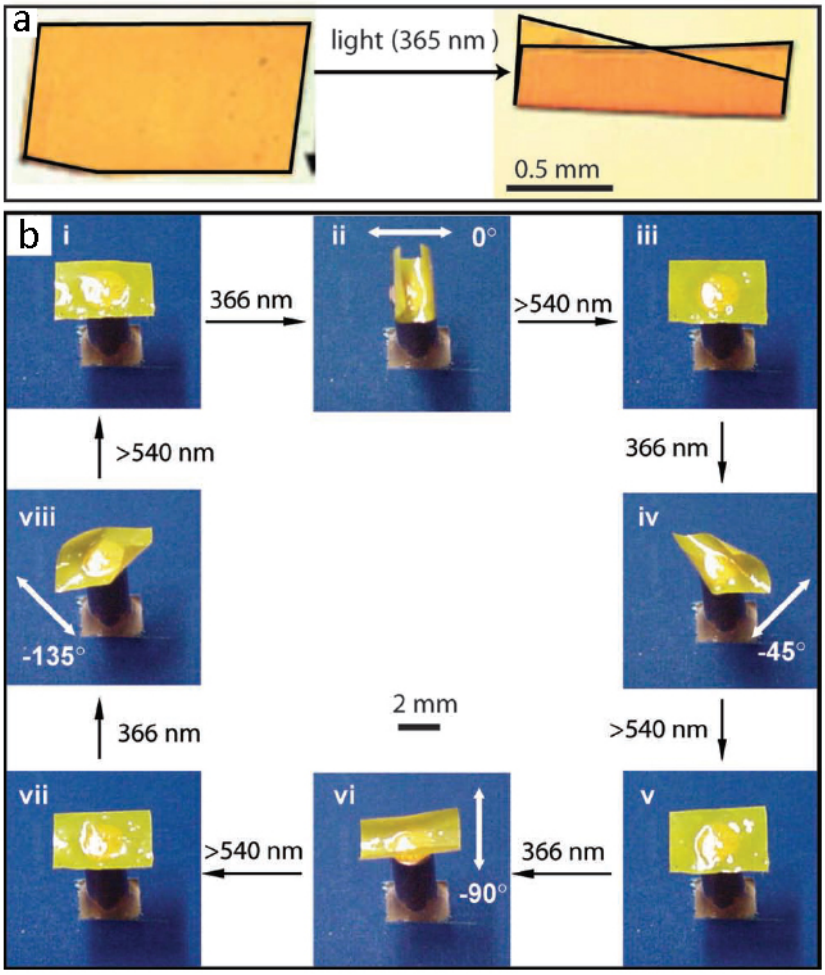

Figure 1.5. Examples of optical actuation schemes. a) Photographs taken during the bending and unbending of an optically actuated liquid crystal gel (LCG) film in toluene. The LCG film bent toward the irradiation direction of UV light and reverted to the initial flat film completely upon irradiation of visible light. Reprinted with permission.[35] © 2003 WILEY-VCH Verlag GmbH & Co. KGaA, Weinheim b) Photographic frames of the film bending in different directions in response to irradiation by linearly polarized light of different angles of polarization (white arrows) at 366 nm, and being flattened again by visible light longer than 540 nm. Reprinted with permission from Macmillan Publishers Ltd: Nature,[32] copyright 2003.

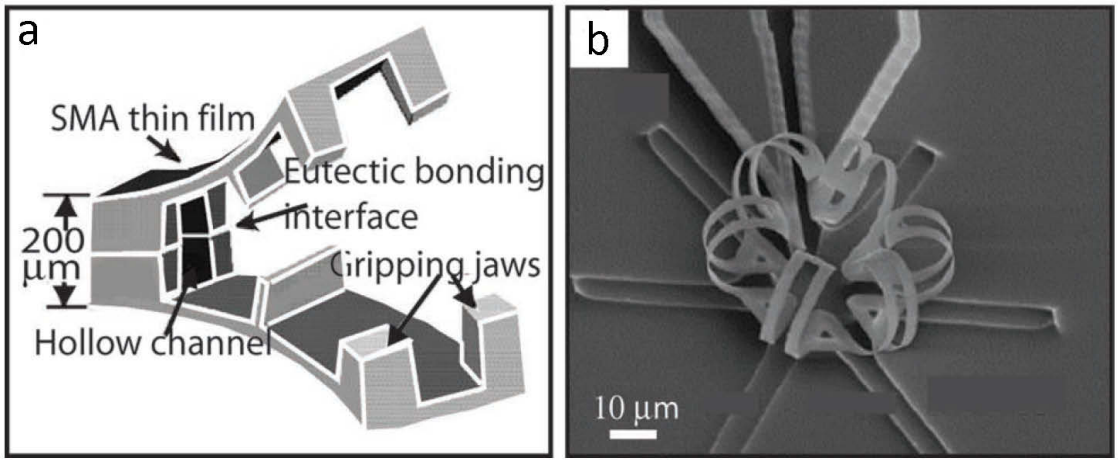

Figure 1.6. Examples of thermal actuation schemes. a) Redrawn schematic of a shape memory alloy-actuated microgripper. The gripper is 900 µ m long, 380 µm wide, and 200 µ m tall. Five microns Ni-Ti-Cu coat the top and bottom surfaces. Heating 30°C above body temperature causes the jaws to open 110 µm. Adapted from [40] © 1996 IEEE. b) SEM image of an SU-8/DLC electro-thermally actuated microcage with finger length of 50 µ m. Reprinted from [43], Copyright 2006, with permission from Elsevier.

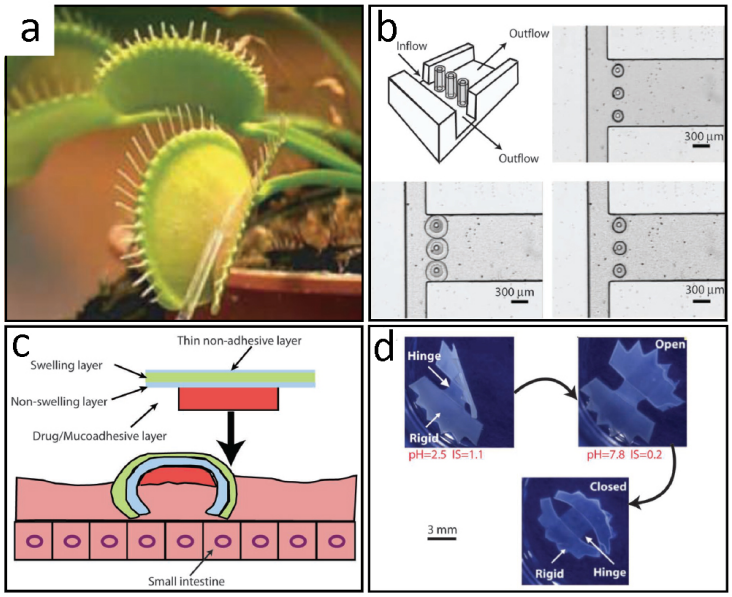

Figure 1.7. Examples of natural and synthetic chemomechanical actuation. a) Optical image of the Venus flytrap in its open state. Reprinted with permission from Macmillan Publishers Ltd: Nature,[45] copyright 2005 b) Schematic and operation of a pH-sensitive hydrogel valve. A diagram of the hydrogel jackets around the posts; the actual device after polymerization of the hydrogel; the swollen hydrogel jackets block the side channel branch in their expanded state; the contracted hydrogels allow fluid to flow down the side branch. Reprinted with permission from Macmillan Publishers Ltd: Nature,[70] copyright 2000. c) Self-folding hydrogel device for drug delivery. Schematics of the 3-layer device from the side view and when folded on the small intestine surface. Adapted from [66], copyright 2006, with permission from Elsevier. d) Venus flytrap shaped polymeric actuator constructed from rigid SU-8 segments with a NIPAm-AAc/PEODA bilayer hinge. Reversible folding occurred when the structure was transferred from a pH 2.5/IS (IS = Ionic Strength) 1.1 M solution to a pH 7.8/IS 0.2 M solution. The folding was reversible over 15 cycles. Adapted from [83], copyright 2010, with permission from Elsevier.

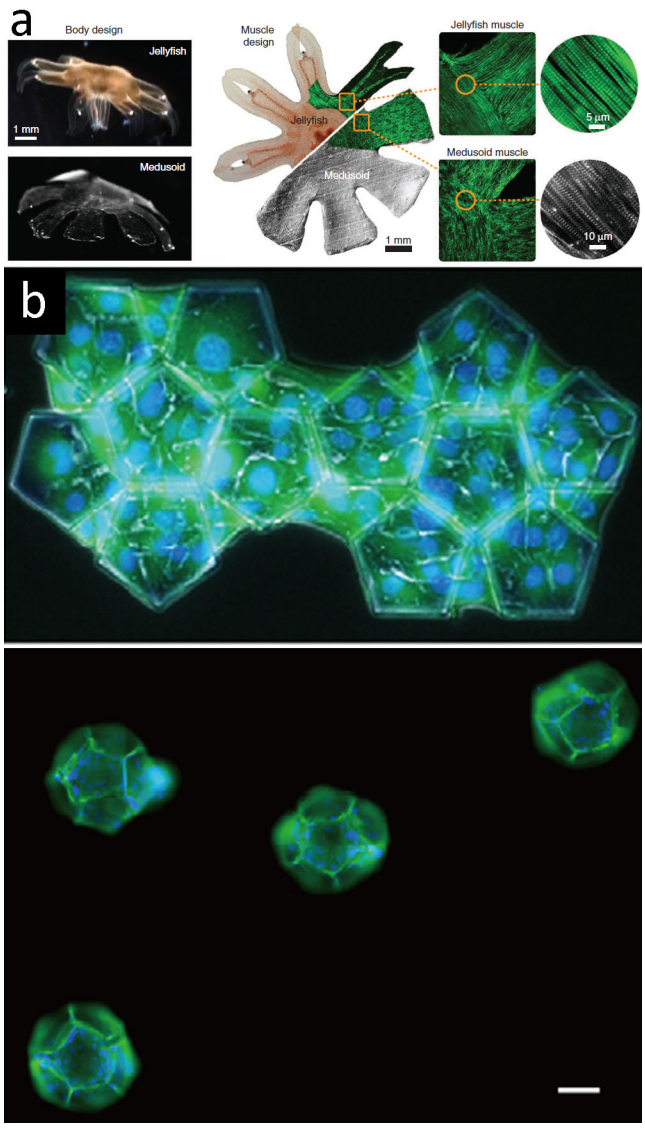

Figure 1.8. Examples of biological actuation. a) Biomimetic jellyfish reversibly actuates when cardiomyocytes seeded atop a PDMS thin film contract and relax under electrical stimulation. Reprinted with permission from Macmillan Publishers Ltd: Nature Biotechnology[79], copyright 2012. (b) Cell traction force causes a 2D template to fold into a 3D dodecahedron. Scale bar is 50 µm. Reprinted with permission from [80]. © 2012 Kuribayashi-Shigetomi et al.

2 Tetherless self-folding microgrippers

Microgrippers are self-folding, stimuli-responsive tetherless tools shaped like hands with rigid phalanges and flexible joints. They can be made from metals, semi-conductors, or polymers; actuated in response to light, heat, chemicals, or enzymes; and used in liquid or air for a range of applications. In all conformations, they contain all of the energy necessary for gripping in their hinges, eliminating the need for wires of batteries. Metallic- and semiconductor-based microgrippers contain a differentially stressed bilayer, which drives their gripping action. Their movement is controlled by a polymer hinge trigger which is responsive to heat, chemicals, or lasers. As the stimulus softens or degrades the hinge trigger layer, the grippers close. The polymeric microgrippers use a similar mechanism, differential swelling, instead of differential stress. As one layer of the polymeric grippers swells or deswells, the other remains neutral, causing a concerted curling motion.

Using different actuation schemes, the grippers can either be made to close en masse or individually. Their small size, 10 μm to 4 mm, allows them to navigate small spaces, hard-to-reach places, with minimal effect to their surroundings. Previously, they have been demonstrated as *in vitro* microsurgical tools capable of excising tissue in response to thermal[84] and enzymatic triggers.[85] They have been utilized here as tagging and tracking devices for defense applications, *in vivo* microsurgical tools for removing large clumps of tissue, devices capable of capturing single cells for *in vitro* diagnostic analysis and potentially *in vivo* biopsy applications, and as controlled release drug delivery devices.

2.1 Fabrication and actuation of microgrippers

Microgrippers are fabricated in the shape of hands with alternating rigid segments and flexible hinges. They derive their energy for gripping from stress within the bilayer hinge, while their strength and robustness come from the rigid segments. The bilayer is made from two films of differing intrinsic stress and can be made from several material combinations: chromium (Cr) and gold (Au), silicon monoxide (SiO) and silicon dioxide (SiO_2), or polypropylene fumarate (PPF) and poly(N-isopropylacrylamide-co-acrylic acid) (pNIPAM-AAc). Detailed fabrication schemes for each gripper type are described in subsequent chapters.

Briefly, metallic and semiconductor grippers are fabricated atop a copper (Cu) sacrificial layer on a silicon (Si) wafer **(Figure 2.1 a)**. Flexible bilayers in the shape of the gripper are patterned using traditional photolithography and deposited using thermal or e-beam evaporation. One material in the bilayer is highly stressed, while the other layer is relatively neutral. Because they share a common boundary, they curl as the layers seek to release their intrinsic stress. Rigid segments, made from nickel (Ni) or Au for metallic grippers or SiO for semiconductor grippers, are photopatterned atop the flexible bilayers and deposited with electrodeposition or e-beam evaporation. Finally, a stimuli-responsive hinge trigger layer is patterned on top of the bilayers. Finally, the grippers are released from the substrate upon dissolution of the Cu sacrificial layer. They remain flat immediately after release. When the hinge trigger is exposed to an appropriate stimulus which softens, degrades or dissolves it, the stress within the bilayer curls each finger of the gripper **(Figure 2.1 b)**. The folding of these structures can be predicted using a Stoney equation model for thin film curvature.[86]

The polymeric grippers are fabricated atop a polyvinyl alcohol (PVA) sacrificial layer on a Si wafer **(Figure 2.1 c)**. Rigid PPF segments are photopatterned first, followed by thermo-responsive pNIPAM-AAc hinges. The grippers are released from the substrate by dissolving the PVA sacrificial layer in water. When the grippers are cold, the pNIPAM-AAc is hydrophilic and swells, causing the grippers to close with the pNIPAM-AAc hinges on the outside. As the temperature increases above 32°C, the pNIPAM-AAc becomes hydrophobic and collapses, causing the grippers to open and then close in the opposite direction, with the PPF rigid segments on the outside **(Figure 2.1 d)**.

Each combination has advantages and disadvantages associated with it. Metallic grippers have a high gripping force, ideal for excising large clumps of tissue or gripping a heavy payload onto clothing. They can also be fabricated with nickel (Ni) rigid segments so they can be driven or collected by an external magnetic field. Semiconductor grippers have the smallest radius of curvature and can be scaled down as small as 10 μm. Additionally, they are clear, allowing their contents (single cell or clumps of cells) to be imaged easily using optical microscopy. The polymeric grippers have the largest radius of curvature, but can be loaded with drugs for use in drug delivery applications. These materials also enable reversible gripping in both directions over more than 25 cycles, while metallic and semiconductor grippers can only close one time.

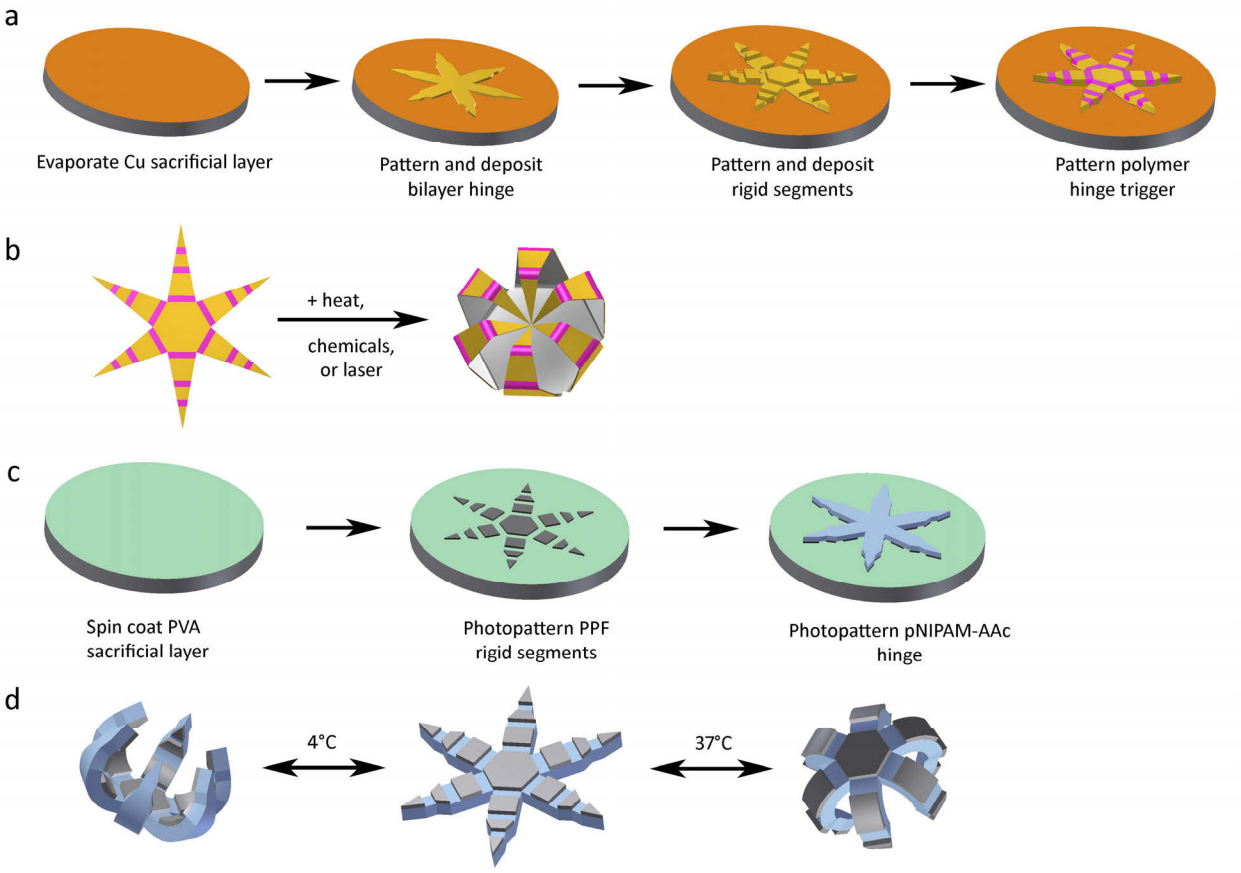

Figure 2.1. Illustration of microgripper fabrication and actuation. (a) Metallic and semiconductor gripper fabrication scheme with bilayer hinges, rigid segments and a polymer hinge trigger. (b) Metallic and semiconductor actuation occurs with thermal, chemical, or optical stimulation. (c) Polymeric gripper fabrication with PPF rigid segments and a pNIPAM-AAc hinge. (d) Polymeric grippers actuate reversibly as temperature changes around NIPAM's 32°C lower critical solution temperature (LCST).

3 Microgrippers for biomedical applications

Metallic, semiconductor, and polymeric grippers have various applications in the field of medicine. Metallic microgrippers, which are very rigid and sharp, are ideal biopsy tools and have several advantages over the current biopsy forceps tool. Primarily, using many small tools improves the probability of discovering gastrointestinal lesions while they are small and treatable. Silicon-based gripper, with an even tighter radius of curvature, can grasp single cells for *in vitro* analysis or a potential *in vivo* biopsy application in the circulatory or central nervous system. Larger polymeric devices make use of biocompatible and biodegradable materials and can be made either thermo- or pH-responsive. They are novel drug delivery tools, able to grip onto the walls of the GI tract and elute drugs with a desirable release profile. The following sections will give details on each of these microtools.

3.1 Biologic tissue sampling with tether-free microgrippers*

Surgical techniques have evolved from invasive to minimally invasive methods which currently rely on the use of wired or tethered devices, such as biopsy forceps to sample and access tissue from deep within the body. Although it has been suggested as far back as 1959, that advances in micro and nanotechnology could possibly revolutionize surgery by allowing for the creation of miniaturized, tether-free surgical tools, with moving parts[87], this vision has yet to be realized. Wireless devices ranging from centimeter scale pill-sized cameras[88] to metallic[89] or semiconducting[90] nanoparticles have been developed for medicine, but they do not have any moving parts

*Portions reprinted from Gastroenterology, 144 / 4, E. Gultepe, S. Yamanaka, **K. E. Laflin**, S. Kadam, Y.S. Shim, A. V. Olaru, B. Limketkai, M. A. Khashab, A. N. Kalloo, D. H. Gracias, F. M. Selaru, Biologic tissue sampling with untethered microgrippers, 691-693, Copyright 2013, with permission from Elsevier.

and hence rely on imaging modalities for diagnostics. Imaging based methods are not always sufficient to establish an adequate diagnosis, and even with significant advances in imaging methods for non-invasive diagnosis of diseases such as cancer or inflammation, tissue biopsy coupled with histopathologic examination remains the gold standard in establishing an accurate diagnosis[91-93]. However, present day biopsy techniques have drawbacks, such as their limited ability to access narrow places in a minimally invasive manner[94-96]. In addition, effective tissue diagnosis is fundamentally based on biopsying only lesions that have previously been identified by visual means, but numerous mucosal conditions, such as dysplasia in ulcerative colitis, or in Barrett's esophagus, are not readily visually recognizable, thus mandating surveillance protocols that involve random biopsies[97, 98]. To effectively sample large organs such as the colon numerous biopsies are required[99]. But, due to the large size of current forceps and the associated mucosal trauma, the number of random biopsies that can be realistically carried out is limited.

With the development of minimally invasive surgery, there has been a push to miniaturize tools[100-102] to enable surgeries through natural orifices and with small incisions[103, 104]. However, a dominant feature of present-day minimally invasive surgical tools is that the signal and energy to operate them is transmitted through wires or tethers which connect them to controls on the outside of the body. These tethers restrict their maneuverability, ability to access confined conduits in the body and the incorporation of multiple tools to sample different parts of the organ simultaneously[105]. Consequently, the current standard of care for cancer surveillance in ulcerative colitis patients is performed with at least 33 sequential biopsies (4-quadrant biopsies every 5-10 cm),

which we estimate cumulatively samples less than 0.3% of colonic mucosa. The low sampling coverage may be ineffective at detecting precancerous or cancerous lesions, especially for early, small lesions that are also the most treatable.

Wireless surgical robotic devices have recently been developed, including those with grasping manipulators[106] or inchworm-like robots[107], but they are large, centimeter scale devices. In contrast, since our microgrippers derive mechanical energy from residual stress powered microactuators and close in response to thermal environmental cues, they can be made much smaller with sub-mm sizes. In our previous studies, our laboratory demonstrated the feasibility of similar devices for grasping and retrieving cells from pieces of tissue placed in glass capillaries or acrylic organ models, under static fluid conditions[85, 108], but their utilization in real organs and especially under *in vivo* conditions remained unclear.

3.1.1 Microgrippers as surgeons

Parallel fabrication, deployment and thermal actuation make the microgrippers ideal to achieve statistical tissue sampling of large organs such as the colon. Our results suggest a new paradigm in medicine whereby large numbers of small, tether-free microsurgical tools could complement individual, large, tethered biopsying devices. These microgrippers, described in detail in section 3.2, resemble biological appendages, with rigid phalanges and flexible joints **(Figure 3.1 a-b)**. The rigid phalanges of the microgrippers are composed of nickel, and hence they respond to applied magnetic field. A thermo-sensitive trigger layer on the joints keeps the microgrippers flat at 4 ºC, but softens at 37 ºC, causing the microgrippers to close.[109] It is noteworthy that the size of

the microgrippers, 1 mm tip-to-tip, is far smaller than conventional biopsy forceps currently in use **(Figure 3.1 c)**.

The microgrippers are small enough so that hundreds can be deployed at a time and can be actuated en masse; therefore, they can form the basis for a more statistically efficient means to screen large area organs. In a Monte Carlo model, we estimated this effectiveness of detecting a mucosal lesion of a particular size by dividing the organ into bins of the lesion size and determining the probability of sampling the bin with the lesion. Our simulation clearly shows that because large numbers of microgrippers can sample many more bins, the sampling success of utilizing the microgrippers is significantly higher than utilizing conventional biopsy forceps, especially in case of small lesions.

3.1.2 *In vivo* and *ex vivo* tissue sampling

To test the feasibility of biologic tissue sampling with microgrippers, we used a swine colon in *ex vivo* studies. We inserted an endoscope into the anus and advanced it under endoscopic guidance. The microgrippers were suspended in sterile water and deployed on the colon surface using a through-the-endoscope catheter. Since the microgrippers are free to move in the water, there is no preferred orientation when they contact the tissue surface. We uniformly spread hundreds of microgrippers by rotating the endoscope during the deployment and visually verified the closure of the microgrippers using the endoscopic imaging **(Figure 3.1 d, e)**. To simulate the normal human temperature, the colon was submerged in a water bath kept at 37 ºC. After closure, we retrieved the vast majority of microgrippers using a magnetic catheter inserted through the endoscope **(Figure 3.1 f)**. The rest of the microgrippers were suctioned out with the endoscope into a trap bottle.

The tissue retrieved with the microgrippers was then used for genetic diagnostics (RNA and DNA analyses), as well as for cytologic analyses. First, we extracted ribonucleic acid (RNA) and deoxyribonucleic acid (DNA) from the retrieved tissue. We reverse transcribed the RNA into complementary DNA (cDNA), and then designed primers for several highly abundant transcripts in pigs.[110] As **Figure 3.2** demonstrates, cDNA amplification produced bands of expected size. Similarly, we employed DNA primers designed for pig DNA.[111] Figure **Figure 3.2** demonstrates that we were able to amplify all three genes and that the amplified DNA had the expected size. Hence, the tissue retrieved by the microgrippers is of sufficient quality and quantity to allow DNA and RNA extraction, as well as polymerase chain reaction (PCR) amplification in an effort to look for previously identified disease-diagnostic markers. Notable concerns are whether the cells retrieved using the microgrippers are desquamated cells in the mucus and if conventional cytologic studies can be achieved using retrieved tissue samples. In order to address these concerns, additional *in vivo* experiments were also done in the esophagus and tissue retrieved using the microgrippers was layered on a slide and stained using hematoxylin and eosin. Cytologic results **(Figure 3.2 c)** clearly show that high quality sections and both epithelial and desquamated cells can be obtained using the microgrippers.

3.1.3 Conclusions

In contrast to the dominant paradigm of "one task by one tool" used in conventional surgery, the concept of utilizing large numbers of miniaturized and untethered devices suggests a statistical approach to surgery. We have shown that it is possible with tether-free microgrippers to retrieve high quality tissue samples which are

suitable for either conventional cytologic analysis or genetic analysis. Further, the use of alternate polymer triggers could enable responsiveness to alternate stimuli, such as enzymes[85], and other biochemicals, to enable autonomous responses at diseased sites.

The grippers used in these experiments were on the order of 1 mm in size, which is ideal for the large and spacious GI tract. In this case, histological analyses benefit from a larger tissue sample. However, to perform *in vivo* biopsies in the circulatory, central nervous, and urinogenital systems, further minimization of the grippers is required.

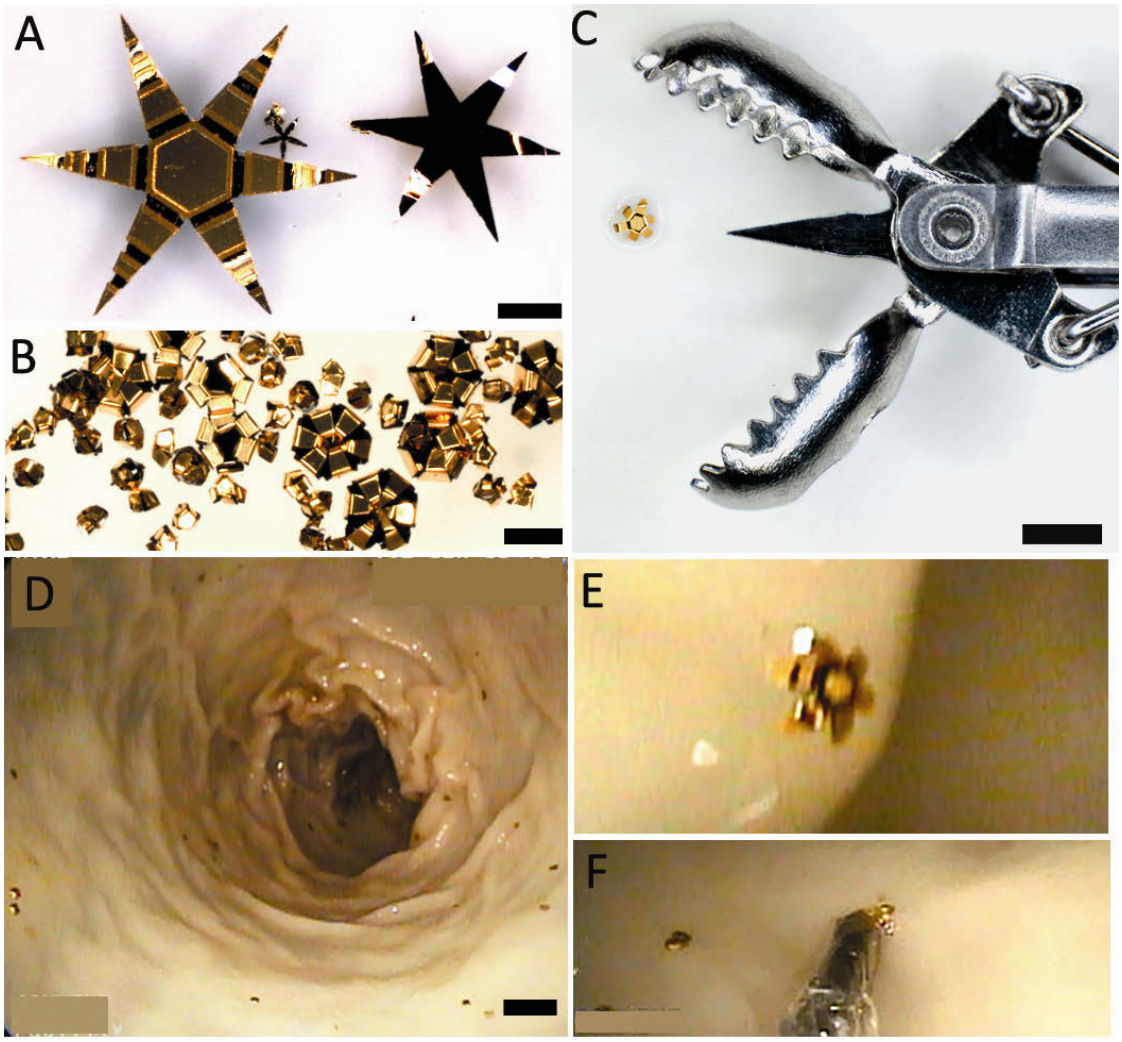

Figure 3.1. Untethered, thermo-sensitive microgrippers for tissue excision. (a-c) Bright field microscopy images of microgrippers in an (a) open and (b) closed state; the scale bars represent 200 μm. (c) The image showing that the microgrippers used in our biopsy experiments were over ten times smaller than the current biopsy forceps; the scale bar represents 1 mm. (d-f) Endoscopic images of deployment and retrieval of the microgrippers in an *ex vivo* porcine model. (d) Microgrippers covering the colon surface, the scale bar represents 2 mm. (e) Close-up image of μ-grippers closing on the colon wall. (f) Retrieval of the microgrippers with a magnetic catheter.

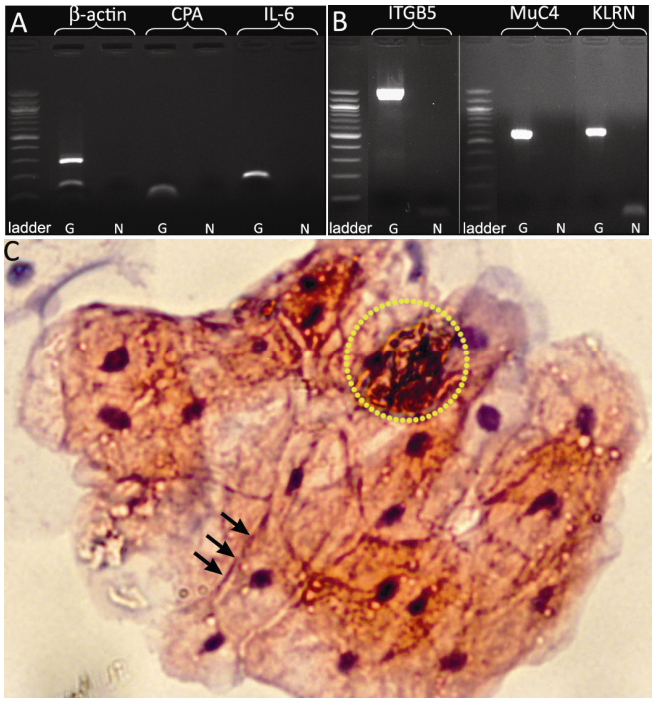

Figure 3.2. Genetic and histological analysis from an *in vivo* biopsy with microgrippers. (a) cDNA (β-actin:164 bp, CPA:62 bp and IL-6:119 bp) and (b) genomic DNA (ITGB5:1300 bp, MuC4 and KLRN: 500-600 bp) from the tissue obtained with μ-grippers (G) compared to the negative control (N). (c) H&E stained section of cells retrieved with the μ-grippers from porcine esophagus in an *in vivo* operation. The image shows viable epithelial cells with clear, abundant cytoplasm, consistent with glycogenated cells originating from the superficial epithelial layer of the esophagus. The black arrows point to junctions between intercellular membranes. The nuclei of these cells are clearly stained and the cells appear healthy, with large cytoplasm to nucleus ratios. Also seen and highlighted in the yellow dotted circle is a separate group of cells with pyknotic nuclei, small cytoplasm-nucleus ratio and deeply stained keratin, indicative of desquamated cells. These cells are probably obtained from the mucus layer overlying the esophageal mucosa.

3.2 Microgrippers for single cell isolation and manipulation*

Due to the large size of tools that are typically utilized for surgical diagnostics and biological analyses, cellular samples are often large in size. Consequently the data collected from tissue biopsied samples and related assays average over a multitude of cells. However, that average often may not accurately represent the behavior of individual cells, particularly if the cells of interest are a small fraction of the population. Further, it can be challenging to draw conclusions about dynamic or transient behaviors of single cells by looking at large populations.[112-114] Tumors have long been known to be heterogeneous populations of cells with varying phenotypes and genotypes, proliferation rate, potential for metastasis, and drug responsiveness, yet we are only beginning to understand how these heterogeneities affect their progression.[115-118] Single cell analyses may be necessary to differentiate the behavior of a cell subpopulation from the bulk measurement, particularly in the fields of cancer biology, genomics, proteomics, stem cell biology, and hematology.[114] This work is especially important as treatments for cancer, immune diseases and tissue regeneration move toward personalized medicine.[119]

A wide range of techniques are available for *in vitro* single cell analysis, and each has advantages and disadvantages in terms of efficiency, cell manipulation, imaging capability, sensitivity, and ability to mimic or actually perform *in vivo*.[120, 121] These methods include flow cytometry,[120] optical traps,[122-127], microfluidic traps and devices,[113, 128-137] microwells,[138, 139] microtubes,[140] and 2D surface patterns.[141-145] Several miniaturized robotic devices have been created to trap and manipulate particles

*An edited excerpt from K. E. Malachowski, M. Jamal, B. Polat, Q. Jin, C. J. Morris, D. H. Gracias, "Self-folding single cell grippers". Under review.

and cells with precise control.[146-148] For example, Chronis et al. demonstrated the manipulation of a 10 μm cell using a wired electrothermally actuated SU-8 gripper.[146] This device can manipulate cells with high precision, but the electrical wires that control its actuation and its large back-end design limit throughput and *in vivo* utility. Another SU-8 device, by Sakar et al, provides untethered manipulation of single cells via magnetic forces with minimal fluid disturbance due to its micrometer size and biocompatibility.[147] However, these devices are passive, trapping cells in a recess and thus may lose their grip on a cell if they moved in the wrong direction or in all three dimensions.

An ideal *in vitro* device would combine the high throughput efficiency of flow cytometry, the incorporation of patterned microfeatures for biomolecular analyses, and the 3D manipulation precision of optical tweezers. An ideal *in vivo* device should be composed of bio-friendly and possibly bioabsorbable materials while facilitating tissue excision or targeted capture, robust gripping and retrieval in an autonomous manner [149] Here, I describe an important step towards achieving tools that combine both these *in vitro* and *in vivo* capabilities for single cell studies. My approach is inspired by previous studies on the self-curling and roll-up of thin films.[84, 150-173] It utilizes high resolution photolithography, which is a high throughput technique capable of fabricating 500,000 to 10 million single grippers on a 3 inch wafer or over 100 million on a 12 inch wafer which is the size of wafers used currently in CMOS fabrication facilities. Additionally, they can be patterned in all three dimensions and actuated to close around single cells en masse. The thickness of the films can be varied to control the fold angle and the sharpness of the tips aids with capture and containment of cells. As compared to previously described

stimuli "μ-grippers" that were used to biopsy cell samples and porcine organs under *in vitro*, *ex vivo* and *in vivo* conditions,[84, 174-176] these grippers are thirty times smaller, requiring significantly thinner hinges and new materials to achieve a tight radius of curvature. As described in the previous section, we previously utilized the larger grippers only in the GI tract; thus, I envision that these grippers could be used in tighter spaces such as within the circulatory, urinogenital or central nervous system; however, there are more stringent requirements on biocompatibility and biodegradability for these applications.

Silicon (Si) and silicon dioxide (SiO_2) react with water via hydrolysis to form $Si(OH)_4$,[177, 178] and thus dissolve into DI water and various biofluids[177, 179] as previously reported by Hwang et al. in their work on dissolvable electronics.[179] That study demonstrated that Si dissolution in PBS at 37°C proceeded at a rate of 4.5 nm/day. Additionally, electronic devices made from Si, SiO_2 and other dissolvable materials were implanted sub-dermally into mice with no significant inflammatory reactions. After 3 weeks, only faint residues of the electronics remained. Silicon monoxide (SiO) is a two-phase, non-homogenous mixture of amorphous Si and SiO_2 and has been previously paired with SiO_2 to form tightly rolled tubes with microscale radii of curvature when e-beam evaporated in nanometer thicknesses.[140, 163, 168, 169] Thus, we selected these two materials for our single cell grippers for their biocompatibility, bioabsorption, and self-curling properties.

3.2.1 Microgripper fabrication

Grippers were fabricated with flexible, pre-stressed bilayer hinges, connected to rigid segments **(Figure 3.3a)**. Initially, we deposited a copper (Cu) sacrificial layer on a

silicon (Si) wafer. We photo-patterned a pre-stressed bilayer in the shape of the gripper using photolithography on an ASML stepper mask aligner with 500 nm resolution. We used e-beam evaporation to deposit silicon monoxide (SiO) and silicon dioxide (SiO_2). The thicknesses of these layers depended on the desired folding angle and the size of the microgrippers, but ranged from 2 nm to 30 nm thick. Examples of SiO/SiO_2 thickness combinations are given below for several gripper sizes.

Table 3.1 Gripper fabrication dimensions and bilayer thicknesses

Gripper diameter, tip to tip (μm)	SiO thickness (nm)	SiO_2 thickness (nm)
10	3	3
35	8	15
50	9	27
70	10	30

These thicknesses achieved folding angles between 90 and 115°. Subsequently, we used photolithography to define the rigid segment regions which were made of 150 to 350 nm of e-beam evaporated SiO. An optional hinge trigger made from paraffin could be molded atop the grippers to control actuation. Paraffin remains stiff at room temperature, but begins to melt around 37°C, allowing the grippers to close. To create the hinge trigger, we defined an outline of the gripper using SPR-220 photoresist to create a mold for the polymer hinge. We molded warm liquid paraffin on top of the grippers and scraped the excess with a razor blade. We dissolved the photoresist in acetone, which left just the paraffin hinge atop the gripper. The microgrippers were released from the Si wafer using either phosphate buffered saline (PBS) or APS-100 Cu etchant (Transene).

These devices can either be arrayed on a substrate for use as a single cell *in vitro* analytical device or completely released to be used as free-floating tools. **(Figure 3.3 b-c)**.

We created several designs with three or four arms, varying in size from 10 μm to 70 μm in length (tip-to-tip when open) **(Figure 3.4 a)**. The alternating rigid frames and flexible hinges are evident in the open grippers **(Figure 3.4 b, d)**. Grippers folded at angles ranging from 90° to 115° depending on the bilayer film thickness. The film thickness could be adjusted to create tightly folded grippers in a range of sizes. For example, 9 nm of SiO and 27 nm of SiO_2 were deposited to create the 50 μm grippers in **Figure 3.4 b and c** while a bilayer of 3 nm of SiO and 3 nm of SiO_2 was used to make the 10 μm grippers in **Figure 3.4 d and e**. Despite their small size, these grippers were fabricated using standard photolithography on a projection mask aligner with 500 nm resolution. Photolithography and registry became increasingly difficult as the size of the grippers decreased and 10 μm was the lower limit of well-resolved grippers. Using parallel photolithography instead of serial e-beam lithography afforded rapid, en masse production.

We also created magnetic single cell grippers, made from a nickel bilayer. The use of ion beam assisted deposition (IBAD) significantly alters the stress in thin films as compared to e-beam deposition without ion beam assistance. For example, the stress in nickel films evaporated using traditional e-beam evaporation is on the order of 500 MPa tensile, whereas the stress in nickel films deposited with IBAD is approximately -350 MPa compressive. This differential in stress can be utilized to achieve tightly curling films such as the ones described in the main text of the paper with SiO and SiO_2. We began to investigate these Ni/Ni single cell grippers with paraffin hinge triggers as free-

floating single cell capture tools that could be controlled via a magnetic field and thermally actuated at body temperature **(Figure 3.5)**. However, the SiO/SiO_2 were better suited to our goals of single cell imaging and assaying, so few experiments were performed using these nickel grippers.

3.2.2 Stress and folding angle characterization and modeling

The radius of curvature of the grippers depends directly on the film thickness, mechanical properties of the materials, and residual stress of each layer within the pre-stressed bilayer. It is noteworthy that previous designs of microgrippers were made from either a chromium/copper (Cr/Cu) bilayer or a chromium/gold (Cr/Au) bilayer.[84, 175, 176] In these designs, the Cr layer had significant compressive stress (~1 GPa), while the Cu or Au layer was relatively neutral. This stress differential caused the grippers to fold due to the shared boundary between the two layers. These metallic combinations, however, were unable to curl tightly enough to close grippers less than 200 μm in length. However, the SiO/SiO_2 combination provided a sufficiently small radius of curvature for single cell grippers.

To better understand the gripper curvature, we characterized residual stress within each of the SiO and SiO_2 layers. We investigated the effect of film thickness and time on film stress for both SiO and SiO_2. Using a wafer curvature measurement tool, we calculated the stress in varying thicknesses of SiO on a Cu sacrificial layer and varying thicknesses of SiO_2 on Cu and SiO layers. There was significant variation in the stress for each film, due to the large radii of the original Si wafers. Therefore, we included only data collected on wafers with a radius lower than 700 m. We found the stress in both SiO and SiO_2 to be compressive and became more tensile as thicknesses increased from 10

nm to 100 nm **(Figure 3.6)**. These stress values varied significantly with thickness below 100 nm, but were consistent with the expected range of compressive stress for the deposition conditions used.[180, 181] However, a more important parameter for film stress is the time of exposure to room air following deposition in an evaporation chamber. The absorption of water vapor and room temperature annealing both significantly alter the stress in SiO_2 films over time **(Figure 3.7)**. So while the stress in SiO films remained mostly constant over time, the absorption of water by SiO_2 caused its tensile stress to grow linearly with the logarithm of aging time, as has been previously reported in the literature.[182] By using SiO_2 films to form the top of each concave folded hinge, we ensured that the growth of this tensile stress component helped each hinge fold with a sufficiently small radius of curvature.

We examined the effect of bending strain and film thickness on folding angle using an analytical curvature model[86] and a computational finite element analysis (FEA) simulation in Abaqus **(Figure 3.8 and 3.9)**. The finite element model simulates the complete process of gripper folding triggered by pre-loaded initial strain. The gripper is simplified as a thin bilayer, composed of one fixed palm, a deformable hinge, and a stiff panel. The layers are made of elastic isotropic material with following properties. Mechanical properties for SiO_2 are well defined in the literature,[183, 184] but properties for SiO are less commonly reported. Hence we assumed mechanical properties of SiO to be between that of amorphous Si[185] and SiO_2, given that SiO is a two-phase, non-homogenous mixture of amorphous Si and SiO_2 with some chemical bonding occurring at the interface of the phases.[186, 187] The mechanical properties we used in our models are given in **Table 3.2**.

Table 3.2 Mechanical properties used for modeling

Property	**SiO**	**SiO_2**
Young's Modulus (E, in GPa)	77	75
Possion Ratio (υ)	0.2	0.17
Initial stress (σ, in MPa)	-344	-2

The bilayer is considered as a composite shell due to large aspect ratio between length and thickness (about 1000:1). Each layer is assigned with designed thickness, with 3 integration points in the Simpson integration rule. Further incrementing of integration points to 9 does not affect final results. Deformation is only applied to the hinge. One end of the hinge is fixed in all three directions while the other is free to bend with a fixed length. Displacement of the palm (middle part of gripper) is zero in all x, y, and z directions. The initial strain determines final folding angle. In Abaqus, the initial strain is simulated by assigning the two materials in bilayer with different thermal expansion coefficients, and applying temperature field only to the hinge region, where $\Delta\varepsilon = \Delta\alpha \cdot \Delta T$. The center and each hinge is meshed with 20×20 structured elements, and the nondeformable panel is meshed with 10×10 structured elements. Further incrementing of mesh numbers to 30×30 do not change the results. Large deformation is expected. Therefore, nonlinear effects of large deformation and displacement are considered during strain ramp from zero to the measured value.

We modeled the effect of strain on bending angle for a 70 μm and a 10 μm gripper **(Figure 3.8)** and found that as strain increases the folding angle also increases which is expected. We also modeled folding angle versus SiO and SiO_2 film thickness for a 70 μm and a 10 μm gripper **(Figure 3.8, 3.9)**. For this particular analysis, stress is considered to be constant with film thickness since the variation in thickness is slight for each material. For a 70 μm gripper, as SiO thickness increases, the folding angle increases slightly; as SiO_2 thickness decreases, the folding angle decreases considerably. For a 10 μm gripper, the folding angle decreases with the increase of film thickness. These plots can serve as a design guide for determining the necessary thicknesses for each layer within the pre-stressed bilayer to achieve a desired folding angle.

Using both the analytical model and the simulation, we compared the measured folding angle for the two different gripper designs and the predicted folding angle values for each design. Folding angles predicted by the analytical curvature model are given in **Table 3.3,** while folding angles predicted by the finite element simulation are given in **Figure 3.10**. These results demonstrate agreement between the analytical model and the computational simulation, and are within 25% of what we observed, which is a level of agreement reasonable for design purposes.

Table 3.3. Comparison of observed and predicted folding angle

Gripper diameter (μm)	SiO/SiO_2 Thickness (nm)	Hinge Gap (μm)	Predicted folding angle	Observed folding angle
70	10 / 30	9.55	82°	110°
10	3 / 3	1.35	103°	101°

3.2.3 *In vitro* single cell capture by gripper arrays

To demonstrate an application as an *in vitro* arrayed analytical tool that could contain single cells for biological experiments, we fabricated 50μm grippers that remain attached to the substrate upon release. The arms were patterned on the Cu sacrificial layer and thus able to fold. The base of the gripper was patterned directly onto the Si wafer and remained attached during the release and folding process. We pipetted L-929 fibroblasts in media on top of the open grippers. The grippers closed around individual cells after two to six hours in warm culture media due to the slow etching action of the ions in the media **(Figure 3.11)**. The gripper arms closed tightly around each cell, trapping it within its grasp, but not crushing it as evidenced by an intact cell membrane in a live/dead assay. Some grippers were empty, but when occupied, each of the grippers only contained one cell. The best observed yield for successfully filled grippers was 48% for an area of approximately 75 grippers and the most important factor modulating yield was the concentration of cells used in the suspension. The SiO/SiO_2 grippers also are transparent, and thus are ideal for imaging the cells trapped within using optical microscopy techniques. These grippers have slit openings at the intersection of the arms and consequently, nutrients, waste and other biochemicals can flow easily to and from the cells, yet we observed that the force is strong enough so that the cells do not escape during staining and imaging. We performed a live/dead assay by staining with calcein AM and ethidium homodimer after the cells were captured **(Figure 3.11 a-c)**. The cells were successfully stained, demonstrating that they are alive, and that the assay chemicals successfully penetrated the grippers. Thus, grippers do not harm the cells, and they allow the cells access to any chemicals within the media.

We also fixed the cells and performed scanning electron microscopy on an array of grippers with isolated fixed cells **(Figure 3.11 d)**. This image confirms that the cell is contained within the arms of the gripper, as opposed to floating on top of the gripper. It is noteworthy that the cells conformed to the shape of the gripper highlighting potential interactions with the faces of the gripper **(Figures 3.11c-d)**.

3.2.4 *In vitro* red blood cell capture

We also investigated applicability of 35 μm grippers to capture red blood cells from a beagle blood sample **(Figure 3.12)**. Red blood cells were pipetted onto partially released grippers. Many grippers were able to trap single blood cells within their arms. Optical profilometry and microscopy on the grippers confirmed that the cells were trapped within the grippers. This experiment highlights the potential for these devices as *in vivo* cell capture tools, with a thermoresponsive hinge trigger adapted from previous gripper designs; such devices could easily navigate the intricate conduits of the human body, allowing surgeons to extract single cells in a non-invasive manner from hard-to-reach areas deep within the body. It is also noteworthy that Si and SiO_2 (and by extension, SiO, a mixture of Si and SiO_2) have been shown to be biodegradable over time when used in dissolvable electronics, making them ideal materials for an *in vivo* application.[179] If needed, such tools could also be created with magnetic elements using highly stressed bilayers of nickel (Ni) with rigid Ni panels for guidance through narrow conduits using magnetic fields. As an additional form of motion control, patterned biomarkers on the gripper could enable targeting of specific diseased cells *in vivo*.

3.2.5 Conclusions

In summary, we have designed and fabricated grippers capable of capturing and isolating single cells. These single cell grippers, made from biocompatible, optically transparent materials, can be arrayed for high throughput *in vitro* assays and imaging or released for use as free-floating tools. We employed varying sizes of these grippers to capture individual fibroblasts and red blood cells. These cells were alive and could be assayed or fixed for imaging. Because these devices are fabricated in 2D and subsequently folded into 3D, future studies could explore patterned topography such as spikes, holes, and nanoscale roughness, and biochemical surface functionalizations in specific designs onto one or more device walls. This approach could enable multiple assays to be run at one time on a single cell. Additionally, our group has previously demonstrated the fabrication of many different shaped of polyhedra.[162, 188] Future studies could utilize these pyramidal grippers and other regular polyhedra to study the effect of 3D confinement on cell growth and morphology. Additionally, our process is amenable to other lithographic approaches such as e-beam or nanoimprint lithography for sub-cellular gripping capabilities. Finally, this work highlights the potential for these tools as *in vivo* cell capture tools, capable of navigating intricate conduits within the circulatory, central nervous, and urinogenital systems.

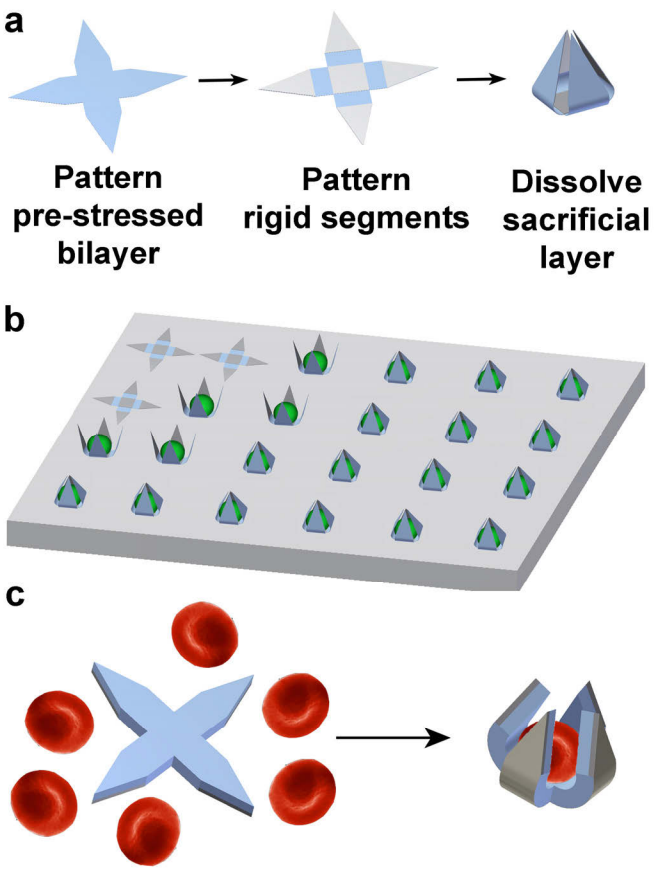

Figure 3.3. Illustration of single cell gripper fabrication and use on substrates or as free-floating tools. (a) Fabrication scheme for creating single cell grippers. The pre-stressed bilayer is a SiO/SiO_2 bilayer, while the rigid segments can be made of SiO. Upon dissolution of the sacrificial layer, the arms can be released to close around cells. An optional thermo-responsive trigger layer can be molded atop the grippers. (b) Illustration of cells captured by single cell microgrippers arrays. (c) Illustration of free-floating single cell grippers and red blood cell capture.

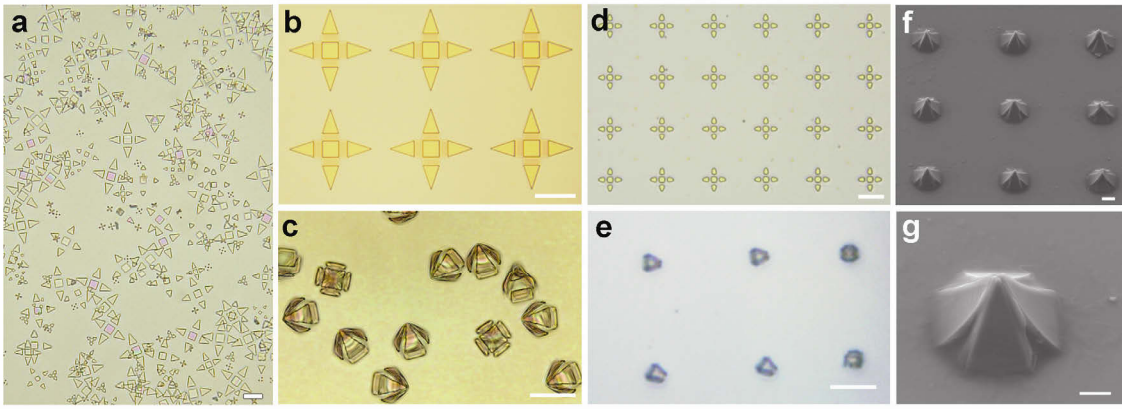

Figure 3.4. Optical images of single cell grippers before and after closing. (a) Optical image of grippers released from the substrate with open arms prior to closing, in sizes ranging from 10 µm to 50 µm. (b-c) Zoomed optical images of 50 µm grippers (b) prior to release from the substrate and (c) closed tightly after release. (d-e) Optical images of 10 µm grippers (d) open and (e)closed. Scale bars are (a, b, c) 25 µm and (d, e) 10 µm. (f-g) SEM images at different magnifications of closed single cell grippers attached to the substrate. Scale bars are (f) 10 µm and (g) 5 µm.

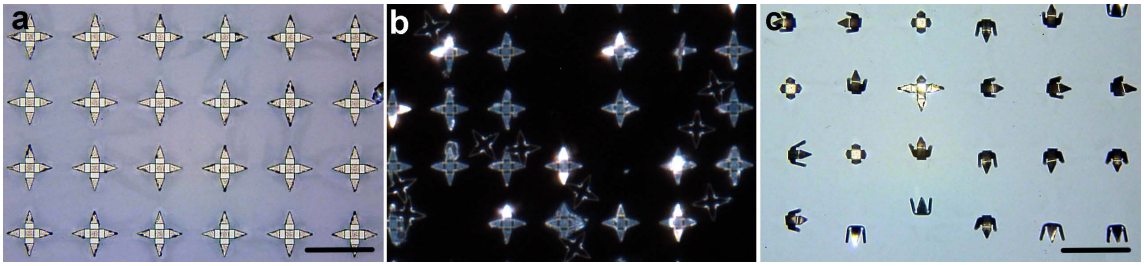

Figure 3.5. Optical images of magnetic nickel single cell grippers. (a) Ni/Ni grippers prior to release from the substrate. (b) Unfolded Ni/Ni single cell grippers released from the wafer substrate with paraffin hinge triggers. (b) Folded Ni/Ni single cell grippers with a folding angle of approximately 85°.

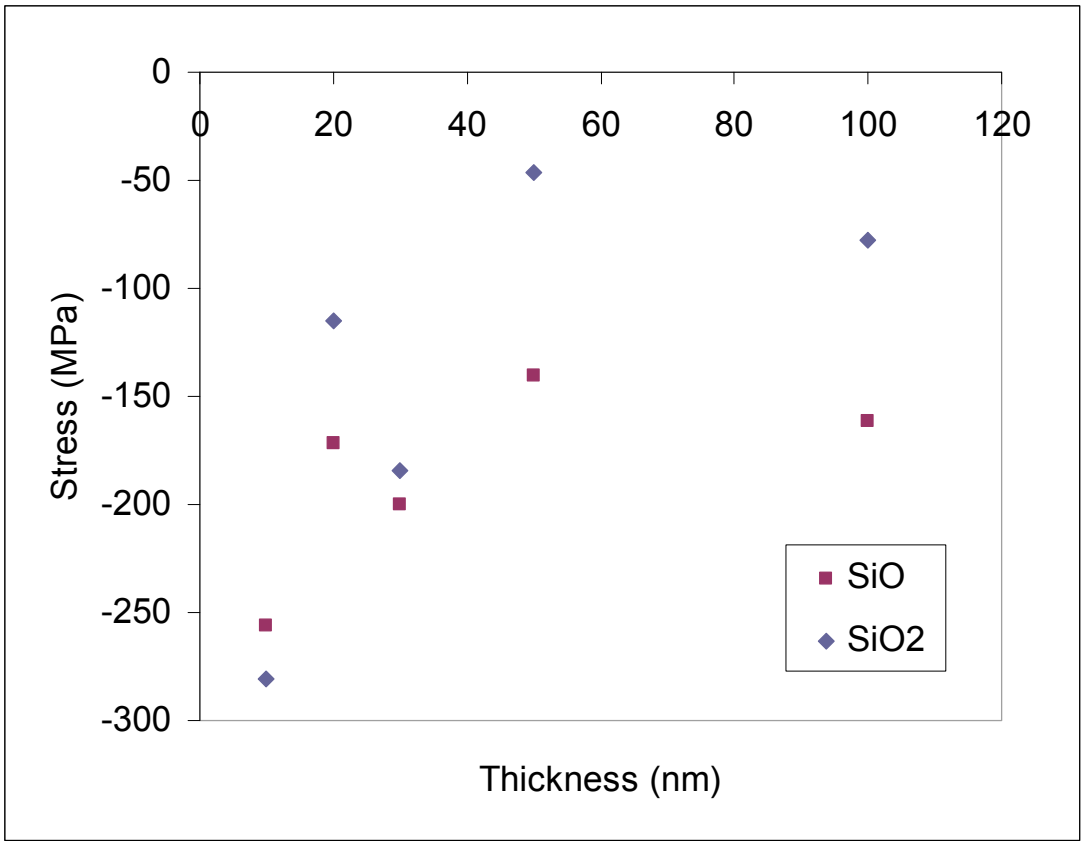

Figure 3.6. Film stress as a function of thickness. Stress changes more drastically with thickness for SiO_2 films compared to SiO films. Both change from more compressive to more neutral as thickness increases.

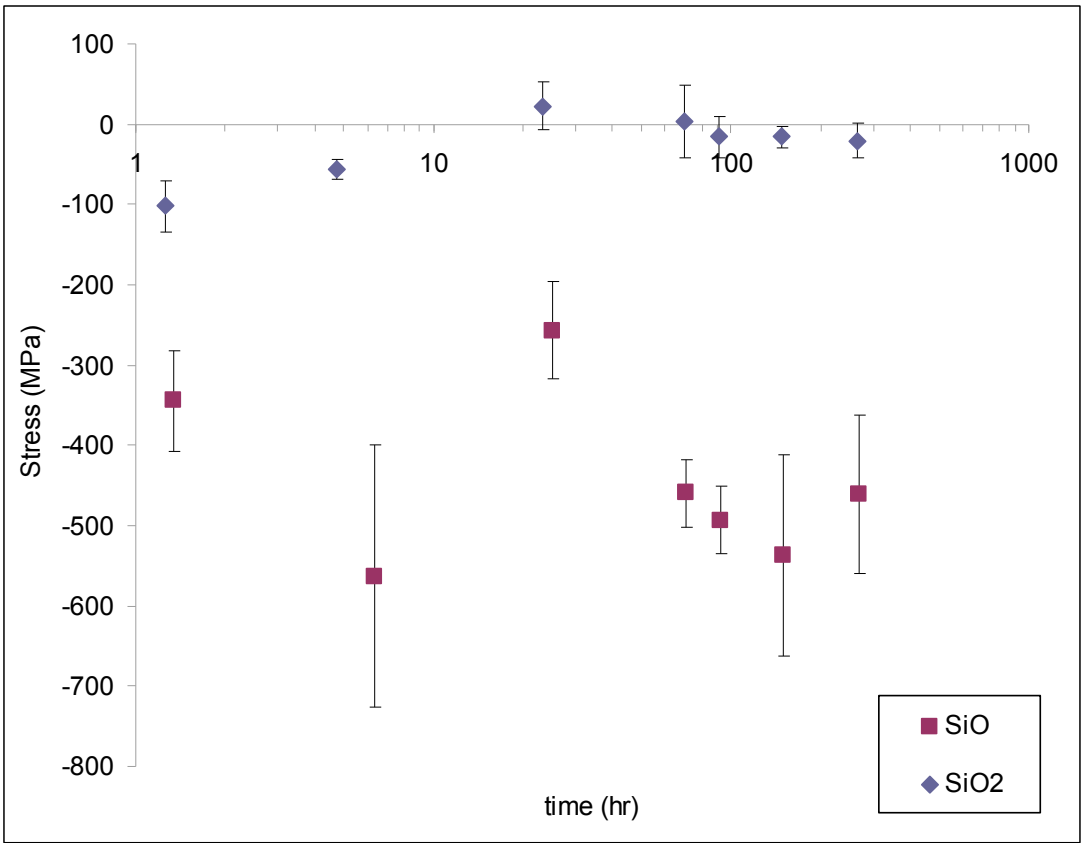

Figure 3.7. Effect of time on SiO_2 film stress. Film stress in evaporated SiO_2 vs. time, measured in SiO and SiO_2 films deposited directly following evaporation. SiO_2 is evaporated on top of SiO and its stress is calculated assuming a constant SiO compressive stress of 256 MPa.

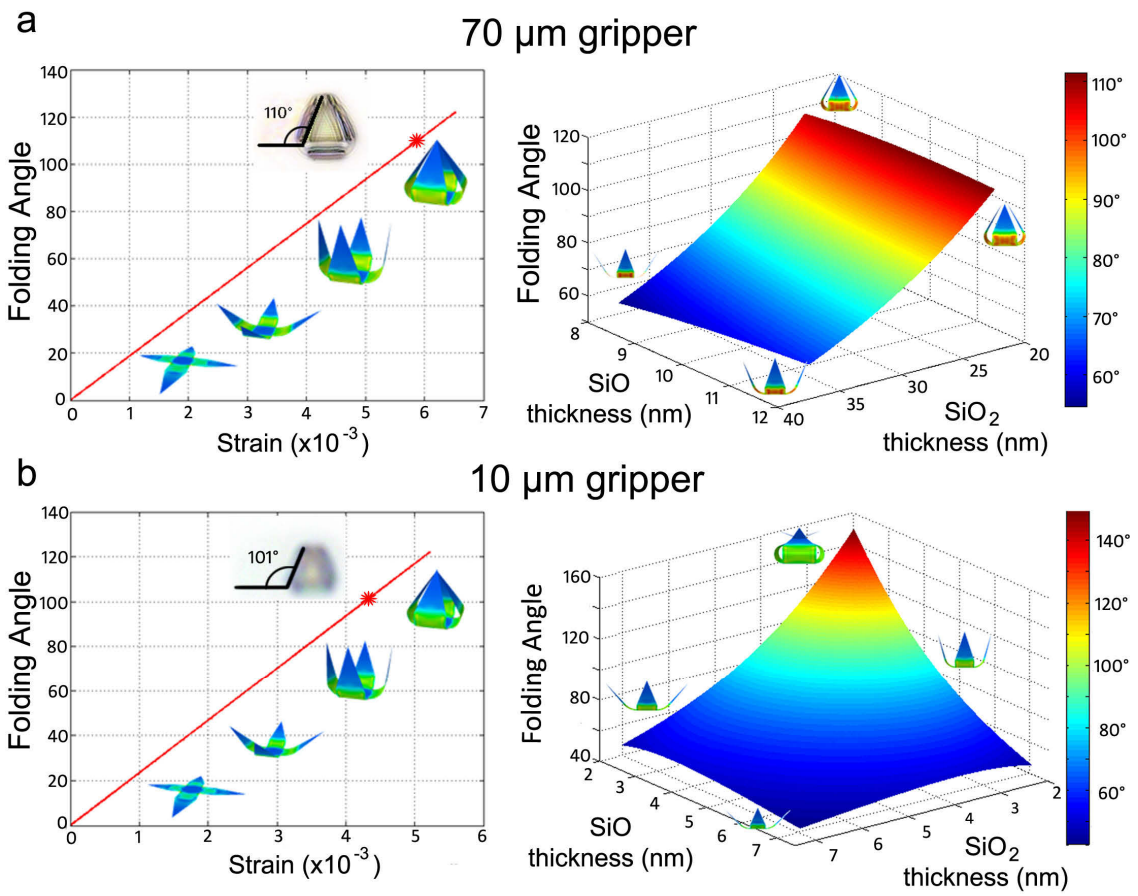

Figure 3.8. Characterization of thin film stress and gripper folding angle. (a) Graphs depicting the effect of strain and bilayer thickness on folding angle for a 70 µm gripper. (b) Graphs depicting the effect of strain and bilayer thickness on folding angle for a 10 µm gripper. The red star on the two left graphs indicates the observed folding angle for each gripper size.

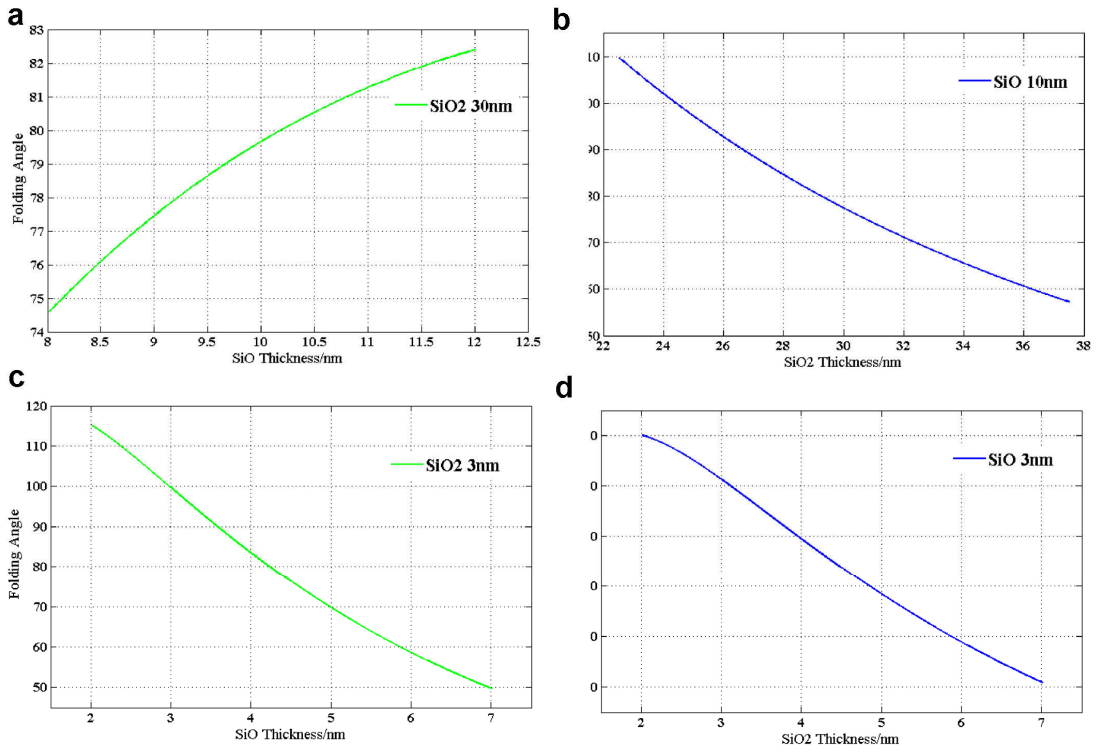

Figure 3.9. Folding angle versus bilayer thickness. (a) Folding angle changes with SiO thickness when SiO_2 is fixed as 30 nm. (b) Folding angle changes with SiO_2 thickness when SiO is fixed as 10 nm. In both cases, the mismatched strain is 0.0043 for a 70 μm gripper. (c) Folding angle change with SiO thickness when SiO_2 is fixed as 3 nm. (d) Folding angle change with SiO_2 thickness when SiO is fixed as 3 nm. In both cases, the mismatched strain is 0.0043 for a 10 μm gripper.

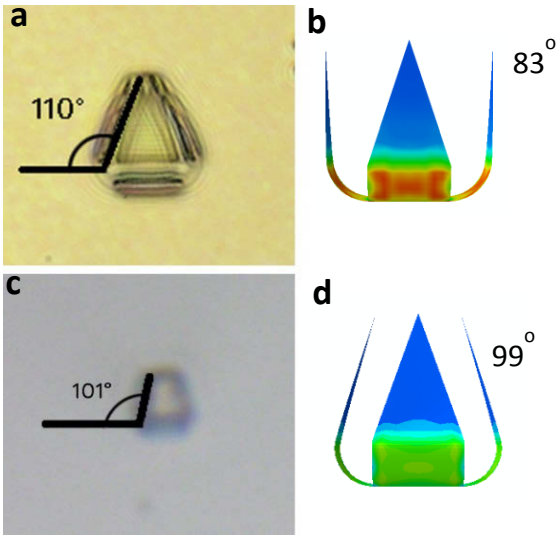

Figure 3.10 Estimation of gripper folding angle. (a-b) Experimentally observed (a) and model calculated (b) folding of a 70 µm gripper. (c-d) Experimentally observed (a) and model calculated (b) folding of a 10 µm gripper. There is an approximately 25% difference in model prediction and experimental results. We attribute this difference to the error of stress measurement and film thickness during evaporation, particularly due to the difficulties associated with measuring wafer bow and stress in such thin films.

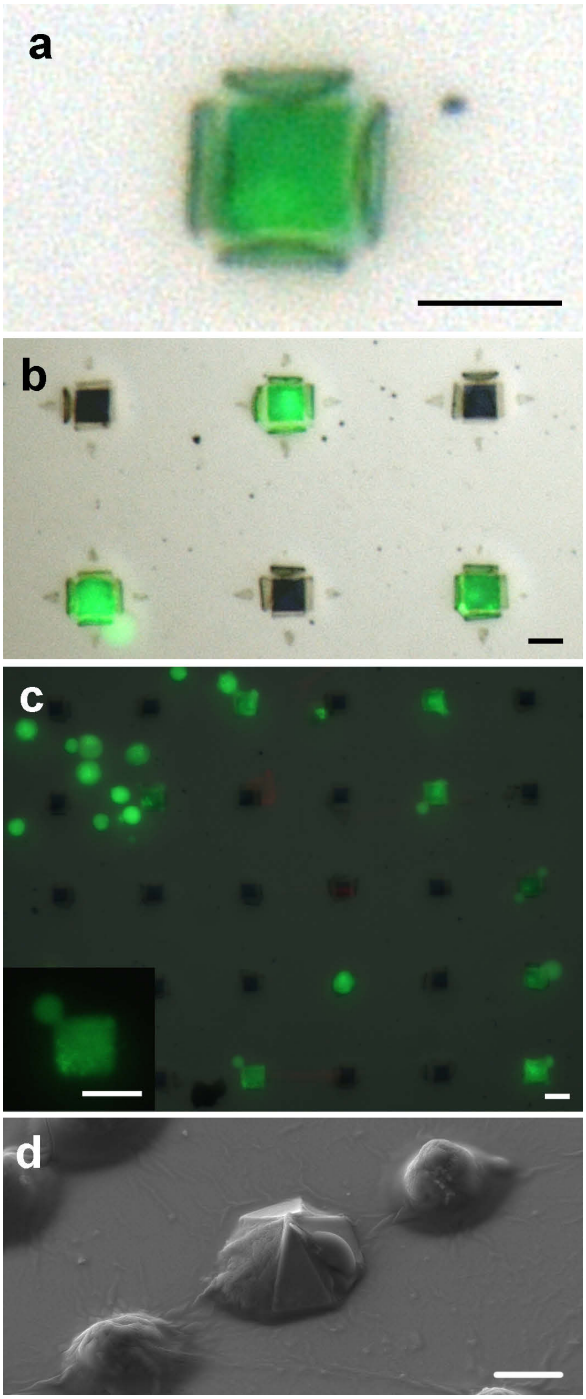

Figure 3.11. Single cell microgripper arrays.(a-c) Individual cells captured within the arms of grippers. (c, inset) The cell inside the gripper has conformed to the square shape of the gripper base. (d) SEM image of a cell trapped within the arms of a gripper, with several untrapped cells surrounding. Scale bars are 10 μm.

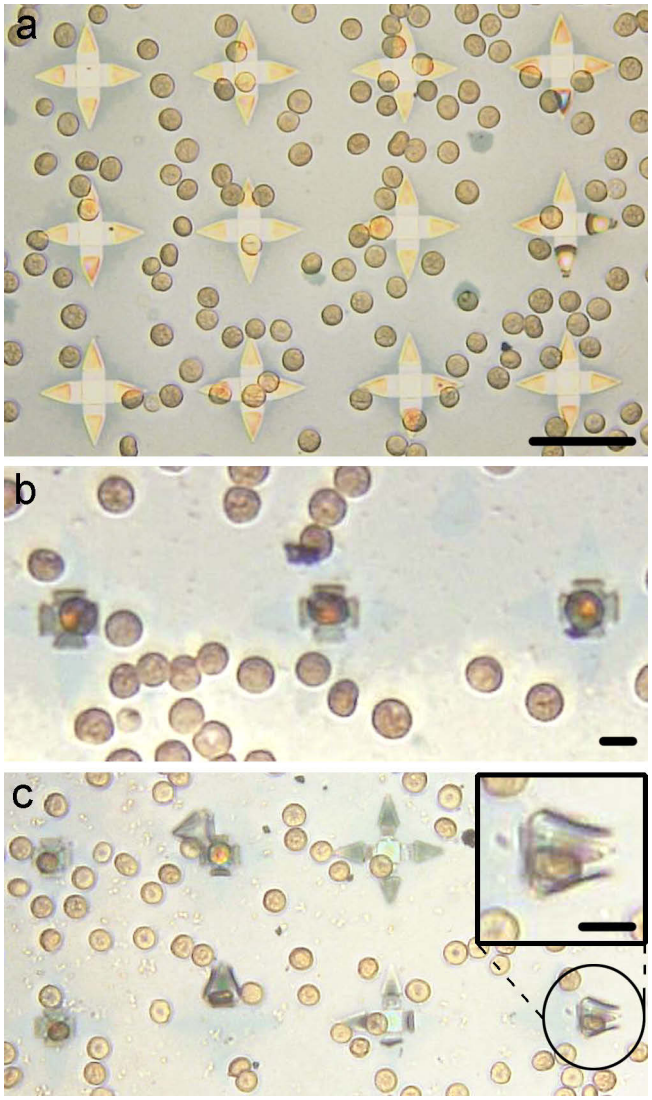

Figure 3.12. Capture of single red blood cells and free-floating single cell grippers. (a-c) Optical images of red blood cells trapped in 35 μm SiO/SiO_2 grippers. (a) Grippers with red blood cells prior to folding and release from the substrate. Scale bar is 35 μm. (b-c) Red blood cells captured by grippers. Scale bars are 10 μm.

3.3 pH- and ionic-strength sensitive hydrogel microgrippers*

Metallic and semiconductor components have been used as precursors for self-folding of sheets, containers, and microgrippers, using either surface tension or intrinsic thin film stresses, including my own work in the previous two sections.[26, 189, 190] However, in many applications such as biological devices, there is a need to incorporate biocompatible and quickly biodegradable materials such as polymers. The incorporation of smart polymers such as hydrogels offers the possibility for stimuli-responsive structures. The reversibility of such polymers is well-known and would be a desirable trait for self-folding devices. Guan et al. developed polymeric self-folding chitosan/poly(ethylene glycol methacrylate-co-ethylene glycol dimethacrylate) bilayers which fold in the presence of water.[191] Related bilayers patterned from poly(methyacrylic acid)/poly(hydroxyethyl methacrylate) folded in solution as a result of pH-related swelling differential, and were used as a drug delivery platform in the digestive tract.[192] We sought to design an all-polymer scheme with a focus on direct patterning using photocrosslinking. We demonstrate the development of photopatterned hydrogels composed of co-polymerized N-isopropyl-acrylamide (NIPAM), Acrylic Acid (AAc), poly-hydroxyl ethyl methacrylate (HEMA), and poly-ethylene glycol diacrylate (PEGDA) and their integration using photolithography. Our approach does not require plasma etching or stamping;[73] rather the polymer is directly crosslinked with UV light. This direct patterning allows for integration of bilayer actuators with rigid panels to enable the construction of complex, patterned, 3D structures that are biocompatible, are

*Portions reprinted from Polymer, 51, N. Bassik, B. Abebe, **K. Laflin**, D. H. Gracias, Photolithographically Patterned Smart Hydrogel Based Bilayer Actuators, 6093-6098, (2010), with permission from Elsevier.

economical to fabricate, and may be useful in microtools.

NIPAM has been widely investigated for its ability to undergo fast phase transitions as a result of temperature changes. By copolymerizing NIPAM with pH-responsive monomers such as AAc, it is possible to design a dual-responsive (temperature and pH) hydrogel system. It has been previously demonstrated that copolymerization of NIPAM with HEMA[193] and poly-ethylene glycol (PEG) can be used to design biodegradable biomaterials that are applicable in medical fields. The effect of ionic strength (IS) and pH on hydrodynamic diameter of NIPAM-based microgel particles has also been studied.[54, 194, 195] A decrease in hydrodynamic diameter was observed when microgels were exposed to an increase in IS. However, previous studies utilized solution-based polymerization techniques, and the results warranted an extension to photopatterned devices. Previously, PNIPAM in an organic solvent (1-butanol) was crosslinked into specific 2D shapes to study solvent-driven motion.[196] A key formulation parameter for enabling photocrosslinking is the inclusion of both the NIPAM monomer and pre-polymerized chains in the precursor solution, which allowed for adequate viscosity and UV sensitivity.

3.3.1 Fabrication of hydrogel-based Venus flytrap grippers

We copolymerized NIPAM with AAc via photocrosslinking to result in a pH- and IS-sensitive component of a bilayer actuator. We were able to design a structure reminiscent of the Venus flytrap (VF) plant [45] using rigid SU-8 panels and a connecting hinge. The VF opened and closed reversibly on exposure to varying pH and IS, demonstrating a straightforward fabrication technique for integration of hydrogel hinged actuators.

NIPAM solution was prepared by mixing of 3 g NIPAM monomer (Scientific Polymer Products Inc.), 0.4 g poly-N-isopropylacrylamide (pNIPAM, 300,000 molecular weight, Scientific Polymer Products Inc.) and 0.18 g BIS-Acrylamide (N,N-Methylenebis-Acrylamide) (Aldrich), dissolved in 7.5 mL of n-butanol (Sigma). The solution was vortexed overnight to aid dissolution of the pNIPAM. We added 0.31 mL acrylic acid and then decanted (after settling) to remove any insoluble crystals. One hundred microliters of photoinitiator, Irgacure 2100 (Ciba), was added to the solution just prior to photolithographic patterning. Polyethylene glycol diacrylate (7mL) (PEGDA, 726 MW Scientific Polymer Products Inc.) was mixed with 10 μL Irgacure 2022 and covered with aluminum foil to protect from prepolymerization.

Solutions were cast or spin-coated onto a glass slide. NIPAM-AAc was exposed to UV light at approximately 50 mJ/cm^2 (measured at 365 nm). PEGDA was exposed at approximately 90 mJ/cm^2. The optimum exposure varied depending on desired sample thickness and photoinitiator concentration. NIPAM-AAc and PEGDA were developed in ethanol and placed in deionized (DI) water for overnight before swelling analysis.

We fabricated Venus flytrap grippers composed of both rigid polymer panels and PEGDA/pNIPAM-AAc bilayer hinges. The rigid panels were prepared by spin coating SU-8 2015 (Microchem) at 2000 rpm on a glass slide to provide an approximately 20 μm thick film. After exposing at approximately 530 mJ/cm^2, the panels were developed for 55 seconds in Propylene glycol monomethyl ether acetate (PGMEA) and rinsed with isopropyl alcohol (IPA). Prior to bilayer coating, the slides were plasma cleaned for 2 minutes. The hydrogel bilayer photopolymerization was performed in noncontact mode. The PEGDA solution was spin-coated on top of the SU-8 rigid frames at 1000 rpm and

exposed at 50 mJ/cm^2. Subsequently, the NIPAM-AAc solution was cast on top and exposed for an additional 90 mJ/cm^2. We observed that pure PEGDA was immiscible with both water and butanol, and therefore the PEGDA monomer solution did not mix with other layers in the photopatterning process. The polymerized patterns were developed in ethanol. The thickness of the bilayer was approximately 225 μm. Multiple VF sizes were fabricated with sizes ranging from several mm to approximately 2 cm. The photopatterned shapes were then released from the glass slide in DI water. The bending of PEGDA/pNIPAM-AAc bilayer system was triggered by changing the IS and pH of the solvents.

Four stock solutions of 200 mL each were prepared at pH 2.5, 4.8, 7.8, and 12.1 with an IS of 0.2M using phosphate salts. In order to study the effect of IS on the swelling of NIPAM-based gels, additional buffers were prepared by taking 50 mL from the stock and adding appropriate amounts of NaCl. It should be noted that we anticipated minimal coupling between pH and IS since we kept one value approximately constant while varying the other.

3.3.2 Effect of IS and pH on swelling

Swelling ratio tests revealed differing swelling behaviors for the polymerized gels. pH-sensitive hydrogels swell or contract in response to pH changes as a result of the charge density of the material. Acidic hydrogels, such as pNIPAM-AAc, swell in solutions with a pH above the pKa of the hydrogel [52] due to the ionization and subsequent dissociation of the acid groups in the hydrogel. As governed by the Donnan equilibrium, osmotic pressure proportional to the difference in mobile ion concentration inside and outside the hydrogel is generated.[59, 197] Changes in IS alter the Debye

screening lengths of hydrogels,[198] causing swelling or contraction due to different degrees of self-repulsion of the hydrogel monomers. Specifically, increasing the concentration of salt in solution causes the mobile ion concentration outside of the hydrogel to approach or even surpass the mobile ion concentration inside the hydrogel. This change in the osmotic pressure causes reduced swelling in ionized hydrogels or de-swelling in neutral hydrogels.[199] Maximum swelling is constrained by the cross-linking of the chains.[200] Transport and diffusion of ions through hydrogels and the resultant kinetics of swelling are complex and explored elsewhere.[200-202]

Overall, NIPAM-AAc showed the most sensitivity to changes in pH due to the dissociation of its acid groups.[59, 197] PEGDA was mostly insensitive to pH. Both showed some sensitivity to IS, specifically showing a decrease in swelling with increasing IS. This can be attributed to the similarity of mobile ion concentration inside and outside of the hydrogels.[199] Detailed data and graphs of swelling ratios for NIPAM, NIPAM-AAc, HEMA, and PEGDA can be found in the original paper. By combining the large swelling capability of NIPAM-AAc with the minimal swelling capability of PEGDA, we can create bilayers which curl and uncurl in response to changes in pH and IS. This curling action occurs due to the shared boundary of the two hydrogels and the increased stress in the layers due to the difference in swelling **(Figure 3.13)**.

3.3.3 Venus flytrap patterning and folding

Hinged structures in the shape of a VF were fabricated with rigid SU-8 panels and PEGDA/NIPAM-AAC bilayer hinges. SU-8 was chosen for the rigid segments because it is structurally rigid and biocompatible. Additionally, it is highly crosslinked and chemically-resistive; for example, it swells only 0.5% in Dulbecco's phosphate buffered

saline.[203] The bilayer polymers adhered well to atmospheric plasma-treated SU-8 and to each other. The structures released easily from the glass substrate in water. Registration of the layers was made easier because of the opacity of the SU-8 panels.

The hinged VF shapes have a different equilibrium state than the bilayer structures due to the difference to initial stress created in the hinge bilayer from patterning over the uneven geometry of the SU-8 rigid panels. Their initial state in a pH 7.8/IS 0.2M was folded to a higher angle (as compared to bilayer folding) due to significant NIPAM-AAc swelling. When transferred to a pH 2.5/IS 1.1M solution, the NIPAM-AAc layer contracted, generating compressive stress, causing the structure to unfold and then fold in the same direction as the bilayer folding, as seen in **Figure 3.14**.

The rigid SU-8 panels maintained the structure of the VF shape and only folded along the bilayer hinge, whereas bilayer shapes actuated along the entire surface, causing a rolling effect. The folding action took place in anywhere from 10 seconds to several minutes, depending on the thickness of the hinge layers. The VF's were reversible over 15 cycles.

3.3.4 Conclusions

We have demonstrated an integrated approach to create hydrogel bilayers via lithographic patterning that fold and unfold in response to changing aqueous conditions. By choosing patternable acrylate derivatives such as PEGDA and NIPAM-AAc, regions with high differential swelling characteristics were created. Of relevance to biological applications, we note that the materials themselves are known to be biocompatible. We constructed VF-shaped hinged structures with SU-8 rigid panels and a hydrogel bilayer

hinge which folded in response to changes in IS and pH. This bilayer closed and re-opened using the energy of the solution, without wires or electricity.

A highlight of this technique is the ease with which a stimuli-responsive polymer can be turned into an actuator. The ease and simplicity of this parallel fabrication scheme makes this technology accessible and highly economical. While our actuator operated on the time scale of minutes, we expect that actuation time will decrease as a function of further miniaturization.[201, 204]

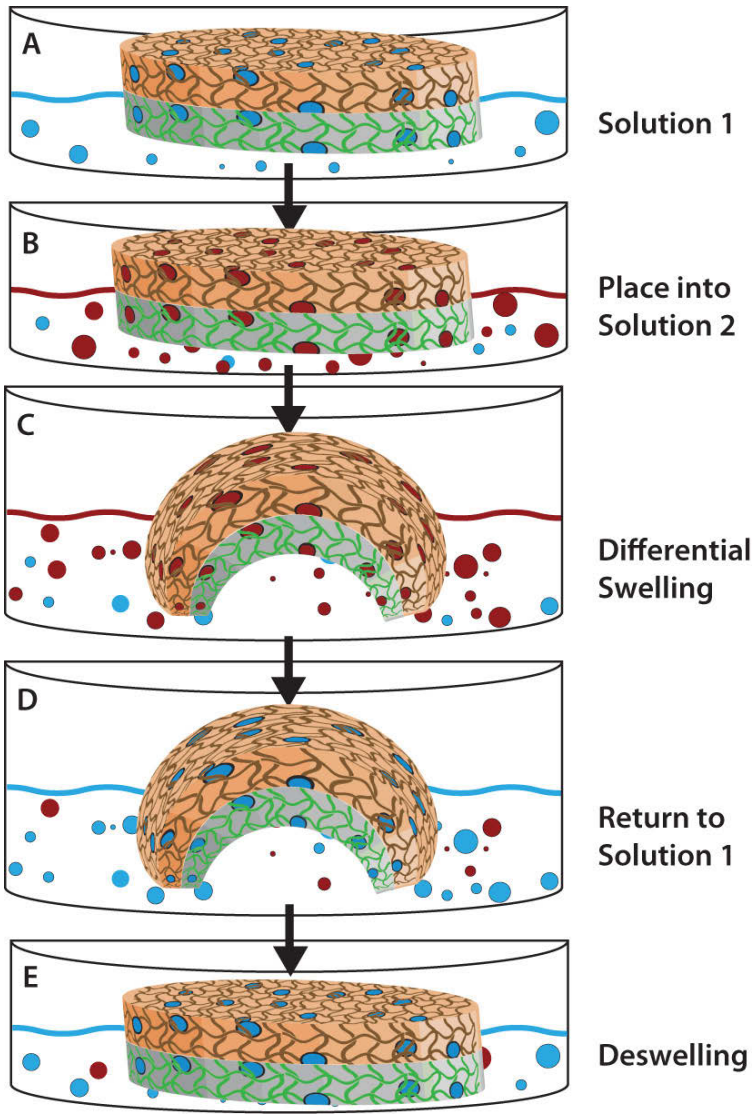

Fig. 3.13. Schematic of PEGDA/NIPAM-AAc bilayer actuation mechanism. A: A hydrogel bilayer is placed in aqueous solution 1 with specific pH and IS. It comes to equilibrium. B: The bilayer is transferred to solution 2 which has different pH and IS. C: Gel 1 swells in response to the environmental changes while Gel 2 does not swell, causing the bilayer to fold. D: The bilayer is transferred back into solution 1. E: Gel 1 deswells in response to the environmental changes and the bilayer unfolds.

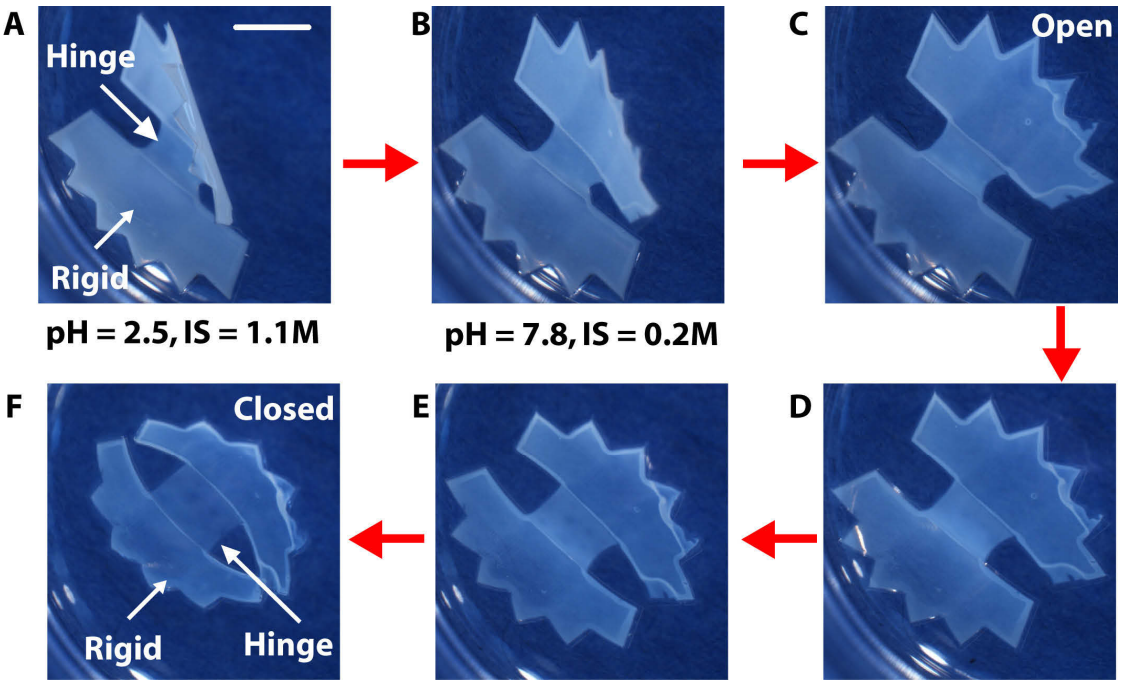

Fig. 3.14. Venus flytrap actuator folding in changing pH/IS. VF-shaped actuator with hinge constructed from rigid SU-8 segments with a NIPAM-AAc/PEODA bilayer hinge. Reversible folding occurred when the structure was transferred from a pH 2.5/ IS 1.1 M solution to a pH 7.8/ IS 0.2 M solution. The folding was reversible over 15 cycles. Scale bar is 3 mm.

3.4 Stimuli-responsive theragrippers for controlled release*

Thus far, I have shown microgrippers applied as diagnostic tools. I have shown their ability to excise tissue for histolotical and genetic analysis for cancer diagnosis and their ability to isolate single cells for assays and imaging. However, I speculated that a stimuli-responsive gripping device would be useful to locally deliver drugs for the treatment of disease, as well.

Drug delivery mechanisms have an enormous impact on the efficacy and bioavailability of pharmaceuticals. There are many accepted routes of administration including but not limited to oral, rectal, buccal, nasal, ocular, vaginal, intravenous, and topical. Controlled release systems offer several advantages: better control over drug concentration, longer residence time, minimized side effects, drug protection from harsh conditions, and lower administration frequency[205]. Inflammatory bowel disease (IBD) and gastrointestinal (GI) cancer patients would benefit from such improvements over current treatments. In the case of IBD, achieving the therapeutic dose is difficult due to unpleasant delivery methods such as rectal suppositories or enemas; the wide range of pH, enzymatic activity, and pressure throughout the GI tract; and low absorption and variable transit time through the GI tract.[206] Patients must often take a combination of up to 16 pills a day, rectal suppositories and enemas, reducing patient quality of life.[207, 208] Likewise, chemotherapy treatments for cancer are often delivered systemically, resulting in painful and unpleasant side effects for patients. An extended, site-specific delivery of drugs could potentially reduce these side effects, improve drug efficacy, and improve

*An edited excerpt from K. E. Malachowski, J. Breger, H. R. Kwag, M. O. Wang, J. P. Fisher, F. Selaru, D. H. Gracias. "Stimuli-responsive theragrippers for controlled release." Under review.

patient quality of life.

Many hydrogels have been developed for controlled release of pharmaceuticals, including micro or nanoparticles,[209-212] capsules or cylinders,[213, 214] and patches or discs,[66, 215-219] made from a variety of materials and fabrication methods.[56, 220] In particular, stimuli-responsive hydrogels are of interest to the drug delivery community due to their responsiveness to the unique range of pH and temperatures within the GI tract, thereby offering the possibility for well controlled drug release.[66, 71, 83, 215] In this paper, we describe a polymeric, biphasic drug eluting theragripper which is capable of closing around tissue in response to body temperature and releasing a drug from its layers and pores. Actuation of the theragrippers is derived from stimuli-responsive soft micro-origami paradigms.[83, 221-225] This device is made from biodegradable, photopatternable polypropylene fumarate (PPF)[226-228] and biocompatible pNIPAM-AAc (see Appendix A).[83] Our central hypothesis is that by combining, (a) the thermally responsive properties of NIPAM, (b) the tissue gripping capabilities of a photolithographically shaped multi-fingered device with sharp tips, (c) the high stiffness of biodegradable PPF, and (d) the controlled release properties of porous polymers, that we can deliver sustained doses of drugs more effectively using a combined chemical and mechanical approach.

3.4.1 Theragripper fabrication

Considerable thought was given to the choice of materials and fabrication processes for the theragripper design and actuation and this distinguishes our work from prior uses of stimuli responsive polymers in drug delivery. We realize that pNIPAM and other hydrogels have been used extensively in active drug delivery devices due to their stimuli-responsiveness.[66, 71, 83, 229] Below 32°C, pNIPAM-AAc is hydrophilic and swells

in water; above 32°C it becomes hydrophobic and collapses as a result of the dehydration of its hydrophobic groups.[230] However while this mechanism makes PNIPAM an ideal hinge material, on its own, this hydrogel suffers from a low modulus that makes them weak and floppy as actuatorsand gripping devices. Importantly, by combining PNIPAM with PPF which has a modulus three orders of magnitude greater than that of most hydrogels, and has been previously used in bone tissue engineering,[231-235] we are able to create a robust gripping device to latch onto cells and tissue. Further, by developing a photolithographic approach, we could precisely shape this stiff, bone-like material to create sharp tips that can dig into tissue to secure the theragrippers in place (Figure 1a). Thus, pNIPAM-AAc hinges swell and collapse in response to temperature, while the PPF panels provide rigidity and strength to the device, causing the theragrippers to open and close at body temperature **(Figure 3.15 a-b)**. These grippers are similar in shape to our metallic microgrippers which have been used for *in vitro* and *in vivo* tissue biopsies.[84, 236, 237]

PPF was synthesized using a previously published protocol; the molecular weight was determined to be 952 Da with a polydispersity of 1.9. To make photopatternable PPF solution, we mixed three parts PPF stock solution with one part diethyl fumarate (DEF, Sigma Aldrich) at 65˚C and added 5% Irgacure 2100 (Ciba) by weight. To make photopatternable pNIPAM-AAc solution, we dissolved 3 g NIPAm monomer (Scientific Polymer Products Inc.), 0.4 g poly-N-isopropylacrylamide (pNIPAM, 300,000 Da molecular weight, Scientific Polymer Products Inc.) and 0.18 g N,N-Methylenebis-Acrylamide (Sigma Aldrich) in 7.5 mL of n-butanol (Sigma Aldrich) and let the solution stir overnight. We added 0.31 mL acrylic acid (Sigma Aldrich) to the solution and stirred

to dissolve. Finally, we added 5% w/w Irgacure 2100. The theragrippers can store and elute drugs from the polymer networks in one or both layers. These grippers are also transparent, allowing visualization of the grasped tissue if needed. Thus, the material composition and properties of the theragrippers make them ideal as drug delivery devices, as they could grip onto and elute a drug in close proximity to a targeted tissue such as in the GI tract **(Figure 3.15 c)**.

The theragrippers can be engineered using three different methods **(Figure 3.16)**. Method 1 theragrippers (TG1) were fabricated on a silicon wafer with photolithographically patterned chromium (Cr) and copper (Cu) alignment markers. We spin-coated a 30% solution of polyvinyl alcohol (PVA, Sigma Aldrich, 9000 Da molecular weight, 80% hydrolyzed) on top of the wafers as a sacrificial release layer and baked for 1 minute at 115˚C. We spin coated PPF solution on top of the silicon wafers at 3000 rpm and exposed at 650 mJ/cm^2 on a mask aligner (Quintel). Without developing, we cast 1 mL of pNIPAM-AAc solution on top of the PPF layer by hand and exposed at 100 mJ/cm^2. We developed both layers by rinsing vigorously with ethanol and deionized (DI) water. Finally, we released the theragrippers from the substrate by dissolving the PVA sacrificial layer in DI water for approximately 20 minutes. We increased the extent of loading by developing a second method (TG2), wherein we created pores in the PPF via salt leaching during fabrication.[231] To do this, we incorporated 5% by weight finely ground sodium chloride (NaCl) into the PPF solution prior to patterning. pNIPAM-AAc hinges were photopatterned in the same way as Method 1. After release, the NaCl was dissolved away in DI water overnight to leave pores in the PPF. Subsequently, TG2 theragrippers were released from the substrate by dissolving the PVA sacrificial layer in

DI water for approximately 20 minutes and soaked in a dye or drug solution. Method 3 theragrippers (TG3) were fabricated by mixing 10 mg of dry chemical in 10 mL of PPF prior to patterning. pNIPAM-AAc hinges were photopatterned in the same way as Method 1. TG3 theragrippers were released from the substrate by dissolving the PVA sacrificial layer in DI water for approximately 20 minutes and used immediately.

3.4.2 Characterization of drug and dye release

We observed the drug release profiles of the theragrippers by loading fluorescein sodium salt into each layer and allowing the dye to elute into DI water at 32°C **(Figure 3.17)**. Fabrication and loading mechanisms for each style of theragripper are detailed in **Figure 3.16**. We observed in TG1 theragrippers that the chemical was loaded primarily in the pNIPAM-AAc. We attribute this to the pNIPAM-AAc's high capacity for swelling because it is a hydrogel, compared to the non-swelling PPF layer.[238] Additionally, the pNIPAM-AAc layer is hydrophilic at 4°C, while the PPF is hydrophobic and thus less able to accept the aqueous hydrophilic drug solution. We observed that TG2 theragrippers contained dye in both the pNIPAM-AAc hinge layer and the large pores in the PPF, leading to a larger total amount of dye released **(Figure 3.17 b).** TG3 theragrippers contained dye primarily in the interstitial spaces of the PPF network. They demonstrated extended release over a longer period of time due to the dense crosslinking and narrow interstitial spaces of the PPF polymer network **(Figure 3.17 c).**[234]

We quantified the chemical elution profiles and plotted cumulative release over a period of 7 days using a fluorescein dye which eluted into DI water at 37°C **(Figure 3.18 a-b)**. Six theragrippers of each type were taken at random, rinsed three times with 25˚C DI water, and added to a vial of 20 mL of 37˚C DI water. 300 μL samples of the solution

were taken at each time point, and were excited and analyzed at 485 nm and 538 nm on a plate reader (Spectramax Gemini XPS, Molecular Devices). The cumulative release profile signifies the total amount of drug released over that period and plotted per gripper. We note that burst release effects from concentrated drug or dye on or near the surface of the theragrippers were minimized by rinsing the grippers well in DI water prior to each study. Although all three samples were prepared using the same 1 mg/mL solution, we observed that the cumulative elution from each was very different. Cumulative elution from TG2 was more than double that from TG1 and we attribute this to high loading of dye into the salt-leached PPF pores. This rationalization is based on prior material characterization of salt-leached porous PPF.[231, 233] TG3 showed the least cumulative elution. We attribute this slow release to the dye being trapped in the interior of the PPF polymer network. Further, the release rate from TG1 and TG2 is much faster than TG3; both these grippers eluted 90% of the plateau concentration in the first 6 hours and reached a plateau in 24 hours, while TG3 continued eluting consistently over 7 days and did not plateau.

In addition to fluorescent dyes, our processing methodology is also applicable with real drugs which are often formulated as powders. We highlight this applicability using Mesalamine, a well-known anti-inflammatory drug for inflammatory bowel diseases. Mesalamine was removed from Pentasa® capsules (Shire) and ground with a mortar and pestle into a fine powder. 5% mesalamine by weight was added to the PPF solution prior to patterning of theragrippers (Method 3). 60 theragrippers were rinsed with DI water three times and added to 15 mL of 37˚C DI water. 300 μL samples of the solution were taken at each time point and analyzed using liquid chromatography mass

spectroscopy (Waters Acquity H Class UPLC) **(Figure 3.18 c)**. The drug eluted over a period of 7 days before it reached a plateau and showed a slow and steady release profile consistent with TG3.

GI cancers would also benefit from delivery of a low but consistent concentration of chemotherapeutic drugs directly to targeted tumor sites. To study this application, we quantified the elution profile of doxorubicin from standard theragrippers soaked in a 400 μg/mL doxorubicin (DOX) solution (TG1) **(Figure 3.18 c)**. Six theragrippers were taken at random, rinsed three times with 25˚C DI water, and added to a vial of 20 mL of 37˚C DI water. 300 μL samples of the solution were taken at each time point, and were excited and analyzed at 485 nm and 590 nm on a plate reader. Although the DOX-TG1 were prepared in the same way, they showed a more extended release as compared to the fluorescein-TG1. We attribute this difference to the higher hydrophobicity of DOX as compared to fluorescein which is hydrophilic.

After examining and fitting a number of kinetic models, including zero order, first order, Higuchi, and Korsmeyer-Peppas, to the release data, we observed that our data best fits a first order kinetic model **(Figure 3.18 d)**, which goes as $C = C_s\left(1 + e^{-kt}\right)$ where C is the drug concentration in the surrounding solution and C_s is the initial drug concentration in the matrix. First order kinetics is common with diffusion-controlled polymer matrix systems with the assumption that the dye or drug is uniformly distributed within the polymer layer.[205, 239-243] Unlike reservoir systems that have a highly concentrated drug solution acting as a sink, the concentration of drug within the polymer matrix is decreasing with time, thus the rate is concentration-dependent. If we rearrange the above

equation for concentration, we get $\ln\left(\frac{C_s - C}{C_s}\right) = -kt$. Thus, in **Figure 3.15 d**, we plotted the natural log of the fraction of drug remaining in the matrix versus negative time, where the slope of the line is the first order rate constant. The first order rate constants are given in **Table 3.4**.

Table 3.4. Rate constant and R^2 value for theragripper first order kinetic models

Gripper Style	K (hr^{-1})	R^2
Fluorescein TG1	0.128	0.9007
Fluorescein TG2	0.138	0.8994
Fluorescein TG3	0.007	0.9662
Mesalamine TG3	0.003	0.9617
Doxorubicin TG1	0.015	0.9093

The widely varying rate constants explain the different rates of elution and are affected by the drug solubility in both the polymer and the solution, drug-polymer interactions in the matrix, diffusivity and morphology of the polymers, and the method of loading as described in a comprehensive review on polymer drug delivery.[238]

3.4.3 Biphasic release from theragrippers

In addition to rate control from a single layer, we note that the use of multi-layered polymeric drug delivery systems offers the possibility of achieving biphasic release profiles to rapidly achieve the therapeutic dose and enables the delivery of multiple drugs from a single device. We illustrated this point by demonstrating biphasic release of two differently colored fluorescent dyes, rhodamine 6G (red) and fluorescein

(green) at 37°C **(Figure 3.19)**. We incorporated rhodamine 6G into the PPF pre-polymer using Method 3 and loaded fluorescein into the pNIPAM-AAc by soaking the grippers as per Method 1. We observed that the fluorescein dye was expelled quickly from the pNIPAM-AAc layer, while the rhodamine eluted significantly more slowly during a 3 hour time period from the PPF layer. The dyes appear to remain isolated from each other in their individual layers. This experiment illustrates that a combination of methods and/or drugs can be tailored for specific therapeutic applications.

3.4.4 Doxorubicin delivery to an *in vitro* model

An important hypothesis in this work is that the gripping action of multi-fingered theragrippers would enhance drug delivery efficacy compared to a non-gripping patch. We developed an *in vitro* model to compare the DOX delivery efficacy of a flat square patch versus a theragripper to a clump of cells subjected to medium flow (5 mL/min) as would occur under *in vivo* conditions in the GI tract. The patch was designed with the identical pNIPAM-AAc bilayer composition and volume. However, in contrast to the theragrippers, these bilayers were not patterned with segmented fingers; hence they could not grip onto cells or tissue and curved only slightly. After loading both the theragrippers and patches with 0.75 μM DOX, we pipetted each onto a clump of MDA-MB-231 breast cancer cells at 37°C. The gripper closed around the cells, while the patch retained its slight curvature **(Figure 3.20 a, c)**. Hence, during flow, the gripper remained attached to the cells the entire time while the patch drifted away from the cells in the direction of the flow after an average of 20 minutes. Thus only the theragrippers eluted DOX in the vicinity of the cells for the entire two hours.

After this period, we removed the grippers and patch, and rinsed with PBS for 20 minutes at 5 mL/min to remove any residual DOX. We tested the efficacy of DOX in killing cells by staining the DOX-exposed cells to a viability stain composed of calcein AM and ethidium homodimer. The patch shows lower numbers of dead cells as compared to the theragripper **(Figure 3.20 b, d; Figure 3.21)**. The results show that DOX was more efficiently delivered directly to the cells via the gripper than the patch and that the gripping action played a critical role in achieving this effectiveness. Additionally, the effectiveness of the gripping action could be gauged by analyzing the retrieved theragrippers which contained cells within their grasp **(Figure 3.20 e, f)**. This result suggests that the theragrippers could grasp mucosal tissue and resist being carried away along with the frequent shedding of mucus lining in the GI tract. It is noteworthy that patches have been previously developed with mucoadhesive coatings to enhance attachment to the GI mucosa[66, 244]. One limitation of this approach is that the initial application force and contact time significantly affect bonding strength.[244, 245] And, while it is possible for patients or doctors to apply a large initial application force to a buccal patch, it is significantly more challenging to firmly apply a patch with sufficient force to the lower GI tract by oral or endoscopic delivery. The autonomous gripping action of the theragrippers reduces this requirement for application of high forces to enable attachment. Further, if enhancement of adhesion is needed, our approach facilitates inclusion of mucoadhesive coatings by dip-coating or spin coating.

3.4.5 Porcine *in vivo* model of controlled dye release

In order to demonstrate feasibility of drug delivery in clinical conditions, we also performed an *in vivo* experiment using theragrippers loaded with an endoscopically

visualizable blue food dye in a porcine GI model. We used a porcine GI model because these best resemble the human GI anatomy. Experimental protocols were approved by The Johns Hopkins University IACUC and met guidelines of the National Institutes of Health guide for the Care and Use of Laboratory Animals. Theragrippers were soaked in blue food coloring for 24 hours (Method 1) and stored in an ice bath until use. After an endoscope was introduced into the esophagus of the pig, the theragrippers were delivered by injection through a catheter placed in one of the ports of the endoscope. We used a standard double channel endoscope (EG-3830TK PENTAX, Tokyo, Japan). The theragrippers remained open and began to close after sliding into the stomach due to the large quantity of fluid and the forceful contractions of the esophagus **(Figure 3.22)**. We observed that the grippers were scattered around the stomach with good coverage. The model drug was observed to be contained in the gripper **(Figure 3.22 a)** and then eluting from the gripper **(Figure 3.22 b)** over time. Some grippers did not show visible drug elution possibly due to the majority of the drug being washed away during the endoscopic delivery in water. Closing of the grippers occurs spontaneously on warming up from the cold temperatures in the ice bath to the body temperature, which typically occurred within a few minutes. In order to delay or accelerate the time-to-close, cold or hot water could be introduced into the catheter along with the theragrippers, thereby facilitating gripping in different regions of the GI tract.

3.4.6 Conclusions

In summary, we have demonstrated a new approach for sustained drug release from therapeutic all-polymeric multi-fingered grippers with sharp tips for gripping into tissue. The theragrippers can be fabricated in a high throughput, parallel and cost-

effective manner using lithographic processes. These processes also facilitate enable accurate design modifications using AutoCAD tools and photomasks. Due to the stimuli-responsive gripping action of these devices, they function autonomously and can be deployed en masse. They can absorb small molecule drugs, and their biphasic release can eluteone or more drugs, rapidly or slowly up to 7 days, enabling a highly tunable device. Their extended release period of a week offers a significant improvement over the daily rectal drug delivery currently used in the treatment of IBD, yet is short enough to avoid concerns of the breakdown of pNIPAM. Their multi-fingered design shows improved site-specific delivery under flow compared to a patch design. Thus, these devices can more effectively provide rapid or extended site-specific administration of one or more drugs by actively gripping into tissue with the combination of stiff, bone-like tips and thermoresponsive hinges. The theragripperswere small enough to be deployed via catheters and dye delivery was also successful *in vivo*. As a result, patients could experience fewer side effects and higher overall drug efficacy, both of which need to be further evaluated. Future experiments investigating drug stability and bioavailability within the device and the pharmacokinetics of mesalamine when delivered via site-specific controlled release will also need to be evaluated *in vivo*. These studies are limited by the lack an effective porcine IBD model, which is still under development.

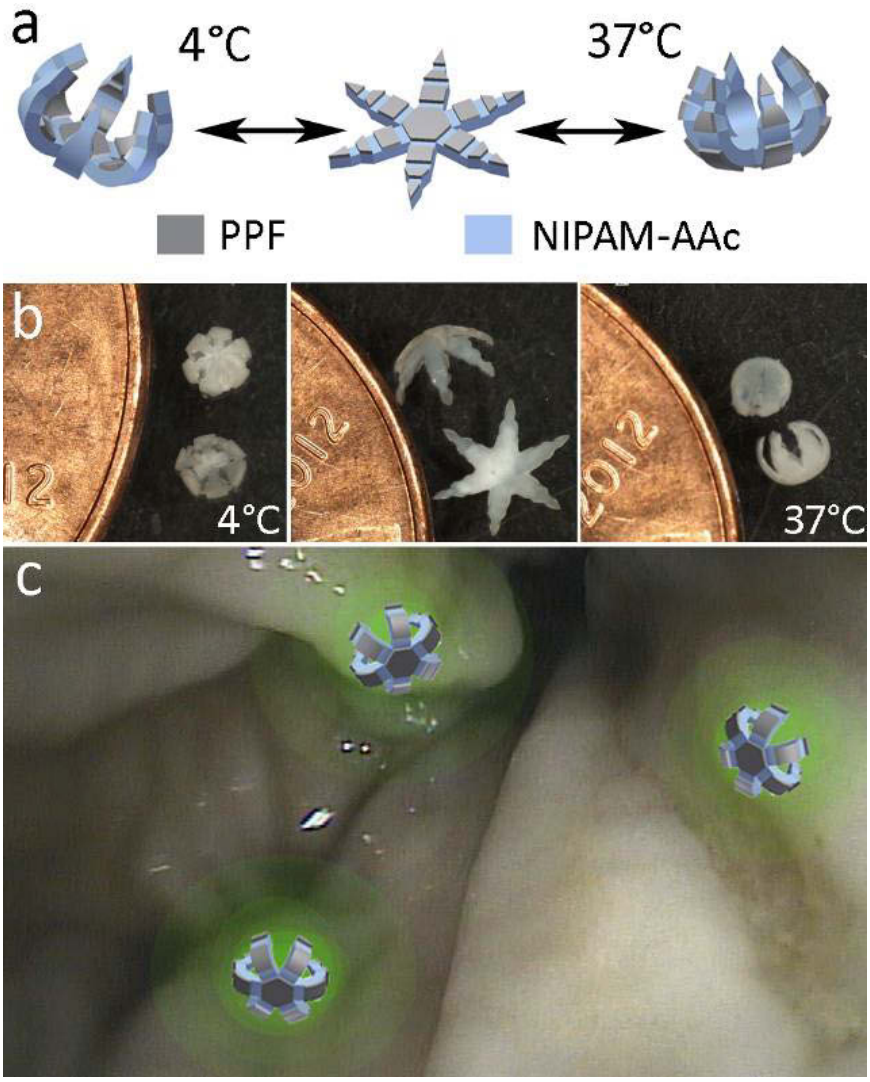

Figure 3.15. Design and proof of principle of drug eluting theragrippers. (a) Schematic of theragrippers with PPF rigid panels and flexible stimuli-responsive pNIPAM-AAc hinges. Due to the thermal responsiveness of the pNIPAM-AAc, the grippers reversibly open and close around body temperature. (b) Theragrippers originally closed at 4°C, open as the solution temperature increases, and finally close again in the opposite direction at 37°C. (c) Conceptual illustration of theragrippers attached to a colon wall, releasing a fluorescent drug to targeted areas of the colon.

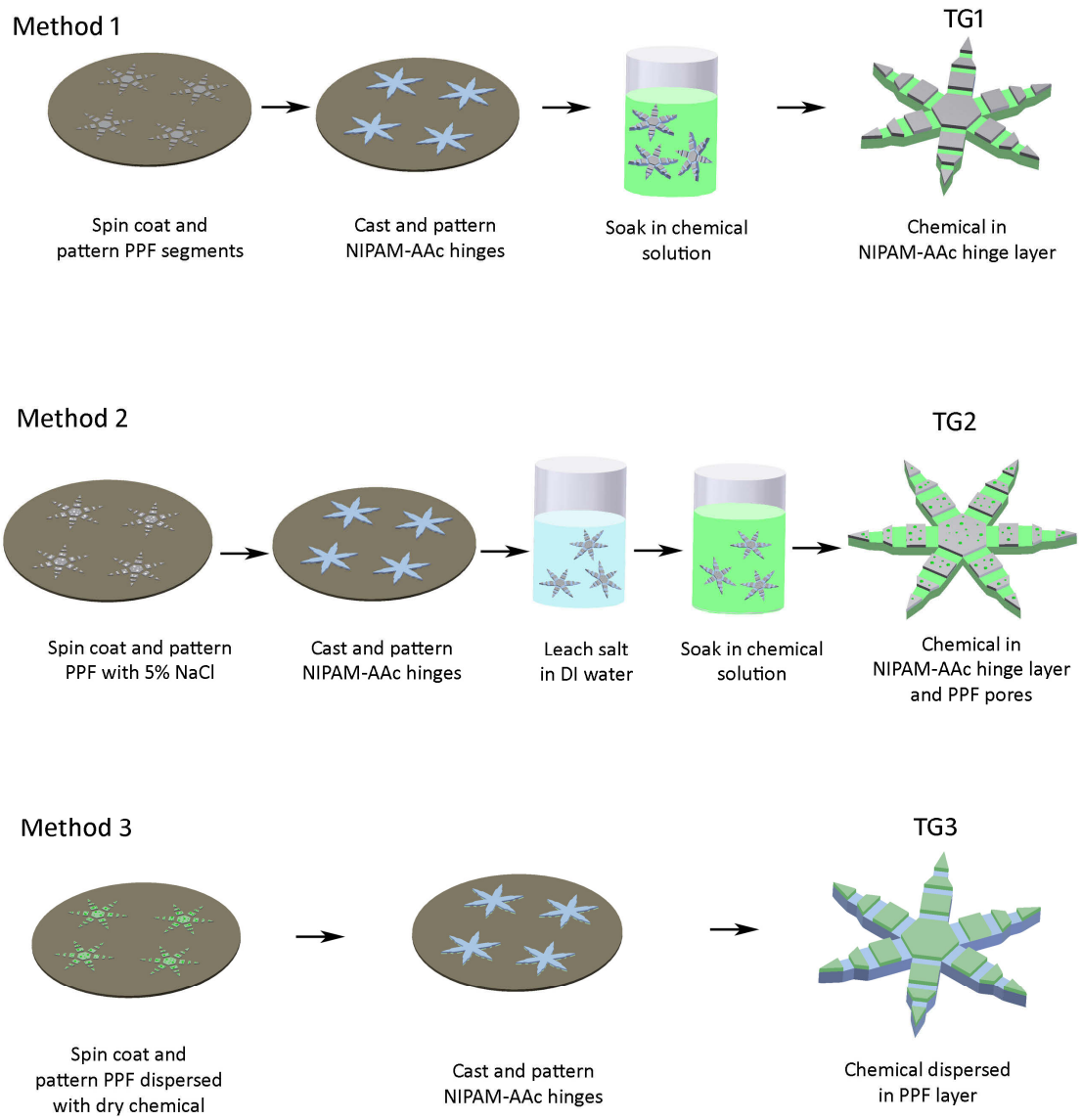

Figure 3.16. Schematic of loading mechanisms for the three types of theragrippers. Chemical is loaded into primarily the pNIPAM-AAc hinge layer (TG1), both the pNIPAM-AAc layer and large PPF pores (TG2), or primarily in the narrow interstitial spaces in the PPF (TG3).

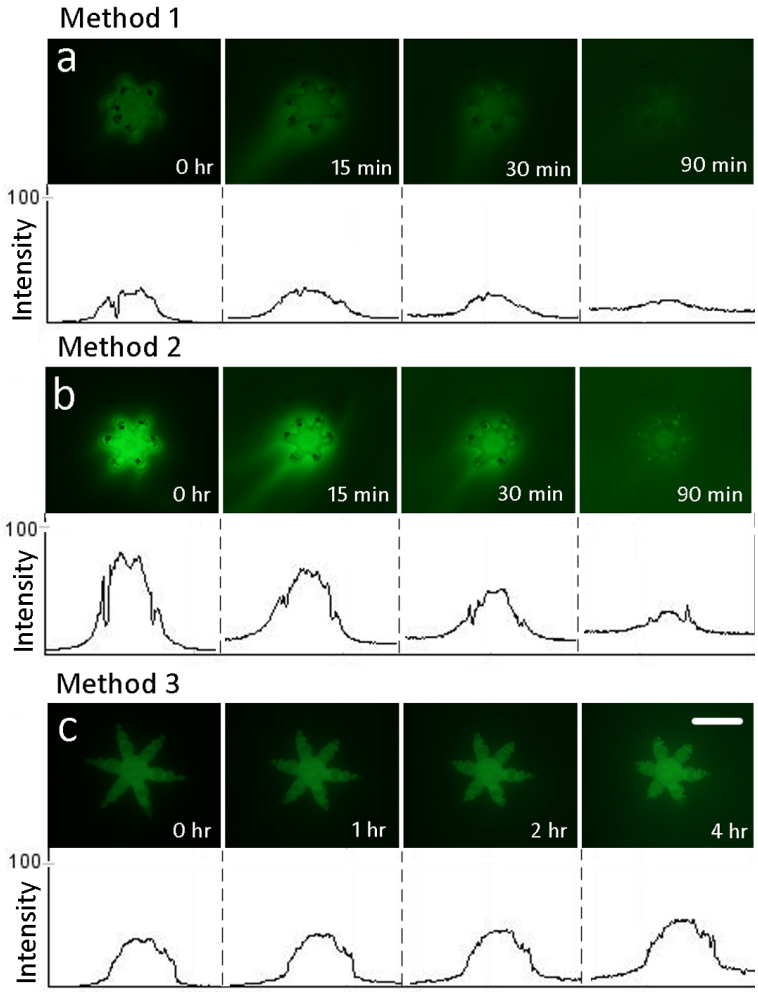

Figure 3.17. Characterization of drug release from theragrippers. Time lapse optical images of fluorescein sodium salt eluting out from theragrippers made via (a) Method 1 (TG1), (b) Method 2 with salt-leached pores in PPF (TG2), and (c) Method 3, where fluorescein is loaded via *in situ* polymerization (TG3). Note the time scale on each set of images, indicating that TG1 and TG2 elute significantly faster than TG3. Pixel intensity graphs below each optical image illustrate the varying fluorescein intensity within and around each gripper as time elapses and the dye elutes. Note that TG2 has the highest intensity due to the dual loading in the pNIPAM-AAc and PPF pores. Scale bar is 1.5 mm.

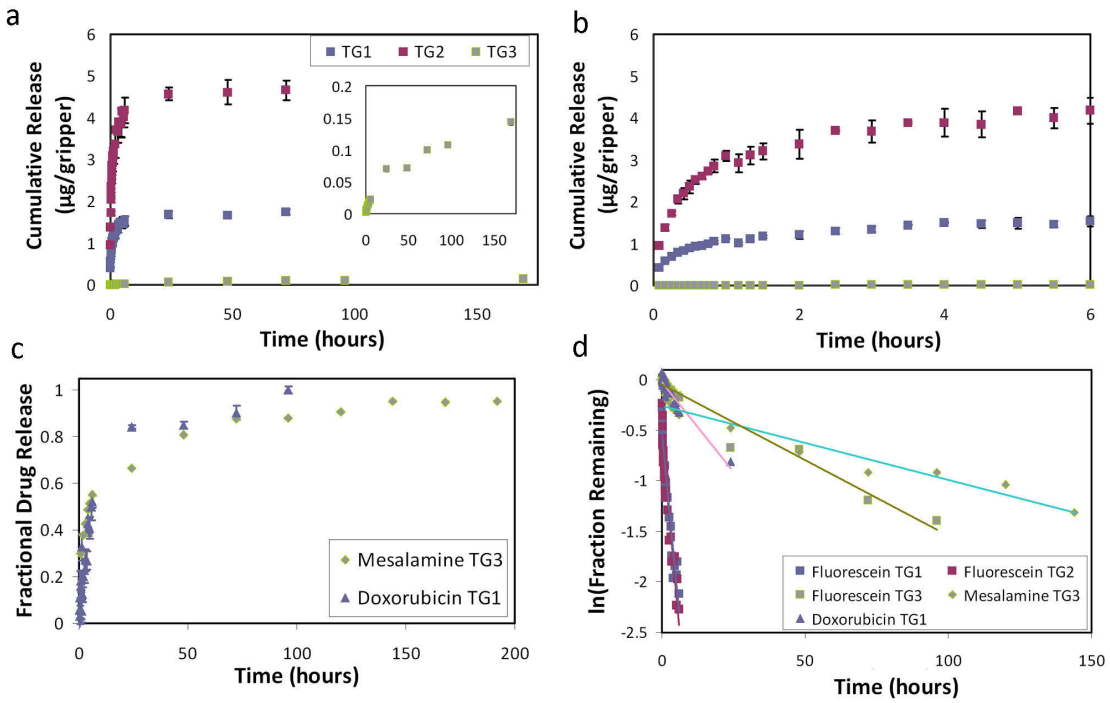

Figure 3.18. Quantified release profiles of dyes, commercial drugs, and kinetic analysis. (a) Graph of the cumulative fluorescein release profiles from the theragrippers. Zoomed graph details TG3 over a smaller y-axis. (b) Zoomed graph shows the cumulative release over the first 6 hours to better define TG1 and TG2 fast release. (c) Graph of the fractional release of mesalamine and doxorubicin from theragrippers. (d) First order kinetic model applied to each release profile.

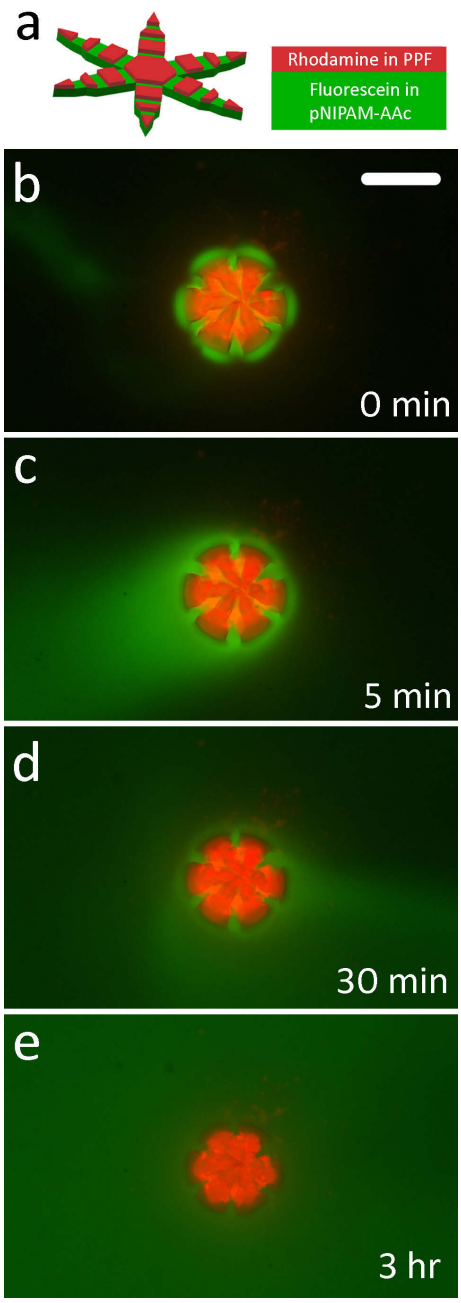

Figure 3.19. Dual release of multiple dyes from a theragripper. (a) Schematic showing the incorporation of rhodamine into the PPF rigid segments and fluorescein sodium salt into the pNIPAM-AAc hinge layer. (b-e) Time lapse optical images showing the rapid release of fluorescein from the pNIPAM-AAc layer and the slow release of rhodamine from the PPF layer. Scale bar is 1 mm.

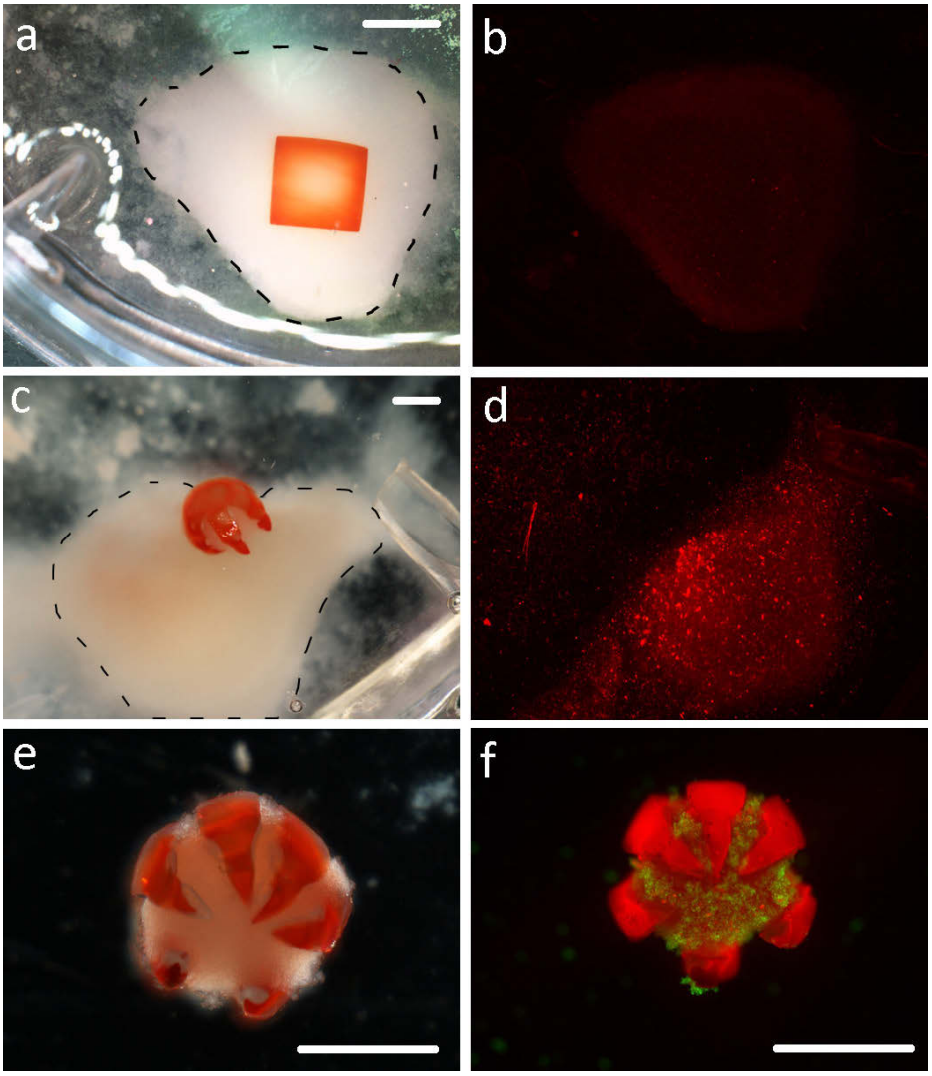

Figure 3.20. ***In vitro*** **model of doxorubicin elution**. (a) The square non-gripping control patch on top of a cell clump (outlined in dotted line). Scale bar is 2 mm. (b) The same cell pellet stained with ethidium homodimer after 2 hr of elution via the control patch. (c) The DOX-TG1 gripping into a cell clump (outlined in dotted line). Scale bar is 1 mm. (d) The same cell pellet stained with ethidium homodimer after 2 hr of elution via the DOX-TG1. (e-f) Optical and fluorescent images of the detached theragripper tightly closed around a clump of cells. Scale bars are 1 mm.

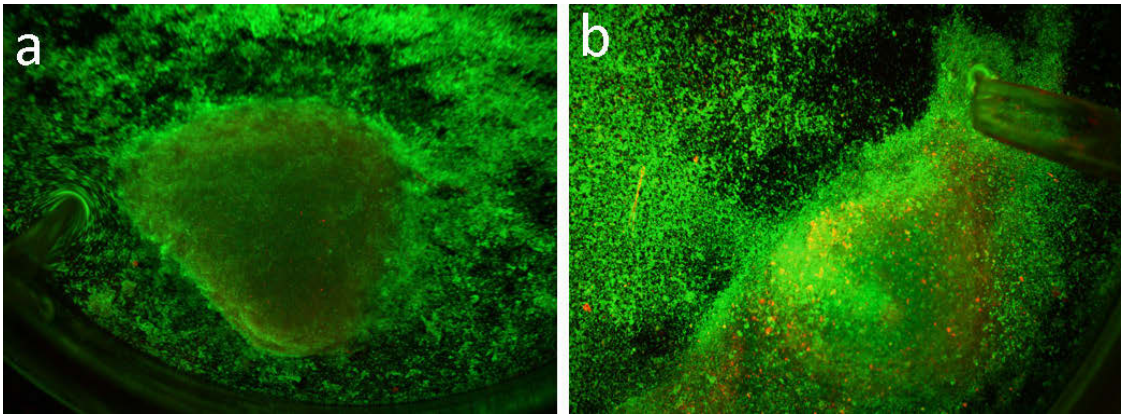

Figure 3.21. Live/dead assay of *in vitro* model. Overlaid fluorescent images of cells stained with calcein AM and ethidium homodimer after 2 hours of doxorubicin delivery via (a) a control non-gripping patch and (b) a theragripper.

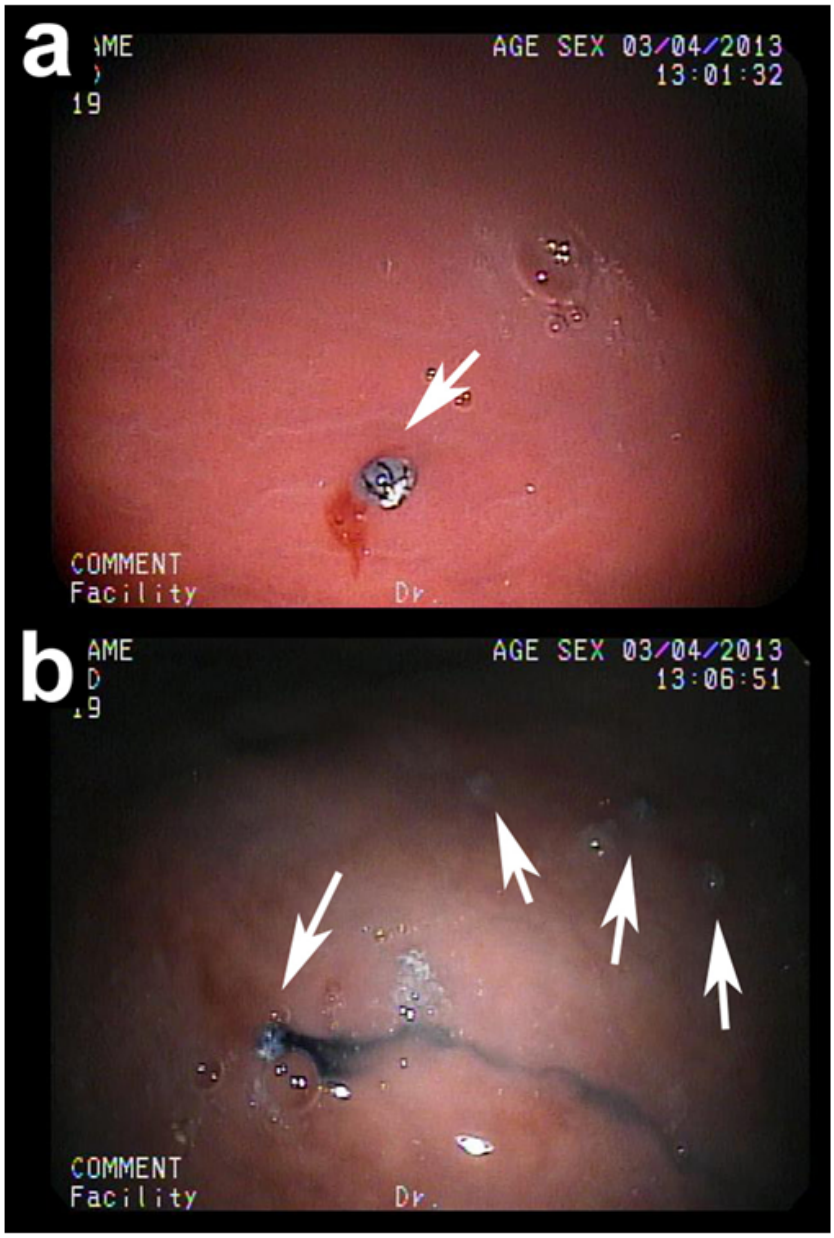

Figure 3.22. Endoscopic *in vivo* delivery of theragrippers to porcine stomach. Drug eluting grippers were loaded by absorption with a blue food dye and delivered to the stomach of a pig through an endoscope. (a,b) Representative grippers inside a porcine stomach containing a model drug (a) and eluting the drug (b). Arrows point to closed grippers throughout the stomach.

4 Microgrippers for defense applications

Self-folding metallic microtools also have applications in the defense world. "Smart" wireless microgrippers and other self-folding devices can fulfill the military and intelligence need for smaller, lighter, and lower power reconnaissance modules. In the following sections, self-folding microtools are demonstrated as remote surveillance devices for tagging, tracking, and locating and as programmable matter. Chemical, thermal, and laser-based actuation schemes are used to show alternatives to the more traditional electrical actuation of MEMS devices. These schemes enable these devices to respond to their environment, actuate wirelessly, and with low to no power requirements.

4.1 Tetherless microgrippers with transponder tags*

There is a pressing need for the development of "smart", wireless microscale devices for a variety of applications in security and defense[246], medicine[247, 248], remote surveillance[249] and distributed networks[250]. These devices typically require a variety of functionalities for imaging, communication, logic/memory processing, sensing, and actuation. Functional modules are often fabricated using varied processes (e.g. MEMS, CMOS, soft-lithography) and may come from a variety of different foundries, post-fabrication methods are needed to enable wafer-scale assembly in a parallel manner to create multi-functional devices. On the macroscale, robotic pick-and-place can be used to align and attach parts to specific devices on wafers. However, this serial procedure becomes increasingly difficult at sub-mm length scales[1]. Self-assembly has emerged as an attractive method to achieve heterogeneous wafer-scale integration in a highly parallel, scalable and cost-effective manner[251-256]. It can also be applied to a variety of functional

*Portions reprinted, with permission, from K. E. Laflin, C. J. Morris, N. Bassik, M. Jamal, D. H. Gracias, Tetherless microgrippers with transponder tags, IEEE/ASME Journal of Microelectromechanical Systems (JMEMS) 20, 2, 505-511 (2011). © 2011 IEEE.

modules including Si-based, polymeric, or other inorganic-based modules. Of the various forces that have been used to direct such assembly, molten-solder-based assembly using capillary forces[1, 252, 254, 255] is especially attractive for heterogeneous integration because solder is electrically conductive, has high surface tension when molten, and has considerable mechanical strength when solidified. Additionally, solder can be deposited by vapor deposition, electrodeposition, or dip-coating[252, 254, 255, 257]. Moreover, molten solder preferentially wets metallic surfaces as compared to Si or polymeric surfaces; hence molten solder can be localized in specific surface regions to direct assembly of devices to those regions[252, 254, 255].

4.1.1 Microgripper fabrication

Grippers were fabricated in the shape of a hand with rigid segments and flexible hinges[84]. The hinges were composed of a thin film metallic chromium (Cr) / gold (Au) bilayer[258]. Hinge bending is driven by the release of differential stress between the stressed Cr and unstressed Au layers. This bilayer was stabilized with a third rigid polymer layer to prevent spontaneous closing. In principle, a variety of polymers could serve as triggers for different events. The grippers were released from the wafer by dissolving a sacrificial layer. When the rigid polymer layer was softened or dissolved by exposure to heat or specific chemicals, each of the Cr/Au bilayer hinges bent, allowing the fingers of the grippers to close.

Figure 4.1 shows our fabrication scheme and integration approach. We deposited 77 nm of Cr and 300 nm of Au on a 250-nm-thick copper (Cu) sacrificial layer using thermal evaporation, and patterned the Cr and Au layers via lift-off[84, 258]. We electrodeposited 5-μm-thick Au to define rigid gripper segments, and electrodeposited an

additional 1 μm of Cu on top of the Au in a 500 μm squared pattern at the center of each gripper. Grippers were also fabricated with 1-μm-thick ferromagnetic nickel (Ni) segments with an additional step of electrodeposition prior to Cu electrodeposition. Leaving the photoresist (SPR-220 7.0, Microchem) intact, we dip-coated each wafer in a Bi-Pb-In-Sn-Cd solder alloy (melting point 47ºC, Indium Corporation), following methods outlined in [255] with a 15% ethylene glycol/water mixture (v/v) floating over the solder. The resulting solder bond pads were approximately 90 μm high at their peak. Finally, we patterned 3-μm-thick Shipley 1827 photoresist (Microchem) to serve as the polymer trigger on top of the metal bilayer hinges between each of the rigid segments, as shown in **Figures 4.1 a and 4.1 b**. It should be noted that alternate polymer triggers can also be used to enable a closing response to different chemical or thermal environments.

4.1.2 Integration of microtransponder tags and applications

To maximize the functionality of these microgrippers, we explored the potential of assembling microelectronic devices onto the backs of the microgrippers. A large number of functionalities (e.g. logic/memory, RFID, CMOS imagers) are fabricated using Si-based foundry processing. In order to show applicability of attaching commercial device chips, we demonstrated assembly of silicon-based RFID-like microtransponders onto the grippers. Transponder tags such as RFID's enable remote data acquisition in a variety of applications, including the tracking of retail products, equipment, animals, people, and waste; authentication of people or products; contactless payment for mobile phones and toll booths; and access management for public transportation or buildings. The size of RFID's is typically limited by an antenna which governs read distance; for example, Hitachi produces a 50 μm x 50 μm sized RFID chip which is sold with a

significantly larger cm-sized antenna [259]. We utilized transponder chips which have all their transponder components housed within a 500 μm square chip. These microtransponders are similar to RFID's in that they can transmit their unique identification number to an ID reader; however, they do not actually use RF power to accomplish this task. They are instead powered by light emanating from a laser diode on the ID reader, allowing transponder miniaturization to the sub-millimeter scale. This size, although easily incorporated into our grippers, limits the read distance to roughly 5 mm.

These commercial transponder chips have been utilized in applications in the pharmaceutical industry and behavioral biology fields. For example, Robinson et al.[260] glued these same transponder tags to ants to study individual behavior. Their application highlights the need for a small transponder-based tag that can be securely attached. While it is relatively straightforward to glue large tags onto large items, attachment of small tags presents a significant challenge, especially if it needs to be achieved in a parallel and cost-effective manner. Although gluing was effective in the previous demonstration, it was achieved in a serial manner and required three to six hours for the glue to fully harden. Smart gripping devices could enable the secure attachment of microscale transponders as an alternative to gluing, implantation, and other serial integration methods.

4.1.3 Silicon chip and transponder fabrication and assembly

We prepared diced Si chips by first bonding one Si chip wafer to a Si carrier wafer with Crystalbond™ 509 (SPI Supplies). We then diced only the chip wafer into square sections in the size range of 250-500 μm squares using a Disco DAD320 dicing saw and an NBC-ZH 2050-SE27HAAA saw blade. We diced partially through the chip

wafer, leaving approximately 100 μm of the chip wafer intact and still bonded to the carrier wafer. The carrier wafer was then removed by dissolving the CrystalbondTM layer with acetone. We then flipped the chip wafer over and remounted it to another carrier wafer using the same bonding method so that the diced side of the chip wafer was protected and the undiced side was exposed. We lapped this exposed side with 9 μm alumina (Al_2O_3) grit to thin it down from approximately 400 μm to 75 μm using a Logitech PM5 Precision Lapping Machine, thereby exposing the trenches created by the previous dicing step. We then sputtered 20 nm of titanium (Ti) and 200 nm of Au onto the diced chip wafer, still bonded to the carrier wafer, to define a bonding pad for solder assembly. Finally, we released the diced chips from the carrier wafer in acetone.

Commercial transponder tags from PharmaSeq, Inc. (Fort Monmouth, NJ) were diced and prepared for assembly in a similar method. The commercial wafer had dimensions of 2 cm by 2 cm and contained 1024 microtransponders. Each transponder chip wafer had been previously thinned to 100 μm, polished, and passivated with silicon nitride by PharmaSeq to protect the devices from further processing steps. We bonded the transponder chip wafer, device-side down, to a carrier wafer with CrystalbondTM 509 and lapped roughly 25 microns with 9 μm Al_2O_3 grit to roughen the back of the transponder chip wafer (9-27 μm roughness by optical profilometry). We then sputtered Ti and Au on the back of the transponder chip wafer and released it from its carrier wafer. We re-bonded the transponder chip wafer with the devices exposed (in order to visualize individual transponder chips), and diced the wafer to separate the transponders from each other. Finally, we released individual transponder chips from the carrier wafer in acetone.

Laser cutting may also be an appropriate technique for creating diced chips, with possible advantages in precision and speed. The technique may also reduce the number of carrier wafer bonding steps. However, we utilized conventional dicing because these tools are widely available.

After gripper fabrication, we achieved wafer scale assembly of the diced Si chips onto the grippers. Assembly of the chips was done after gripper fabrication but prior to sacrificial layer dissolution and gripper release. The addition of a low melting point solder pad in the center of the gripper provided a site for the adhesion of a metalized chip. The chips were self-assembled onto the grippers using capillary forces from the molten solder and were attached due to the minimization of solder interfacial energy[255]. The sequential position of this step was important. If the assembly were done after release of the grippers from the wafer, grippers would close in the hot assembly solution. Alternatively, if this assembly step were done earlier, prior to gripper hinge patterning, the 75-100 μm thick chips would introduce significant topography, impeding resist spinning and photolithographic alignment. Additionally, the assembly step was achieved in relatively mild solutions so as to not dissolve or degrade the polymer hinges prior to use.

To accomplish the assembly, we placed the chips in a glass vial with 20 mL of water and 500 μL of acetic acid and heated the liquid to 65˚C. Once the liquid was at the desired temperature, we added a section of the gripper-patterned wafer to the vial. The chips were swirled around the upward facing tilted wafer and allowed to settle onto the gripper-patterned wafer, and then shaken down the face of the wafer. This process was repeated for two minutes. Incorrectly assembled chips, such as multiple chips attaching to

a single bond pad, were removed by tapping the jar. The gripper-patterned wafer piece with attached chips was removed and rinsed with cool deionized water **(Figure 4.1 c)**.

After assembly, we released the grippers with attached chips from the wafer by dissolving the Cu sacrificial layer in an 8% ferric chloride solution **(Figure 4.1 d)**. Grippers with integrated chips were stored in water. These tetherless grippers could then be actuated in liquid or air in response to heat or several organic chemicals **(Figure 4.1 e)**.

4.1.4 Solder dipping and self assembly yield

Capillary forces from the molten solder alloy adhesion pad directed the self-assembly of the Si-based and commercial transponder chips by enabling bonding of the metalized side of the chips to the solder pad on each unreleased gripper, as shown in **Figure 4.2**. Solder dip-coating yields averaged 68% over 14 full wafers of medium- and large-sized grippers and were dependent on the type of metal used for the bonding pad, type of solvent, and solution temperature. Dip-coating yield was defined as the ratio of the number of solder-coated bond pads to the total number of bond pads. We observed yields of approximately 60% with the use of either Au or Cu as the bond pad metal. Yields as high as 99% were observed for bond pads coated with both Cu and Au.

Yields were highest in an aqueous solution of ethylene glycol (EG, 15% v/v) whose pH was adjusted to 2 using hydrochloric acid (HCl). EG enhanced the solubility of salt byproducts during HCl cleaning, but a higher concentration of EG tended to dissolve the photoresist. The ideal dip-coating temperature was 10-15˚C above the melting temperature of the solder which was approximately 60-65˚C in our case. This temperature ensured complete solder melting without adverse effects on the photoresist.

Additionally, we were careful to remove the wafer slowly from the solder to ensure equilibrium wetting and a relatively uniform solder volume on each bond pad.

After bond pads were coated with solder by dip-coating, chips were assembled onto these bond pads. Chip assembly yield, defined as the ratio of the number of bond pads with assembled chips compared to the total number of solder bond pads, averaged 78% with yields as high as 93% observed. The average assembly was based on six full wafers, two half wafer sections, and nine quarter wafer sections. In general, smaller wafer sections had a higher yield due to higher parts-to-bonding-site ratios.

The assembly yield was dependent on the chip assembly conditions, including the fluid temperature, type of agitation, and chip concentration. We obtained assemblies with the highest yields using a temperature approximately 10-15˚C above the melting point of the solder. Additionally, a high part-to-binding-site ratio (2000 chips to 50-100 sites) was necessary for optimal yields. Minimization of the solder interfacial energy helped secure and attach chips at the center of each gripper.

We also observed alignment and tilt defects at the lower assembly temperatures and shorter assembly times required by our process. Higher temperatures or longer self-assembly times resulted in further energy minimization and therefore self-alignment, but also led to a degraded polymer material needed for eventual actuation of the gripper hinges.

We found that the use of chips larger than the bond pad caused poor alignment, while the use of smaller-sized chips often caused multiple chips to assemble onto a single bond pad. Similarly-sized chips and bond pads were ideal. Additionally, a large amount of solder on the bond pad led to significant tilt relative to the substrate. However, it

should be noted that the functionality of the integrated gripper-transponder system was tolerant of these tilt and alignment defects, so the minimization of these types of defects was not critical.

The order of steps during dicing of the chips and back-side metallization significantly affected chip assembly yields. Lapping the parts created a microscale level of surface roughness on the back of the chips, which is known to enhance capillary-force-driven wetting and spreading[257]. It was also important to metalize the back-side of the chips after dicing (as opposed to before), which allowed metal to also deposit on portions of the thin sidewalls on each chip. The presence of this metal (Ti and Au) is confirmed in **Figure 4.3**. The figure inset also shows small metallic curls that formed from residual metal deposited between the diced chips, a feature only present when we performed the metal deposition step last. Surprisingly, the presence of the additional metal had a large effect on observed yield. When we carried out metallization before dicing, as we did for the commercial transponder chips, self-assembly yields were between 0% and 5%. If laser cutting were used for this application, it would still be necessary to generate rough metallic edges during cutting, which enhance solder wetting after metallization.

Energy-dispersive X-ray spectroscopy (EDX) on the diced chip side walls, shown in **Figure 4.4**, also established that elements from the solder were present on the side walls following assembly. In addition to the dominant Au and Ti peaks, Bi, Pb, and Sn can be seen in the side wall EDX curve. Quantification of composition from the side wall EDX data did not yield significant levels of Bi or Pb, because the Au peak was so dominant; however their peaks are evident on the EDX curve. We believe these features

explain the difference in yield between the Si chips with metalized side walls and microtransponder chips without metalized side walls.

4.1.5 Microgripper actuation en masse

We demonstrated the actuation of grippers of varying sizes with both Si-based and transponder chips. The lower size limit of the grippers in this study was constrained by the size of the chips, but current studies indicate that gripper operation works at much smaller size scales, as small as 200 μm tip-to-tip. **Figure 4.5 a** shows numerous Si-chip-integrated grippers of three sizes after release from the wafer. It is important to note that these tetherless grippers remained flat and closed only on exposure to the appropriate thermal or chemical cue.

Upon exposure to a temperature greater than 40ºC, the grippers began to close en masse due to softening of the polymer trigger and release of the stress within the metallic bilayer hinge. In the experiment shown in **Figures 4.5 a and b**, the temperature of the water was raised from room temperature to 43ºC. In general, grippers closed faster in hotter water. Grippers also closed upon exposure to solvents such as acetone and isopropyl alcohol, indicating a chemo-mechanical response. As compared to thermal actuation, grippers closed in these liquids at a much faster rate, typically within a second.

In **Figure 4.5**, the large grippers are approximately 3.5 mm when open and 1 mm when closed, and contain a Si chip that is 600 μm by 600 μm. The medium-sized grippers are approximately 2.5 mm when open and 725 μm when closed, and contain a Si chip that is 600 μm by 600 μm. The smallest Si-chip-integrated grippers are approximately 1.6 mm when open and 450 μm when closed, and contain a 250 μm by 250 μm Si chip.

4.1.6 Tagging applications of transponder-integrated microgrippers

The integrated grippers are intended for multifunctional use wherein the chip provides advanced electronic or optical functionalities and the gripper provides secure attachment, triggered by a specific cue. Hence, the integrated gripper should be able to securely attach to small objects upon exposure to a particular thermal or chemical stimulus. On attachment, the chip needs to be well bonded to the gripper, and neither the chip nor the gripper should detach during actuation or subsequent mechanical agitation. In addition, it would be advantageous if the gripper actuation and attachment process were relatively benign and compatible with living organisms.

Figure 4.6 shows images of a microtransponder-integrated gripper attaching onto a single textile fiber placed in water, where the surrounding temperature was increased from 25°C to 43°C on a hotplate. After closing, the transponder remained attached to the back side of the gripper, and the gripper was securely attached to the fiber.

Integrated gripper actuation and attachment can also be achieved in air (**Figure 4.7 a-b**). Here, actuation onto woven textile fibers was triggered by shining a 250 watt halogen bulb heat lamp for roughly 10 minutes from a distance of approximately 10 cm away from the grippers. The temperature of the fibers surrounding the grippers was measured to be 65°C with an infrared probe. We attributed the longer heating time to the fact that the dense fibrous nature of this particular textile prevented complete folding. We verified that the ability of these grippers to attach to fibers was robust and that the grippers did not fall off with shaking.

To demonstrate gripping devices as an alternative to gluing for the attachment of transponder tags, as well as compatibility with living creatures, we closed a Si-chip-

integrated gripper around the bristles of a fall webworm caterpillar (Hyphantria cunea). The gripper was dropped onto the caterpillar in its open conformation and actuated with a 10 μL droplet of acetone that was dispensed using a micropipette. The gripper closed tightly around the small spiny bristles of the caterpillar, and the caterpillar continued crawling on the leaves and eating, as shown in **Figure 4.8**. It should be noted that these grippers have also previously been demonstrated to securely attach to clumps of cells[84], beads[84] and metal wires[261]. From our studies, we observed that attachment was secure. However, grippers were occasionally observed to fall off very thin objects such as the caterpillar bristles. In this case, the grippers did not break, but rather slid off the thin bristles.

After attachment, we verified functionality of the microtransponder-integrated gripper. The transponders were successfully identified by their unique identification numbers using the laser reader provided by PharmaSeq. This verification demonstrated that neither gripper nor transponder functionality was impaired during integration and actuation.

4.1.7 Conclusions

We have demonstrated a technique for the integration of chip-based devices onto thermo-chemically actuating grippers. The integration of Si-based chips onto the grippers is directed at enabling multi-functionality of gripping devices by providing capabilities for imaging, sensing, and communication. Our grippers can be fabricated in a range of sizes to accommodate varying microscale devices. The advantages of the integration scheme include parallel assembly and versatility in the types of functional modules that can be attached. We have shown that commercial unpackaged chips can be

attached to the grippers; hence it is conceivable that other modules such as solar sensors, photodiodes, charge-coupled device (CCD) imagers, light emitting diodes (LEDs), and logic and memory chips could also be commercially obtained and attached.

The grippers' chemo-mechanical actuation lends itself well to actuation en masse and event-based gripping. Here, the choice of polymer determines its sensitivity and selectivity to different thermal and chemical cues. For example, our laboratory has demonstrated elsewhere grippers that utilize biopolymer triggers and actuate on exposure to specific enzymes[85]. Hence, these grippers can be utilized for a variety of event-based cues of relevance to numerous security, defense, and medical applications.

During the application of these integrated grippers, I recognized that our traditional methods of actuation – thermal and chemical – presented challenges for air-based devices. The radiation of heat from a heat lamp, for example, is highly inefficient, with significant energy loss due to convection. Additionally, the ability of specific chemicals to dissolve or degrade the polymer hinge trigger is not conveyed to airborne chemicals or vapors. Thus, new mechanisms for efficient air-based actuation are needed to enable defense applications, many of which take place on land.

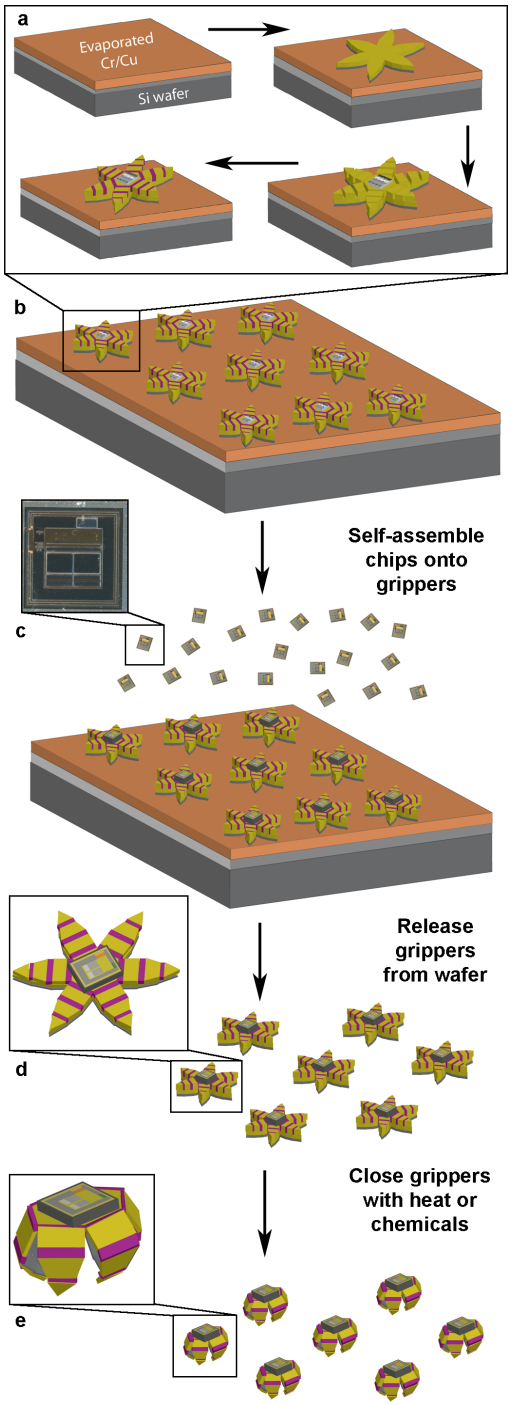

Figure 4.1. Fabrication scheme for grippers integrated with Si-based device chips. (a-b) Fabrication of the grippers with bond pads for chip attachment, (c) self-assembly of chips onto the bond pads, (d) release of integrated grippers from the substrate, and (e) actuation of the integrated grippers en masse.

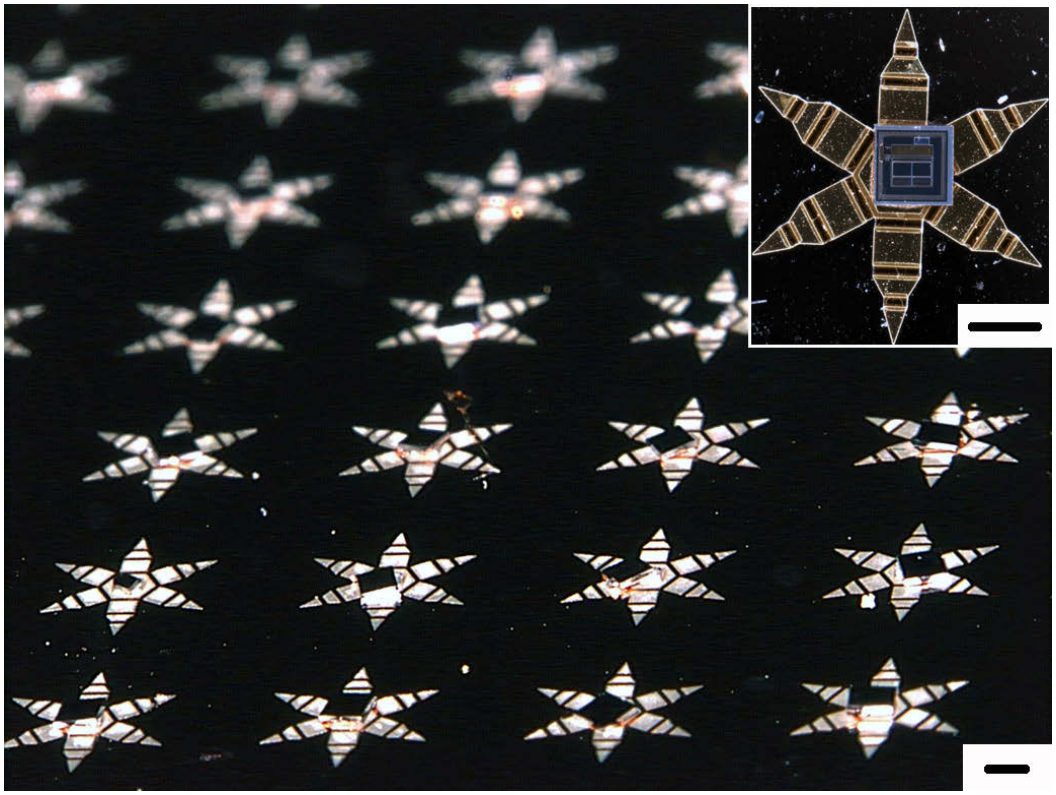

Figure 4.2. En masse self-assembly of Si chips onto grippers. Optical microscopy image of wafer scale assembly of unpatterned Si chips onto grippers. The inset shows an optical image of a commercial transponder tag attached onto a gripper. Scale bar is 500 μm.

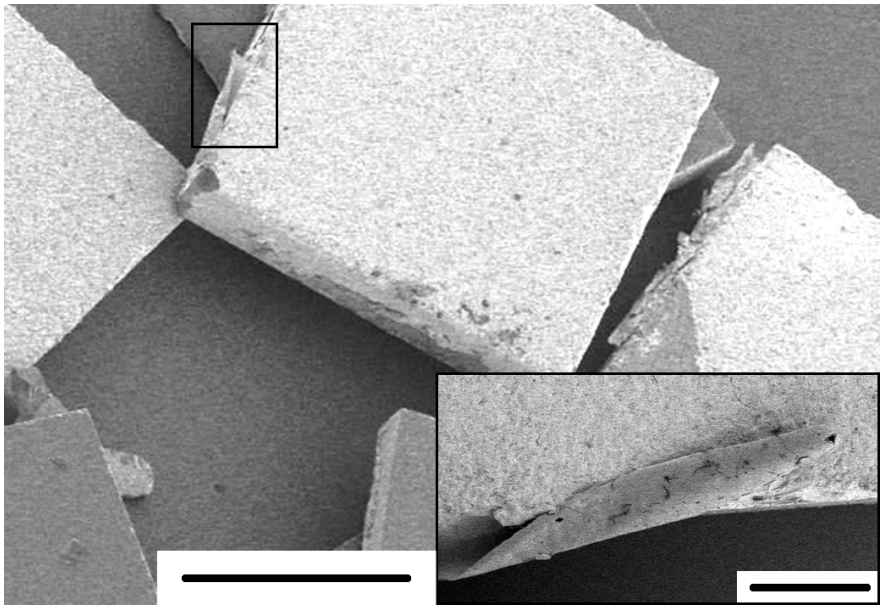

Figure 4.3. Side wall deposition improves assembly yield. SEM image of diced and metalized unpatterned Si chips showing metallization on side walls and residual metal curls, both which aid in assembly. The inset shows a zoomed SEM image of the metallic roughness on the edge of the chips. Scale bar is 300 μm; scale bar in inset is 50 μm.

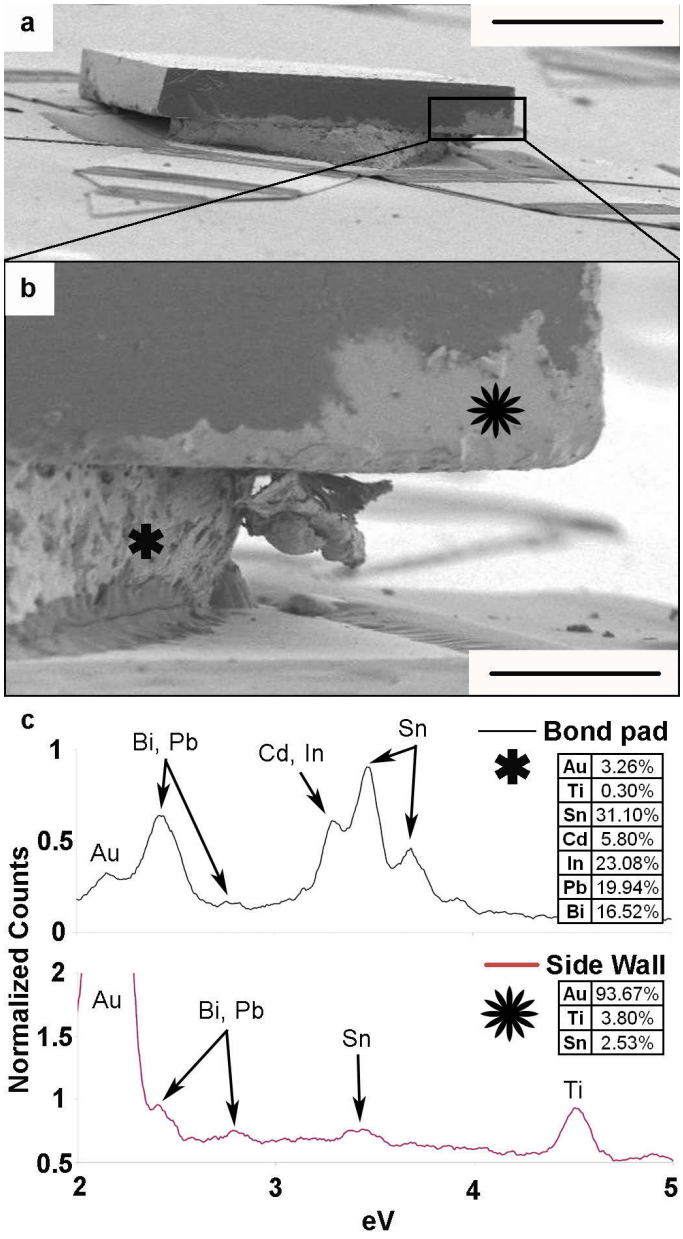

Figure 4.4. Analysis of side wall solder deposition. (a) SEM image of a chip-integrated gripper. An unpatterned Si chip sits on top of a solder bond pad attached to a gripper, (b) an inset of the chip showing metal deposited on the side wall, (c) the EDX analysis of the bond pad and metal deposited on the side wall. Scale bar is 250 μm in (a) and 50 μm in (b).

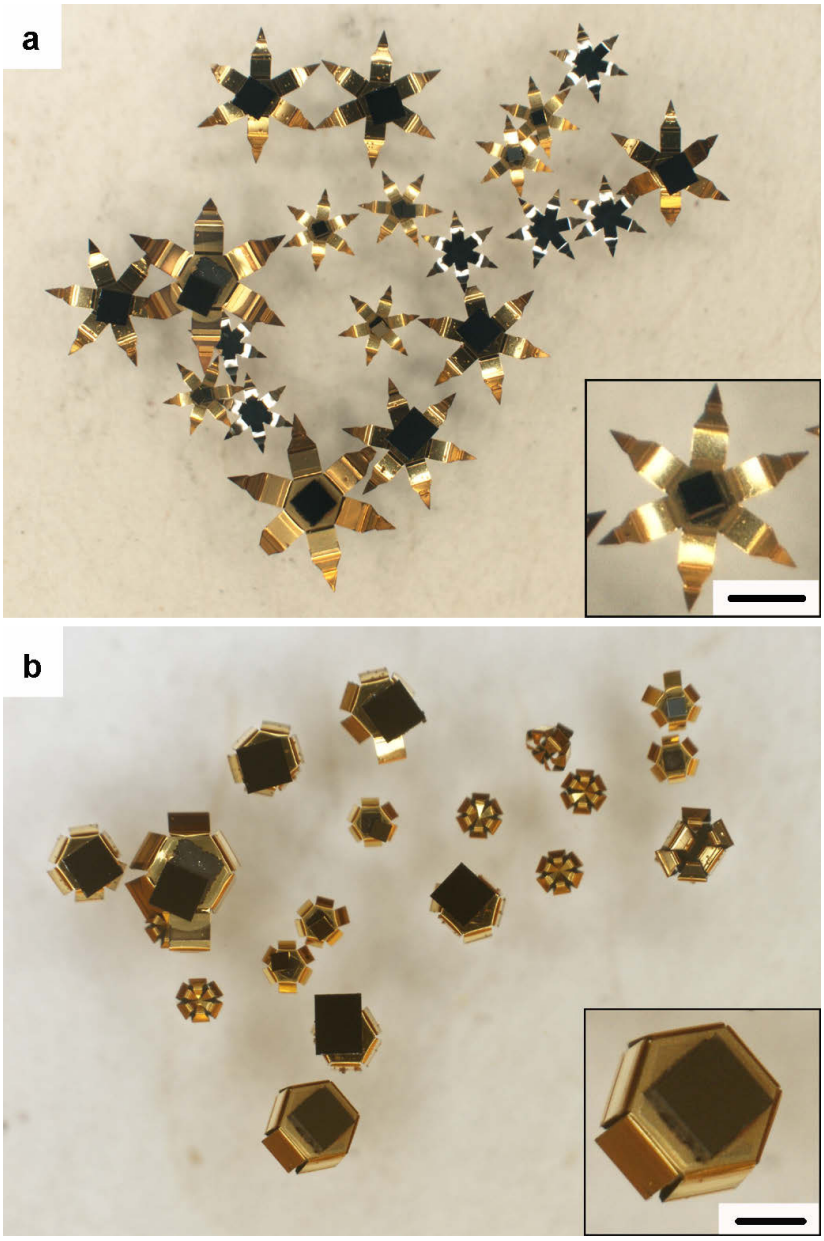

Figure 4.5. Si-chip integrated grippers before and after closing. Optical images and insets of (a) flat Si-chip-integrated grippers in water at room temperature and (b) closed grippers in water at 43ºC. Scale bars are 500 μm. Grippers remain flat and close only on heating; closing occurs en masse.

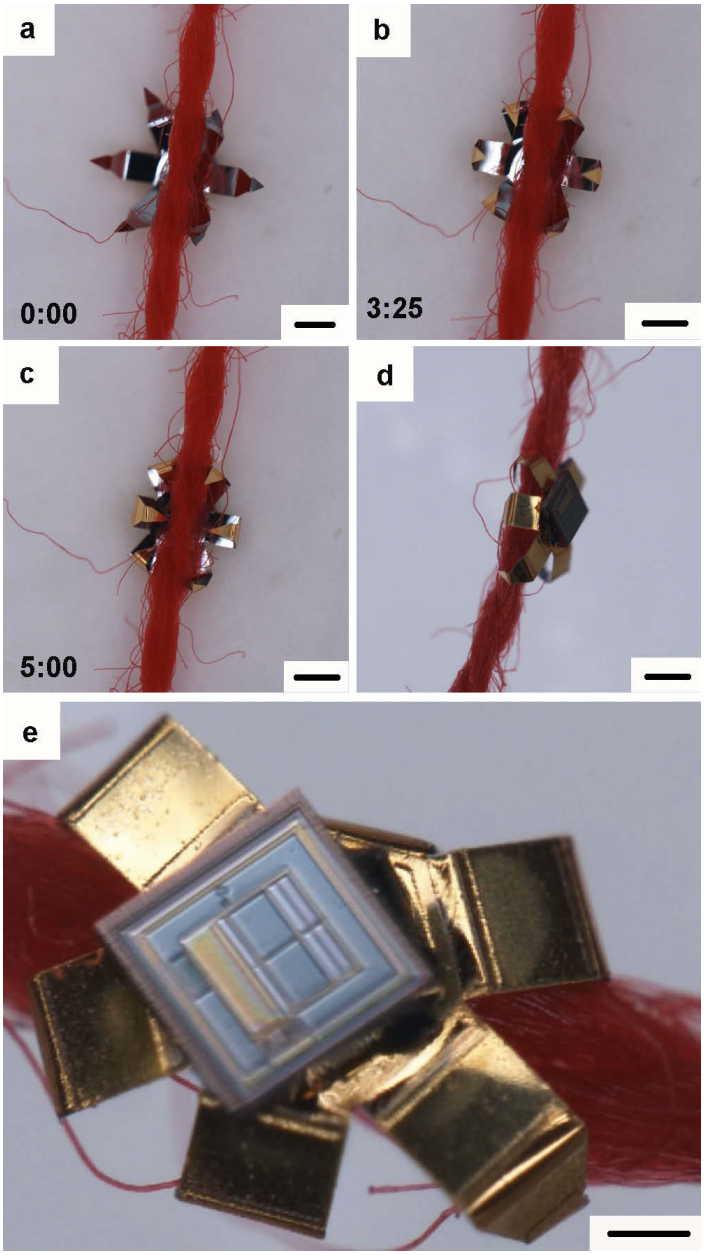

Figure 4.6. RFID gripper closing around a fiber. (a-c) Time lapse optical microscopy images of transponder-integrated gripper thermal actuation around a piece of string. The time is indicated in min:sec. The image in (d) shows gripper attachment from a different angle, (e) zoomed image showing the transponder. Scale bar in (a) – (d) is 500 μm and in (e) is 250 μm.

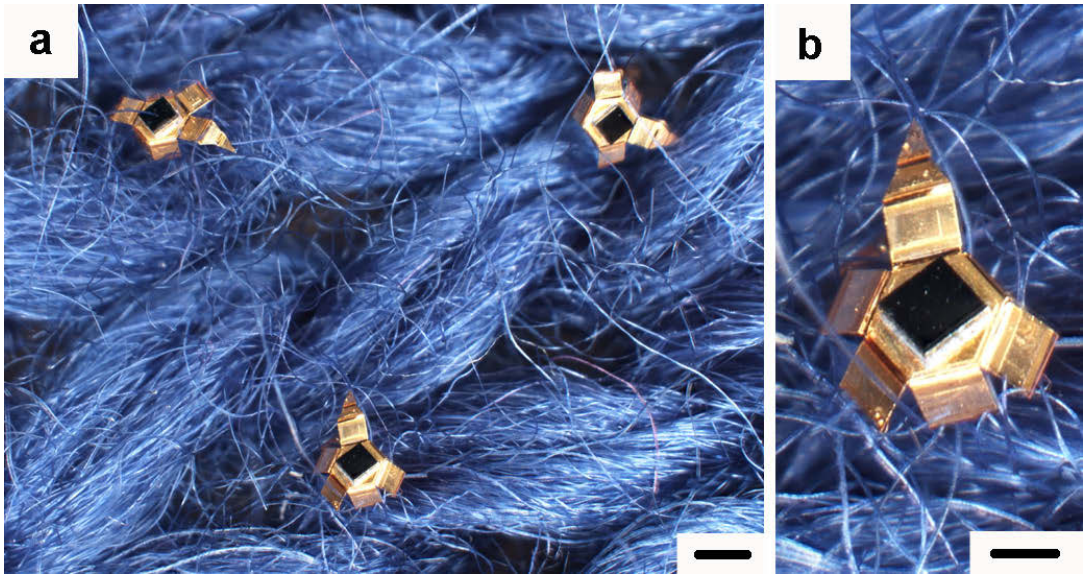

Figure 4.7. Si-chip integrated grippers closing onto a sweater. Optical microscopy image at different magnifications of Si-chip-integrated grippers thermally actuated on woven wool fibers. Scale bar is 1 mm in (a) and 500 μm in (b).

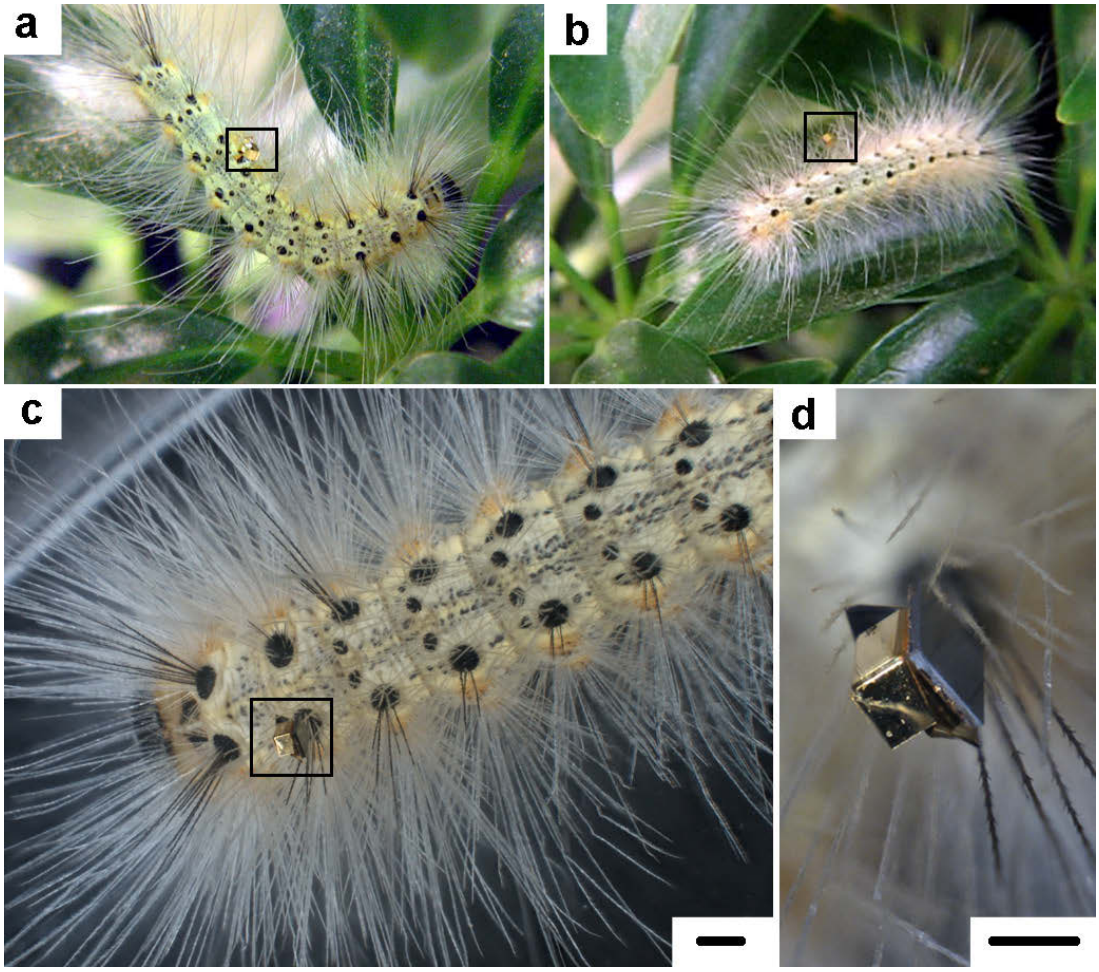

Figure 4.8. Si-chip integrated gripper closing onto a moving caterpillar. (a-b) Optical images of a webworm caterpillar crawling on a plant with attached Si-chip-integrated gripper, (c) optical microscopy image of a Si-chip-integrated gripper on caterpillar, (d) zoomed image of gripper on caterpillar bristles. Scale bar is 1 mm in (c) and 500 μm in (d).

4.2 Laser-triggered sequential folding of microstructures*

In my own work and in the literature, we see examples of how origami-inspired fabrication and actuation schemes provide a means to fold and consequently transform planar lithographically patterned structures into three-dimensional materials and devices in a highly parallel manner.[189, 262-264] While self-folding of somewhat complicated structures such as bi-directionally corrugated sheets[265] or truncated octahedra[266] can be achieved without precise control of folding pathways, sequential control of folding pathways is an essential feature of paper origami and would be needed for folding of more complex and especially nested structures. Further, the accurate and sequential control of folding has been shown to endow programmability.[267]

In order to fold a structure, energy is required to fold flat panels out of the plane, and as comprehensively reviewed by Leong et al.,[189] a variety of strategies has been utilized to enable hinged actuation for controlled folding at small size scales. I have discussed examples of electrical[262] and pneumatic[268] actuation, which allow sequential folding with high accuracy and specificity, but the structures need to be wired to external controls. I have also discussed the need for more efficient methods of actuation required for defense applications. Photothermal or laser-triggered actuation provides a wireless and efficient means to direct folding over large distances. Indeed, optically actuated folding has been achieved using shape memory[269] and other polymers,[270-272] thin metal films,[273] and carbon nanotubes.[39, 274-276] This actuation methodology has opened up applications on a variety of length scales such as force detection on the nanoscale,[39] to

*Portions reprinted with permission from "Laser triggered sequential folding of microstructures", **K. E. Laflin**, C. J. Morris, T. Muqueem, D. H. Gracias, *Applied Physics Letters* 101, 131901 (2012). Copyright 2012, AIP Publishing LLC.

the creation of split ring resonator arrays on the microscale[277] to reconfigurable medical devices on the macroscale.[269]

In some of these applications, however, photothermal actuation necessitated positioning and focusing the laser beam with mirrors or lenses resulting in hundreds to thousands of W/cm^2 for actuation.[270, 278, 279] In a number of defense and medical applications, there is a need to reduce energy consumption, evade detection, and improve portability and maneuverability.[100, 247, 280, 281] Hence, large and complex setups become less desirable and devices which rapidly respond with significant motion to low intensity irradiation via commercially available lasers would provide enhanced capabilities for surgical operations,[100, 247] robotics,[280, 281] and initiation of energetic materials.[282] Previously, we have shown how a polymer trigger on a pre-stressed metallic bilayer can be utilized to enable stimuli-responsive folding based on temperature[283] and chemicals including glucose[84] and enzymes.[85] Here, we demonstrate sequential folding of microstructures using low power laser irradiation, allowing long distance wireless actuation in air with high spatial specificity. Folding is achieved using commercially available hand-held lasers that are lightweight and portable, and require just AA batteries.

4.2.1 Materials and methods of fabrication and actuation

The intrinsic stress built into thin film hinges acts as the driving force for folding, as I have shown in previous devices like the metallic microgrippers used for biologic tissue sampling. The thin film hinges contain a layer of chromium (Cr) with high intrinsic stress and a layer of gold (Au) with low stress. This mismatch of stress along a common boundary causes bending of the hinges.[84] These Cr/Au bilayer hinges are patterned between thicker rigid segments, with multiple hinges on each structure that are used to

facilitate folding sequences. A polymer film is patterned atop each Cr/Au hinge and keeps it flat until the polymer film is heated by the laser and softened.

We fabricated the microstructures on silicon wafers using thermally evaporated copper (Cu, thickness = 100 nm) as a sacrificial layer. We used three steps of photolithography, the first to pattern thermally evaporated Cr/Au hinges **(Figure 4.9 a)**, the second to pattern electrodeposited rigid Au segments, and the third to pattern SC1827 photoresist (Microchem) triggers atop the bilayer hinges. The thicknesses of the different layers varied with size of the structures and desired folding angle, and were obtained using a multilayer thin film curvature model.[86] Structures were released from the substrate in 10% ferric chloride solution through dissolution of the Cu sacrificial layer. They were rinsed and stored in deionized (DI) water until use.

4.2.2 Characterization of laser-triggered actuation

We studied optical folding of microstructures ranging in size from 300 μm to 3 mm using two different hand-held lasers: a green laser (Wicked Lasers, 532 nm, 40mW, 1.5 mm beam diameter) and a near infrared laser (Freak lasers, 808 nm, 100 mW, 3 mm beam diameter). We observed that the microstructures folded when irradiated with either laser beam. We attributed bending of the hinge to heating of the polymer trigger above its T_g of approximately 40ºC, which we have measured in prior studies.[84] On heating, the polymer softens and no longer restrains the stressed Cr/Au bilayer resulting in spontaneous bending.[84] By varying the relative spatial length scale of irradiation as compared to the size of the microstructures, multiple or single integrated microstructures could be folded. Actuation could be tuned to specific size scales by focusing or broadening the laser beam to different diameters with a lens, providing the user

significant control over actuation. For example, upon irradiation with a spatially diffuse laser beam, multiple microgrippers integrated with 40 μm hinges were folded at once **(Figure 4.9 b)**. In contrast, relatively focused laser irradiation was used to fold individual microgrippers **(Figure 4.9 c)**. Hence, parallel or individual deployment of sensors or actuators can be achieved.

We were able to wirelessly fold devices up to three feet away and observed that the time scale of bending of a hinge varied between 67 milliseconds and 21 seconds, depending on wavelength and intensity of laser irradiation. We characterized laser-triggered folding using microgrippers (1.5 mm) and examining the effect of distance **(Figure 4.10 a)** and irradiance **(Figure 4.10 b)** on time-to-close using ten samples for each condition. Here, time-to-close ($\underline{t_c}$) was the time it took for each device to go from its open conformation to a visibly closed conformation, at which point all further folding and movement stopped. The initial time corresponded with the start of laser irradiation. We observed that t_c was directly proportional to d^2 **(Figure 4.10 a)** where d was the distance between the laser and the folding microstructure. We attributed this observation to the fact that t_c was inversely proportional to laser irradiance, following the empirical fit in **Figure 4.10 b** and our theoretical discussion below. Laser irradiance was also inversely proportional to d^2 due to divergence of the laser beam, resulting in an expected proportionality between t_c and d^2. Our observations suggest that lasers with low divergence could enable fast actuation even at larger actuation distances, which is particularly relevant for defense applications in hostile environments.

One of the highlights of optical actuation is the possibility to enable frequency selective actuation that can be facilitated by utilizing materials with different absorption

characteristics. Our method can be engineered to be frequency-selective with the appropriate selection of laser wavelength and irradiance, hinge metal, and hinge polymer trigger. In our system, the absorbance of both the gold metal31 and the polymer trigger material in the flexible hinges is significantly higher at 532 nm than at 808 nm **(Figure 4.11)**. Hence, lower irradiance is required, and faster folding is achieved using a 532 nm laser **(Figure 4.10 b)**. In the experiments used to obtain data shown in **Figure 4.10 b**, we irradiated an identically sized microgripper but varied the irradiance using neutral density filters (Thorlabs) mounted in front of each laser. Although both lasers were able to fold the grippers, the irradiance required to achieve a specific t_c, or indeed, any folding at all, varied significantly. For example, the 532 nm laser could close grippers at irradiances as low as 680mW/cm^2, but more than 2 W/cm^2 was needed with the 808 nm laser.

In our measurements of the dependence of t_c on irradiance I_r, we observed multiple regimes **(Figure 4.10 b)**. We observed a threshold irradiance below which no folding occurred, presumably due to insufficient heating of the polymer trigger. At intermediate irradiance, small decreases led to significantly slower folding times, likely due to heat loss via convection and conduction to the surrounding air as well as conduction to the substrate below. At larger irradiance, we observed an inverse relationship between t_c and I_r. To understand these regimes, we analytically and numerically modeled heat loss from the microgripper due to conduction into a surrounding air domain. Although each microgripper device was initially planar within a short distance from the microgripper surface, heat loss into the surrounding air rapidly approached that of a point source in spherical coordinates. We therefore approximated the microgripper surface from which heat was lost as a sphere with equivalent surface

area to obtain a solution for the steady state temperature rise at the surface ΔT_s. Starting with the heat equation in spherical coordinates, we set the time derivative to zero for the steady state solution.

$$\frac{\partial}{\partial r}\left(r^2 \frac{\partial T}{\partial r}\right) = 0 \tag{1}$$

We integrated this equation once and applied a boundary condition to solve for the constant of integration.

$$\frac{\partial T}{\partial r} = \frac{C_1}{r^2} \tag{2}$$

Using a boundary condition of r = 0 is not feasible, so we approximated a boundary condition at the external surface of a sphere with radius r_0 which has a surface area equivalent to the surface area of heat loss from the microgripper. We equated the area of this heat loss, A_{loss}, to the surface area of this equivalent sphere ($4\pi r_0^2$) and to the actual surface area of the gripper ($2 f_1 \pi R^2$), where f_1 is a fill factor relating the heat loss from a disc to the loss from the microgripper shape.

$$A_{loss} = 4\pi r_0^2 = 2 f_1 \pi R^2 \tag{3}$$

We equated the two areas and solved an expression for r_0 as

$$r_0 = R\sqrt{f_l / 2} \tag{4}$$

When the microgripper is illuminated with a laser with an irradiance of I_0, that heat is absorbed by the microgripper. Thus we modeled the heat loss from the gripper as coming from a point source at the center of the approximated sphere. At steady state, the power provided by the laser is equal to the heat lost from the gripper, where k is the thermal conductivity of air.

$$I_0 A_{abs} = -kA_{loss} \left. \frac{\partial T}{\partial r} \right|_{r=r_0} \tag{5}$$

We applied the previous definitions of surface area of the gripper from equation 3 and rearranged this derivative.

$$\left. \frac{\partial T}{\partial r} \right|_{r=r_0} = -\frac{I_0}{k} \frac{A_{abs}}{A_{loss}} = -\frac{I_0}{k} \frac{f_a \pi R^2}{2 f_l \pi R^2} = -\frac{I_0}{k} \frac{f_a}{2 f_l} \tag{6}$$

where f_a is another fill factor relating the absorption of energy by a disc to the absorption by the gripper. Heat is lost from both sides of the gripper but only absorbed by one side, hence the extra factor of 2 in the denominator of the equation. We then substituted equations 2 and 4 into equation 6 and solved for the constant of integration as:

$$\left. \frac{\partial T}{\partial r} \right|_{r=r_0} = -\frac{I_0}{k} \frac{f_a}{2 f_l} = \frac{2C_1}{f_1 R^2} \tag{7}$$

$$C_1 = -\frac{R^2 I_0 f_a}{4k} \tag{8}$$

We then substituted this equation for C_1 back into the original derivative and integrated.

$$T = \frac{R^2 I_0 f_a}{4kr} + C_2 \tag{9}$$

We solved for C_2 using the boundary condition of r approaching infinity, where $T = T_i$. We used equation 4 again to solve for the steady state temperature at the sphere's surface.

$$\Delta T_s = I_0 \frac{R}{k} \frac{f_a}{2\sqrt{2 f_l}} \tag{10}$$

We also numerically calculated the transient temperature response using a two-dimensional axisymmetric model in ANSYS (v13) for a variety of microgripper sizes and optical power levels, and consistently found calculated steady state microgripper surface temperature changes to be within 7.3% of those predicted by equation (10).

Each transient solution closely followed the exponential relationship, $\Delta T \approx \Delta T_s \left(1 - e^{-t/\tau}\right)$, with a time constant τ depending primarily on microgripper size. We obtained an expression for t_c corresponding to a closing temperature rise of ΔT_c by rearranging the exponential relationship and expressing the resulting natural logarithm as a Taylor series expansion.

$$t_c = -\tau \ln\left(1 - \frac{\Delta T_c}{\Delta T_s}\right) = -\tau\left[\left(\frac{\Delta T_c}{\Delta T_s}\right) - \frac{1}{2}\left(\frac{\Delta T_c}{\Delta T_s}\right)^2 + \frac{1}{3}\left(\frac{\Delta T_c}{\Delta T_s}\right)^3 - \ldots\right] \tag{11}$$

We dropped all higher order terms for $\Delta T_c \ll \Delta T_s$, and substituted ΔT_s from equation (10);

$$t_c \approx \tau \Delta T_c \frac{2k\sqrt{2f_l}}{f_a R I_0} \tag{12}$$

Assuming that I_0 is directly proportional to I_r, equation (12) correctly predicts the $1/I_r$ behavior observed at higher laser irradiances. We also used the empirical power law fit for the 532 nm source in Fig. 2b, the assumption that I_0 was precisely 15% of the applied irradiance[284], a numerically calculated value for τ, and equation (12) to calculate an average ΔT_c of 46°C. This result corresponds to an average closing temperature of 69°C for an initial room temperature of 23°C, which is consistent with past observations of microgripper closure between 40 and 95°C.[84] Although more accurate calculations would require a more detailed knowledge of the relationship between I_0 and I_r, and validation with actual measured values for ΔT_c, the approximated equations (10) and (12) are useful to estimate folding temperatures and times in different environments.

4.2.3 Sequential folding of unique devices and hinges

One major advantage of laser-triggered actuation is the high precision achieved by spatial control over folding. Consequently, by directing a laser beam at individual hinges, it is possible to sequentially fold structures as might be required in reconfigurable systems[285] or programmable matter.[267] We were able to sequentially fold individual arms of a four-membered structure **(Figure 4.12)**. Even though we utilized lasers to heat the hinges, it is noteworthy that laser intensity could be adjusted so that heating of spatially separated hinges can be localized, such that triggering one hinge does not trigger adjacent hinges.

As further demonstration of control over devices, we fabricated sequentially folded, nested three-dimensional (3D) patterned cubes **(Figure 4.13)**. A small, uniquely patterned cruciform was placed in the interior of a larger patterned cruciform. The 40 mW, 532-nm laser-triggered folding of the smaller cruciform without folding the larger one. Subsequently, the same laser was used to trigger folding of each face of the larger cruciform around the already folded smaller cube, creating two nested cubes. This high precision demonstration of sequential folding on two size scales highlights considerable user control over the complexity of structures that can be fabricated via laser-triggered actuation. Such nested structures are reminiscent of vesosomes[286] and cellular organelles offering the possibility for spatially sequestered functional modalities or chemicals within a single package such as would be required in cascading reactions. The possibility for unique functionality is enhanced by the ability to pre-pattern such structures in many different shapes[188] with specific pores or circuits using basic lithographic techniques prior to assembling them into complex nested devices. Further, metallic structures function as micro-Faraday cages and could be used to protect, for instance, highly sensitive electromagnetic devices from noisy environments.

4.2.4 Conclusions

In summary, this work demonstrates the sequential, wireless, low power laser-triggered folding of microstructures. Precisely focused heating afforded by laser actuation allows for sequential, spatially controlled folding, which is a key development especially for defense and robotics applications. Collimated light produced by lasers can theoretically actuate devices at large distances with similarly precise spatial control. The microdevices demonstrated in this work can be utilized in defense applications such as

the remote initiation of energetic materials,[282] which have been demonstrated as microthrusters in robotics,[287] and in the attachment of transponder tags or other electronics to various surfaces[288]. Compatibility of the fabrication process with planar lithographic methods offers the possibility for integration of logic/memory circuits, sensors, transponder tags and optical modules such as light emitting diodes (LEDs) for even greater functionality.

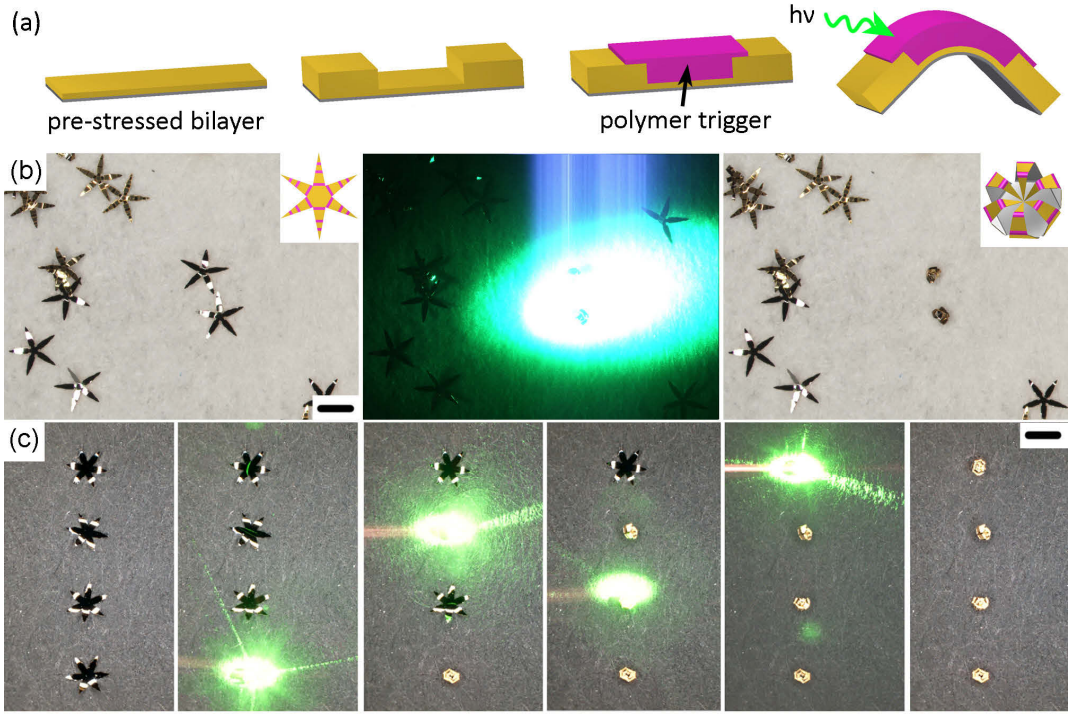

Figure 4.9. Conceptual schematic and experimental realization of laser actuated folding. (a) Schematic showing the fabrication scheme for the microstructures. Flexible Cr/Au bilayer hinges alternate with rigid Au segments. A polymer trigger is patterned atop the flexible hinges. Bending occurs when the polymer is softened on heating by laser irradiation. (b), (c) Optical microscopy images of a 532 nm laser inducing folding of microstructures. Actuation at different scales is possible by focusing or broadening the laser spot. (b) Multiple microgrippers are closed at once by a laser beam. Scale bar is 500 μm. Insets show schematics of open and closed grippers. (c) Individual microgrippers are closed sequentially. Scale bar is 1 mm.

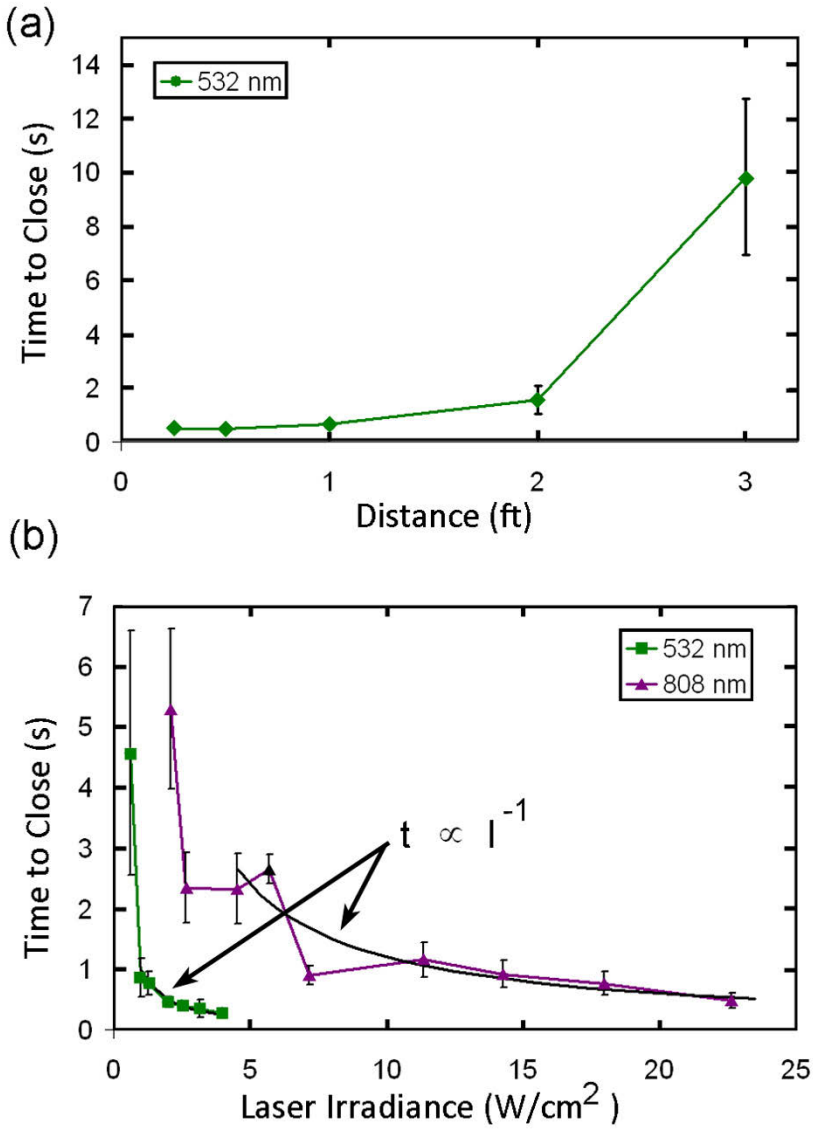

Figure 4.10. Characterization of laser-triggered folding of microdevices. (a) Graph showing the time to close t_c versus distance of the laser from the microstructure, d. (b) Graph showing t_c versus laser irradiance (I_r), from a visible (green diamonds) and near-IR (purple triangles) laser.

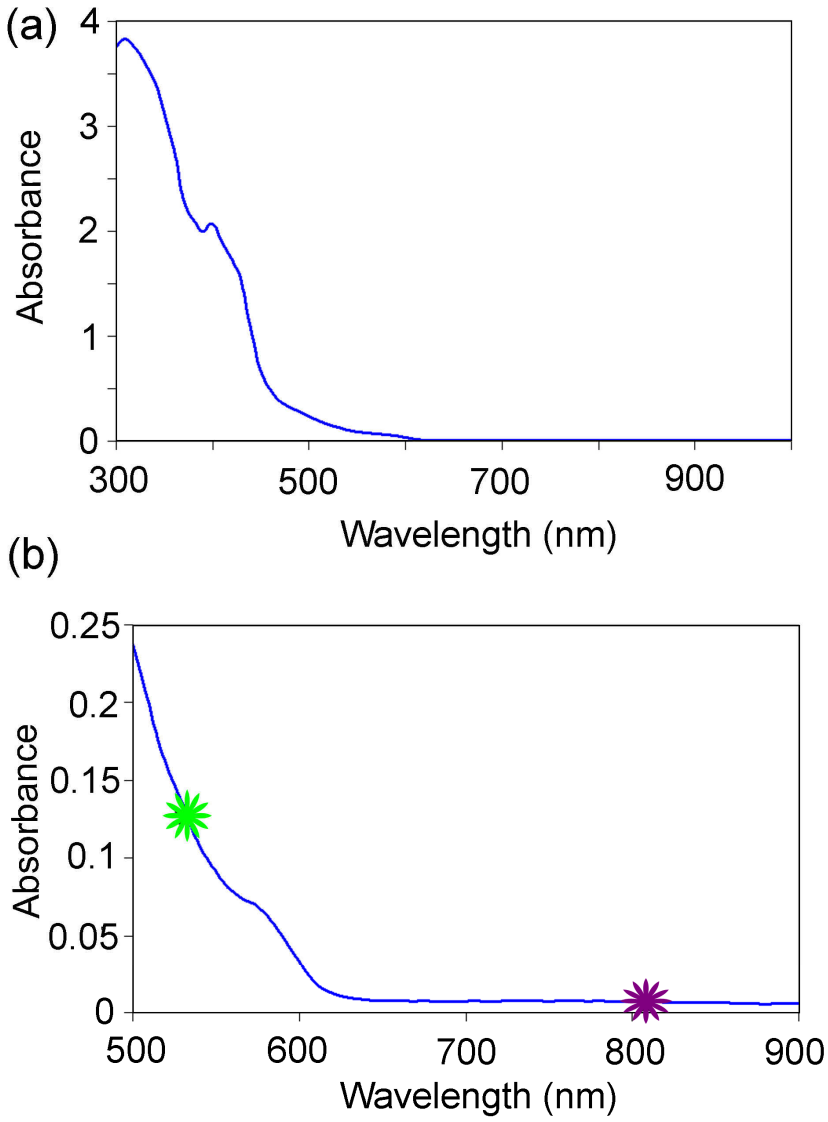

Figure 4.11. Polymer hinge trigger absorbance. (a) Graph of the absorbance spectrum of the polymer trigger as a function of wavelength. (b) Graph of the absorbance spectrum of the polymer trigger, zoomed into the relevant wavelengths for our lasers. The green star indicates the absorbance of the 532 nm laser. The purple star indicates the absorbance of the 808 nm laser. Absorbance measurements were done using a Spectramax Plus 384 microplate spectrophotometer (Molecular Probes).

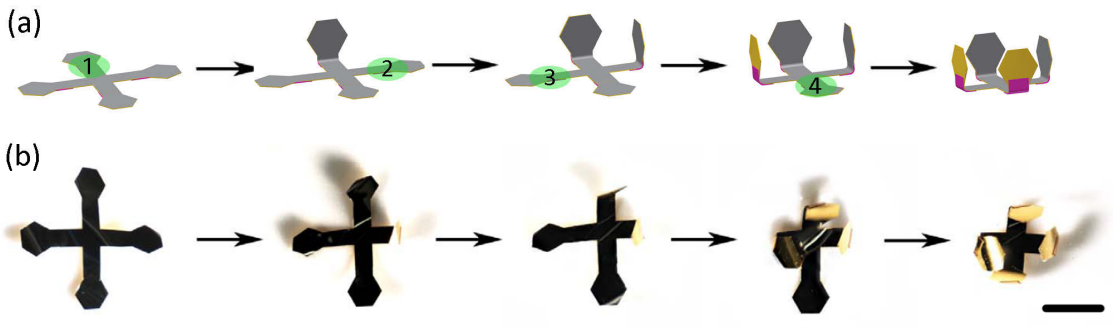

Figure 4.12. Sequential folding with spatial control. (a) Schematic of a four-membered structure folded sequentially. (b) Optical microscopy images of sequential actuation of individual hinges within a single four-membered structure using a 532 nm laser. Scale bar is 1 mm.

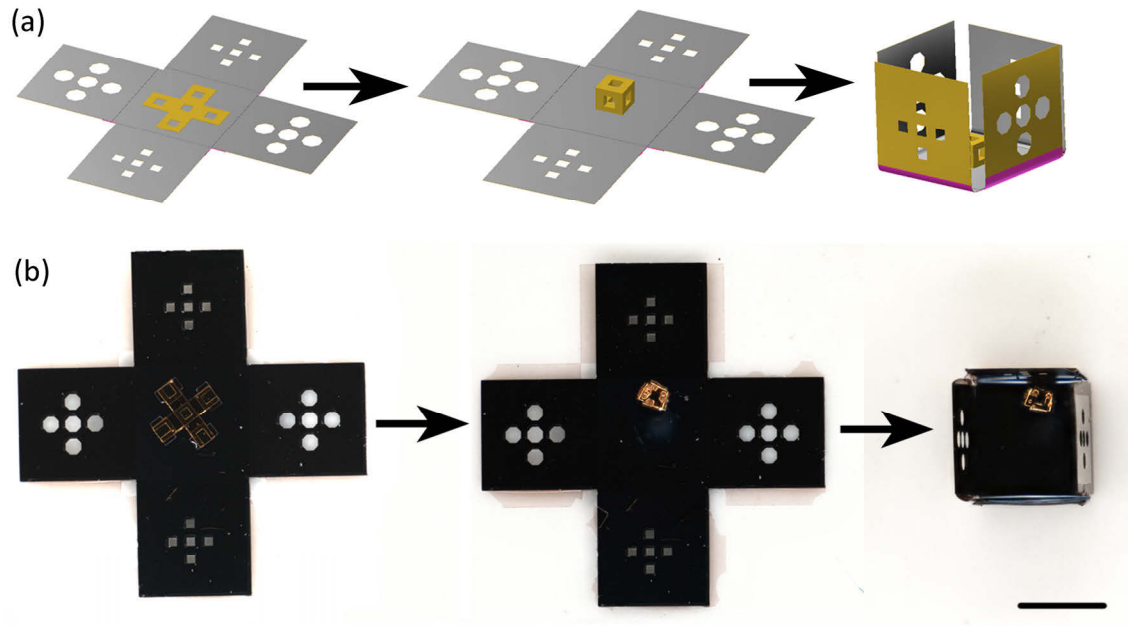

Figure 4.13. Sequential folding of nested cubes. (a) Schematic and (b) optical microscopy images of the sequential folding of two patterned cruciforms into nested cubes, triggered by a low power 532-nm laser. Scale bar is 1 mm.

5 Conclusions

In this thesis, I have demonstrated how stimuli-responsive microtools can be applied to both biomedical and defense applications. In both applications, these tools enable a paradigm shift from one-tool-per-task to a statistical approach. By utilizing many tiny tools, either to collect hundreds of tissue samples for cancer detection or to tag and track a target, the likelihood of achieving our goal are improved. The wireless control of these devices further facilitates their application. This feature allows these tools to wend through narrow conduits of the body, unhindered. It also allows for remote surveillance and covert tagging of targets, keeping soldiers out of harm's way. Because they contain all of the energy necessary for actuation in their hinges, there is no need for a bulky battery or large antenna; thus there is little limiting their miniaturization. Additionally, their stimuli-responsiveness targets their action towards a specific condition or event, increasing their specificity. Their wide application in surgery, drug delivery, tagging and tracking, and programmable matter is a testament to their versatility.

For surgical applications, we demonstrated *in vivo* biopsies of tissue clumps within the GI tract. These tools enable a statistical sampling of a large-area organ, where hundreds of small samples can more effectively detect small lesions as compared to a few large samples taken by the standard biopsy forceps. We developed new material combinations to further miniaturize these grippers for the capture of single cells, with both *in vivo* and *in vitro* applications.

We demonstrated these grippers as drug delivery devices, with the site-specific controlled release of commercial drugs for inflammatory bowel disease and cancer from the polymer layers of the grippers. These therapeutic grippers showed an advantageous

biphasic release pattern, with the potential for quick release to achieve the therapeutic dose paired with slow release to maintain the dose.

For defense applications, microelectronics were integrated onto the grippers for enhanced remote surveillance. These devices are a significant improvement over the large, bulky devices used currently for tagging, tracking, and locating. Their ability to autonomously grip onto hair, clothing, and moving targets is of considerable importance to the intelligence community. The actuation of such devices with lasers is also an improvement for long range robotics and actuation.

The challenges are still great, however, for micro- and nanoscale tools. Specificity and sensitivity are critical to the success of such tools. For biomedical applications, greater specificity could allow the targeting of certain cells or tissues. The ability to seek out and destroy cancer cells, for example, before they grow beyond a single cell would be a huge step towards cancer prevention. Antibodies and enzymes are among the most specific biological and chemical targeting mechanisms and could be incorporated onto the surface, used in an actuation mechanism, or released from within these or other microscale devices. For tagging, tracking, and locating and other covert reconnaissance applications, specificity is also critical. While an operator recognizes a target by sight, the ability to detect targets by other means is desirable. For example, a device that could detect and target specific biological or chemical warfare agents could help national security identify both dangerous equipment and personnel.

Similarly, sensitivity is of utmost importance for the future employment of microscale tools. Sensitivity and specificity go hand in hand because many of the chemicals we wish to sense appear in parts per million (ppm) and parts per billion (ppb)

concentrations in the body and in the air. These devices need both attributes to successful achieve more effective targeting.

For biomedical applications, biocompatibility of materials continues to be a challenge. Our microscale tools are appropriate for use in the GI tract due to the high clearance rate of mucus in the body. However, biocompatible and biodegradable materials that cause no imflammatory or immune response are necessary to move truly inside the body and to gain the confidence of doctors and patients. Many materials currently under investigation, including NIPAM and other polymers, quantum dots, and metallic nanoparticles do not meet these requirements. Significant advances in materials science are required to retain the benefits of these materials while enhancing their biocompatibility.

As miniaturized devices play a “bigger” role in technology and our modern lives, we as engineers and scientists need to consider seriously the limitations of current fabrication methods, actuation mechanisms, materials, and power sources. Novel micro- and nanoscale devices will be built from even smaller components like DNA, utilizing bottom-up fabrication schemes such as self-assembly, and will need to gather energy from and respond to conditions in the environment around them. While this challenge is a great one, the reward is equally great.

6 References

[1] C. J. Morris, S. A. Stauth, B. A. Parviz, *IEEE Trans. Adv. Packag.* **2005**, *28*, 600.
[2] J. Bustillo, R. T. Howe, R. S. Muller, *Proc. IEEE* **1998**, *86*, 1552.
[3] G. T. A. Kovacs, N. I. Maluf, K. E. Petersen, *Proc. IEEE* **1998**, *86*, 1536.
[4] N. Miki, X. Zhang, R. Khanna, A. A. Ayon, D. Ward, S. M. Spearing, *Sensors and Actuators A* **2003**, *103*, 194.
[5] A. Mehra, X. Zhang, A. A. Ayon, I. A. Waitz, M. A. Schmidt, C. M. Spadaccini, *Journal of Microelectromechanical Systems* **2000**, *9*, 517.
[6] L. Jian, Y. M. Desta, J. Goettert, M. Bednarzik, B. Loechel, J. Yoonyoung, G. Aigeldinger, V. Singh, G. Ahrens, G. Gruetzner, R. Ruhmann, R. Degen, "SU-8 based deep X-ray lithography/LIGA", presented at *Micromachining and Microfabrication Process Technology VIII*, San Jose, CA, **2003**.
[7] F. P. W. Melchels, J. Feijen, D. W. Grijpma, *Biomaterials* **2010**, *31*, 6121.
[8] T. Baldacchini, C. N. LaFratta, R. A. Farrer, M. C. Teich, B. E. A. Saleh, M. J. Naughton, J. T. Fourkas, *Journal of Applied Physics* **2004**, *95*, 6072.
[9] C. N. LaFratta, J. Li, J. T. Fourkas, *Proceedings of the National Academy of Sciences* **2006**, *103*, 8589.
[10] K. Sun, T.-S. Wei, B. Y. Ahn, J. Y. Seo, S. J. Dillon, J. A. Lewis, *Advanced Materials* **2013**, *25*, 4539.
[11] M. S. Mannoor, Z. Jiang, T. James, Y. L. Kong, K. A. Malatesta, W. O. Soboyejo, N. Verma, D. H. Gracias, M. C. McAlpine, *Nano Letters* **2013**, *13*, 2634.
[12] R. Bruinsma, W. M. Gelbart, D. Reguera, J. Rudnick, R. Zandi, *Physical Review Letters* **2003**, *90*, 248101.
[13] J. S. Flint, V. R. Rancaniello, R. Krug, *Principles of Virology: Molecular Biology, Pathogenesis, and Control*, American Society Microbiology, **1999**.
[14] T. Leidl, B. Hogberg, J. Tytell, D. Ingber, W. Shih, *Nature Nanotechnology* **2010**, *5*, 520.
[15] L. J. Hornbeck, *MRS Bull.* **2001**, *26*, 325.
[16] Sandia National Laboratories, **2005**, http://mems.sandia.gov/gallery/images_gears_and_transmissions.html.
[17] R. Mariella, *Biomedical Microdevices* **2002**, *4*, 77.
[18] A. Nisar, N. Afzulpurkar, B. Mahaisavariya, A. Tuantranont, *Sensors and Actuators B: Chemical* **2008**, *130*, 917.
[19] D. J. Laser, J. G. Santiago, *Journal of Micromechanics and Microengineering* **2004**, *14*, R35.
[20] M. Staples, K. Daniel, M. Cima, R. Langer, *Pharm. Res.* **2006**, *23*, 847.
[21] R. S. Shawgo, A. C. Richards Grayson, Y. Li, M. J. Cima, *Curr. Opin. Solid State Mater. Sci.* **2002**, *6*, 329.
[22] A. C. Richards Grayson, R. Scheidt Shawgo, Y. Li, M. J. Cima, *Advanced Drug Delivery Reviews* **2004**, *56*, 173.
[23] Y. Haga, M. Esashi, *Proc. IEEE* **2004**, *92*, 98.
[24] D. L. Polla, "BioMEMS applications in medicine", presented at *Micromechatronics and Human Science, 2001. MHS 2001. Proceedings of 2001 International Symposium on*, 2001, **2001**.
[25] C. Moraes, C. A. Simmons, Y. Sun, *CSME Bulletin* **2006**, 15.

[26] E. Smela, O. Inganas, I. Lundstrom, *Science* **1995**, *268*, 1735.
[27] S. Bütefisch, V. Seidemann, S. Büttgenbach, *Sensors and Actuators A: Physical* **2002**, *97-98*, 638.
[28] J. P. Hubschman, J. L. Bourges, W. Choi, A. Mozayan, A. Tsirbas, C. J. Kim, S. D. Schwartz, *Eye* **2009**, *24*, 364.
[29] O. C. Jeong, S. Konishi, *Sensors and Actuators A: Physical* **2007**, *135*, 849.
[30] C. Liu, T. Tsao, Y.-C. Tai, W. Liu, P. Will, C.-M. Ho, "A Micromachined Permalloy Magnetic Actuator Array for Micro Robotics Assembly Systems", presented at *Solid-State Sensors and Actuators, 1995 and Eurosensors IX.. Transducers '95. The 8th International Conference on*, 25-29 Jun 1995, **1995**.
[31] Y. W. Yi, C. Liu, *Journal of Microelectromechanical Systems* **1999**, *8*, 10.
[32] Y. Yu, M. Nakano, T. Ikeda, *Nature* **2003**, *425*, 145.
[33] C. D. Eisenbach, *Polymer* **1980**, *21*, 1175.
[34] H. Finkelmann, E. Nishikawa, G. G. Pereira, M. Warner, *Physical Review Letters* **2001**, *87*, 015501.
[35] T. Ikeda, M. Nakano, Y. Yu, O. Tsutsumi, A. Kanazawa, *Advanced Materials* **2003**, *15*, 201.
[36] T. J. White, N. V. Tabiryan, S. V. Serak, U. A. Hrozhyk, V. P. Tondiglia, H. Koerner, R. A. Vaia, T. J. Bunning, *Soft Matter* **2008**, *4*, 1796.
[37] A. Mamada, T. Tanaka, D. Kungwatchakun, M. Irie, *Macromolecules* **1990**, *23*, 1517.
[38] T. Ikehara, M. Tanaka, S. Shimada, H. Matsuda, *Sensors and Actuators A: Physical* **2002**, *96*, 239.
[39] S. Lu, B. Panchapakesan, *Applied Physics Letters* **2006**, *88*, 253107.
[40] P. Krulevitch, A. P. Lee, P. B. Ramsey, T. C. Trevino, J. Hamilton, M. A. Northrup, *Journal of Microelectromechanical Systems* **1996**, *5*, 270.
[41] Y. Bellouard, *Mater. Sci. Eng., A* **2008**, *481-482*, 582.
[42] A. Bose, M. Hartmann, H. Henkes, H. M. Liu, M. M. H. Teng, I. Szikora, A. Berlis, J. Reul, S. C. H. Yu, M. Forsting, M. Lui, W. Lim, S. P. Sit, *Stroke* **2007**, *38*, 1531.
[43] J. K. Luo, R. Huang, J. H. He, Y. Q. Fu, A. J. Flewitt, S. M. Spearing, N. A. Fleck, W. I. Milne, *Sensors and Actuators A: Physical* **2006**, *132*, 346.
[44] A. Volkov, T. Adesina, V. Markin, E. Jovanov, *Plant Physiol.* **2008**, *146*, 694.
[45] Y. Forterre, J. M. Skotheim, J. Dumais, L. Mahadevan, *Nature* **2005**, *433*, 421.
[46] H. Kirsebom, I. Y. Galaev, B. Mattiasson, *J. Polym. Sci., Part B: Polym. Phys.* **2011**, *49*, 173.
[47] T. Tanaka, *Polymer* **1979**, *20*, 1404.
[48] T. Tanaka, D. Fillmore, S.-T. Sun, I. Nishio, G. Swislow, A. Shah, *Physical Review Letters* **1980**, *45*, 1636.
[49] R. A. Siegel, M. Falamarzian, B. A. Firestone, B. C. Moxley, *Journal of Controlled Release* **1988**, *8*, 179.
[50] L. Brannon-Peppas, N. A. Peppas, *Biomaterials* **1990**, *11*, 635.
[51] A. R. Khare, N. A. Peppas, *J. Biomater. Sci., Polym. Ed.* **1993**, *4*, 275.
[52] N. A. Peppas, A. R. Khare, *Advanced Drug Delivery Reviews* **1993**, *11*, 1.
[53] A. S. Hoffman, *Artif. Organs* **1995**, *19*, 458.
[54] M. J. Snowden, B. Z. Chowdhry, B. Vincent, G. E. Morris, *Journal of the Chemical Society, Faraday Transactions* **1996**, *92*, 5013.

[55] Y. Qiu, K. Park, *Advanced Drug Delivery Reviews* **2001**, *53*, 321.
[56] P. Gupta, K. Vermani, S. Garg, *Drug Discovery Today* **2002**, *7*, 569.
[57] D. Schmaljohann, *Advanced Drug Delivery Reviews* **2006**, *58*, 1655.
[58] S. Chaterji, I. K. Kwon, K. Park, *Progress in Polymer Science* **2007**, *32*, 1083.
[59] S.-k. Ahn, R. M. Kasi, S.-C. Kim, N. Sharma, Y. Zhou, *Soft Matter* **2008**, *4*, 1151.
[60] P. Bawa, V. Pillay, Y. E. Choonara, L. C. d. Toit, *Biomed. Mater.* **2009**, *4*, 022001.
[61] I. Tokarev, S. Minko, *Soft Matter* **2009**, *5*, 511.
[62] K. Nakamae, T. Nizuka, M. Furukawa, T. Nishino, K. Kato, T. Inoue, A. S. Hoffman, Y. Kanzaki, *J. Biomater. Sci., Polym. Ed.* **1997**, *9*, 43.
[63] P. Markland, Y. Zhang, G. L. Amidon, V. C. Yang, *Journal of Biomedical Materials Research* **1999**, *47*, 595.
[64] J. Kost, R. Langer, *Advanced Drug Delivery Reviews* **2001**, *46*, 125.
[65] D. Shenoy, S. Little, R. Langer, M. Amiji, *Mol. Pharmaceutics* **2005**, *2*, 357.
[66] H. Y. He, J. J. Guan, J. L. Lee, *Journal of Controlled Release* **2006**, *110*, 339.
[67] K. M. Gupta, S. R. Barnes, R. A. Tangaro, M. C. Roberts, D. H. Owen, D. F. Katz, P. F. Kiser, *J. Pharm. Sci.* **2007**, *96*, 670.
[68] J. M. Benns, J.-S. Choi, R. I. Mahato, J.-S. Park, S. W. Kim, *Bioconjugate Chem.* **2000**, *11*, 637.
[69] V. A. Sethuraman, K. Na, Y. H. Bae, *Biomacromolecules* **2005**, *7*, 64.
[70] D. J. Beebe, J. S. Moore, J. M. Bauer, Q. Yu, R. H. Liu, C. Devadoss, B.-H. Jo, *Nature* **2000**, *404*, 588.
[71] J. Guan, H. He, D. J. Hansford, L. J. Lee, *The Journal of Physical Chemistry B* **2005**, *109*, 23134.
[72] N. Bassik, B. T. Abebe, K. E. Laflin, D. H. Gracias, *Polymer* **2010**, *51*, 6093.
[73] T. S. Kelby, W. T. S. Huck, *Macromolecules* **2010**, *43*, 5382.
[74] T. S. Kelby, M. Wang, W. T. S. Huck, *Advanced Functional Materials* **2011**, *21*, 652.
[75] M. E. Harmon, T. A. M. Jakob, W. Knoll, C. W. Frank, *Macromolecules* **2002**, *35*, 5999.
[76] R. Toomey, D. Freidank, J. r. RÃ¼he, *Macromolecules* **2004**, *37*, 882.
[77] J. S. Sharp, R. A. L. Jones, *Advanced Materials* **2002**, *14*, 799.
[78] A. W. Feinberg, A. Feigel, S. S. Shevkoplyas, S. Sheehy, G. M. Whitesides, K. Kit Parker, *Science* **2007**, *317*, 1366.
[79] J. C. Nawroth, H. Lee, A. W. Feinberg, C. M. Ripplinger, M. L. McCain, A. Grosberg, J. O. Dabiri, K. Kit Parker, *Nature Biotechnology* **2012**, *30*, 792.
[80] K. Kuribayashi-Shigetomi, H. Onoe, S. Takeuchi, *PLoS ONE* **2012**, *7*, e51085.
[81] http://mems.sandia.gov/tech-info/mems-overview.html, Vol. 2013, Sandia National Laboratories.
[82] D. Goodsell, Vol. 2013 (Ed: http://www.rcsb.org/pdb/101/motm.do?momID=109), Research Collaboratory for Structural Bioinformatics Protein Data Bank, **2009**.
[83] N. Bassik, B. Abebe, K. Laflin, D. H. Gracias, *Polymer* **2010**, *51*, 6093.
[84] T. G. Leong, C. L. Randall, B. R. Benson, N. Bassik, G. M. Stern, D. H. Gracias, *Proceedings of the National Academy of Sciences* **2009**, *106*, 703.
[85] N. Bassik, A. Brafman, A. M. Zarafshar, M. Jamal, D. Luvsanjav, F. M. Selaru, D. H. Gracias, *Journal of the American Chemical Society* **2010**, *132*.

[86] G. P. Nikishkov, *Journal of Applied Physics* **2003**, *94*, 5333.
[87] R. P. Feynman, *Journal of Microelectromechanical Systems* **1992**, *1*, 60.
[88] G. Iddan, G. Meron, A. Glukhovsky, P. Swain, *Nature* **2000**, *405*, 417.
[89] X. Qian, X. H. Peng, D. O. Ansari, Q. Yin-Goen, G. Z. Chen, D. M. Shin, L. Yang, A. N. Young, M. D. Wang, S. Nie, *Nature Biotechnology* **2008**, *26*, 83.
[90] X. Michalet, F. F. Pinaud, L. A. Bentolila, J. M. Tsay, S. Doose, J. J. Li, G. Sundaresan, A. M. Wu, S. S. Gambhir, S. Weiss, *Science* **2005**, *307*, 538.
[91] E. Warner, *New England Journal of Medicine* **2011**, *365*, 1025.
[92] R. H. Collins Jr., M. Feldman, J. S. Fordtran, *New England Journal of Medicine* **1987**, *316*, 1654.
[93] R. D. Odze, *Nature Reviews Gastroenterology & Hepatology* **2009**, *6*, 478.
[94] M. Ramchandani, D. N. Reddy, R. Gupta, S. Lakhtakia, M. Tandan, S. Darisetty, A. Sekaran, G. V. Rao, *Gastrointestinal Endoscopy* **2011**, *74*.
[95] T. Rösch, K. Hofrichter, E. Frimberger, A. Meining, P. Born, N. Weigert, H. D. Allescher, M. Classen, M. Barbur, U. Schenck, M. Werner, *Gastrointestinal Endoscopy* **2004**, *60*, 390.
[96] M. Hattori, M. Nagino, T. Ebata, K. Kato, K. Okada, Y. Shimoyama, *British Journal of Surgery* **2011**, *98*, 704.
[97] S. H. Itzkowitz, D. H. Present, *Inflammatory Bowel Disease* **2005**, *11*, 314.
[98] B. J. Reid, X. Li, P. C. Galipeau, T. L. Vaughan, *Nature Reviews Cancer* **2010**, *10*, 87.
[99] S. Winawer, R. Fletcher, D. Rex, J. Bond, R. Burt, J. Ferrucci, T. Ganiats, T. Levin, S. Woolf, D. Johnson, L. Kirk, S. Litin, C. Simmang, *Gastroenterology* **2003**, *124*.
[100] M. J. Mack, *Journal of the American Medical Association* **2001**, *285*, 568.
[101] P. W. Dhumane, M. Diana, J. Leroy, J. Marescaux, *Journal of Minimal Access Surgery* **2011**, *7*, 40.
[102] L. L. Swanstrom, M. Whiteford, Y. Khajanchee, *Surgical Endoscopy* **2008**, *22*, 600.
[103] A. N. Kalloo, V. K. Singh, S. B. Jagannath, H. Niiyama, S. L. Hill, C. A. Vaughn, C. A. Magee, S. V. Kantsevoy, *Gastrointestinal Endoscopy* **2004**, *60*, 114.
[104] N. T. Nguyen, M. W. Hinojosa, B. R. Smith, K. M. Reavis, *Obesity Surgery* **2008**, *18*, 1628.
[105] R. Fernandes, D. H. Gracias, *Materials Today* **2009**, *12*, 14.
[106] S. R. Platt, J. A. Hawks, M. E. Rentschler, *IEEE Transactions on Biomedical Engineering* **2009**, *56*, 1700.
[107] H. Li, G. Yan, G. Ma, *The International Journal of Medical Robotics and Computer Assisted Surgery* **2008**, *4*, 355.
[108] T. G. Leong, C. L. Randall, B. R. Benson, N. Bassik, G. M. Stern, D. H. Gracias, *Proceedings of the National Academy of Sciences* **2009**, *106*, 703.
[109] E. Gultepe, J. R. Randhawa, S. Kadam, *Advanced Materials* **2013**, *25*, 514.
[110] M. Collado-Romero, C. Arce, M. Ramírez-Boo, A. Carvajal, J. Garrido, *Veterinary Research* **2010**, *41*, 23.
[111] J. Ren, H. Tang, X. Yan, X. Huang, B. Zhang, H. Ji, B. Yang, D. Milan, L. Huang, *J Anim Breed Genet* **2009**, *126*, 30.
[112] S. J. Altschuler, L. F. Wu, *Cell* **2010**, *141*, 559.

[113] C. Ma, R. Fan, H. Admad, Q. Shi, B. Comin-Anduix, T. Chodon, R. C. Koya, C.-C. Liu, G. A. Kwong, C. G. Radu, A. Ribas, J. R. Heath, *Nature Medicine* **2011**, *17*, 738.
[114] D. Di Carlo, H. T. K. Tse, D. R. Gossett, in *Single-Cell Analysis: Methods and Protocols*, Vol. 853 (Eds: S. Lindstrom, H. Andersson-Svahn), Springer Science+Business Media, **2012**.
[115] N. Navin, A. Krasnitz, L. Rodgers, K. Cook, J. Meth, J. Kendall, M. Riggs, Y. Eberling, J. Troge, V. Grubor, D. Levy, P. Lundin, S. Maner, A. Zetterberg, J. Hicks, M. Wigler, *Genome Research* **2010**, *20*, 68.
[116] J. Calbo, E. van Montfort, N. Proost, E. van Drunen, H. B. Beverloo, R. Meuwissen, A. Berns, *Cancer Cell* **2011**, *19*, 244.
[117] A. Pietras, *Advances in cancer research* **2011**, *112*, 255.
[118] F. Mannello, *BioMed Central Medicine* **2013**, *11*, 169.
[119] R. A. Beckman, G. S. Schemmann, C.-H. Yeang, *Proceedings of the National Academy of Sciences* **2012**.
[120] S. Lindstrom, H. Andersson-Svahn, *Lab on a Chip* **2010**, *10*, 3363.
[121] S. Lindstrom, H. Andersson-Svahn, *Single Cell Analysis: Methods and Protocols*, Vol. 853, Springer Science + Business Media, New York **2012**.
[122] A. Ashkin, J. M. Dziedzic, J. E. Bjorkholm, S. Chu, *Optics Letters* **1986**, *11*, 288.
[123] E. Townes-Anderson, R. S. St Jules, D. Sherry, J. Lichtenberger, M. Hassanain, *Molecular Vision* **1998**, *4*.
[124] M. W. Berns, Y. Tadir, H. Liang, B. Tromberg, *Methods Cell Biol.* **1998**, *55*.
[125] C. Xie, M. A. Dinno, Y.-q. Li, *Optics Letters* **2002**, *27*, 249.
[126] A. Lúcio, R. Santos, O. Mesquita, *Physical Review E* **2003**, *68*, 041906.
[127] H. Zhang, K.-K. Liu, *Journal of The Royal Society Interface* **2008**, *5*, 671.
[128] A. R. Wheeler, W. R. Throndset, R. J. Whelan, A. M. Leach, R. N. Zare, Y. H. Liao, K. Farrell, I. D. Manger, A. Daridon, *Analytical Chemistry* **2003**, *75*, 3581.
[129] X. Peng, P. Li, *Analytical Chemistry* **2004**, *76*, 5273.
[130] X. Peng, P. Li, *Analytical Chemistry* **2004**, *76*, 5282.
[131] A. Valero, F. Merino, F. Wolbers, R. Luttge, I. Vermes, H. Andersson, A. van den Berg *Lab on a Chip* **2005**, *5*, 49.
[132] D. Di Carlo, L. Y. Wu, L. Lee, *Lab on a Chip* **2006**, *6*, 1445.
[133] D. Di Carlo, N. Aghdam, L. Lee, *Analytical Chemistry* **2006**, *78*, 4925
[134] G. T. Roman, Y. Chen, P. Viberg, A. H. Culbertson, C. T. Culbertson, *Analytical and Bioanalytical Chemistry* **2007**, *387*, 9.
[135] J. Nilsson, M. Evander, B. Hammarström, T. Laurell, *Analytica Chimica Acta* **2009**, *649*, 141.
[136] S. Park, Y. Zhang, T. H. Wang, S. Yang, *Lab on a Chip* **2011**, *11*, 2893.
[137] X. Ding, S.-C. S. Lin, B. Kiraly, H. Yue, S. Li, I.-K. Chiang, J. Shi, S. J. Benkovic, T. J. Huang, *Proceedings of the National Academy of Sciences* **2012**, *109*, 11105.
[138] M. Charnley, M. Textor, A. Khademhosseini, M. Lutolf, *Integrative biology* **2009**, *1*, 625.
[139] S. Lindstrom, H. Andersson-Svahn, *Biochimica et Biophysica Acta* **2011**, *1810*, 308.

[140] E. J. Smith, W. Xi, D. Makarov, I. Monch, S. M. Harazim, V. A. Bolanos Quinones, C. K. Schmidt, Y. Mei, S. Sanchez, O. G. Schmidt, *Lab on a Chip* **2012**, *12*, 1917.
[141] R. S. Kane, S. Takayama, E. Ostuni, D. E. Ingber, G. M. Whitesides, *Biomaterials* **1999**, *20*, 2363.
[142] A. Azioune, M. Storch, M. Bornens, M. Thery, M. Piel, *Lab on a Chip* **2009**, *9*, 1640.
[143] J. E. Gautrot, B. Trappmann, F. Oceguera-Yanez, J. Connelly, X. He, F. M. Watt, W. T. S. Huck, *Biomaterials* **2010**, *31*, 5030.
[144] A. M. Leclair, S. S. G. Ferguson, F. Lagugne-Labathet, *Biomaterials* **2011**, *32*, 1351.
[145] K. Mandal, M. Balland, L. Bureau, *PLoS ONE* **2012**, *7*, e37548.
[146] N. Chronis, L. P. Lee., *Journal of Microelectromechanical Systems* **2005**, *14*, 857
[147] M. S. Sakar, E. B. Steager, D. H. Kim, M. J. Kim, G. J. Pappas, V. Kumar, *Applied Physics Letters* **2010**, *96*, 043705.
[148] S. Kim, F. Qiu, S. Kim, A. Ghanbari, C. Moon, L. Zhang, B. Nelson, H. Choi, *Advanced Materials* **2013**, *25*, 5863.
[149] R. Fernandes, D. H. Gracias, *Materials Today* **2009**, *12*, 14.
[150] V. Y. Prinz, V.A Seleznev, A.K Gutakovsky, A.V Chehovskiy, V.V Preobrazhenskii, M.A Putyato, T. A. Gavrilova, *Physica E: Low-dimensional Systems and Nanostructures* **2000**, *6*, 828.
[151] O. G. Schmidt, K. Eberl, *Nature* **2001**, *410*, 168.
[152] K. Kazuyoshi, T. Fleischmann, S. Saravanan, P. O. Vaccaro, T. Aida, *Japanese Journal of Applied Physics* **2003**, *42*, 4079.
[153] C. L. Chua, D. K. Fork, K. van Schuylenbergh, J.-P. Lu, *Journal of Microelectromechanical Systems* **2003**, *12*, 989=995.
[154] V. Y. Prinz, *Russian Physics Journal* **2003**, *46*, 568.
[155] L. Zhanga, S. V. Goloda, E. Deckardta, V. Y. Prinz, D. Grützmachera, *Physica E: Low-dimensional Systems and Nanostructures* **2004**, *23*, 280.
[156] M. Sasaki, D. Briand, W. Noell, N. F. de Rooij, *IEEE Journal of Selected Topics in Quantum Electronics* **2004**, *10*, 455
[157] M. Huang, C. Boone, M. Roberts, D. E. Savage, M. G. Lagally, N. Shaji, H. Qin, J. A. Naim, F. Liu, *Advanced Materials* **2005**, *17*, 2860.
[158] W. J. Arora, A. J. Nichol, H. I. Smith, G. Barbastathis, *Applied Physics Letters* **2006**, *88*, 053108.
[159] E. Moiseeva, Y. M. Senousy, C. K. Harnett, *Journal of Micromechanics and Microengineering* **2007**, *17*, N63.
[160] P. Stellman, T. Buchner, W. J. Arora, G. Barbastathis, *Journal of Microelectromechanical Systems* **2007**, *16*, 932.
[161] N. Bassik, G. M. Stern, M. Jamal, D. H. Gracias, *Advanced Materials* **2008**, *20*, 4760.
[162] T. G. Leong, B. R. Benson, E. K. Call, D. H. Gracias, *Small* **2008**, *4*, 1605.
[163] Y. Mei, G. Huang, A. A. Solovev, E. Bermudez Urena, I. Monch, F. Ding, T. Reindl, R. K. Y. Fu, P. K. Chu, O. G. Schmidt, *Advanced Materials* **2008**, *20*, 4085.
[164] Alexander A. Solovev, Yongfeng Mei, Esteban Bermúdez Ureña, Gaoshan Huang, O. G. Schmidt, *Small* **2009**, *5*, 1688.

[165] G. Huang, Y. Mei, D. J. Thurmer, E. Coric, O. G. Schmidt, *Lab on a Chip* **2009**, *9*, 263.
[166] N. Bassik, G. M. Stern, D. H. Gracias, *Applied Physics Letters* **2009**, *95*, 091901.
[167] Y. Mei, D. J. Thurmer, C. Deneke, S. Kiravittaya, Y.-F. Chen, A. Dadgar, F. Bertram, B. Bastek, A. Krost, J. Christen, T. Reindl, M. Stoffel, E. Coric, O. G. Schmidt, *ACS Nano* **2009**, *3*, 1663.
[168] V. B. Shenoy, D. H. Gracias, *MRS Bulletin* **2012**, *37*, 847.
[169] S. M. Harazim, W. Xi, C. K. Schmidt, S. Sanchez, O. G. Schmidt, *Journal of Materials Chemistry* **2012**, *22*, 2878.
[170] W. Xi, A. A. Solovev, A. N. Ananth, D. H. Gracias, S. Sanchez, O. G. Schmidt, *Nanoscale* **2012**, *5*, 1294.
[171] E. J. Smith, W. Xi, D. Makarov, I. Mönch, S. Harazim, V. A. B. Quiñones, C. K. Schmidt, Y. Mei, S. Sanchez, O. G. Schmidt, *Lab on a Chip* **2012**, *12*, 1917.
[172] L. Soler, V. Magdanz, V. M. Fomin, S. Sanchez, O. G. Schmidt, *ACS Nano* **2013**, *7*, 9611.
[173] K. Chalapat, N. Chekurov, H. Jiang, J. Li, B. Parviz, G. S. Paraoanu, *Advanced Materials* **2013**, *25*, 1.
[174] N. Bassik, A. Brafman, A. M. Zarafshar, M. Jamal, D. Luvsanjav, F. M. Selaru, D. H. Gracias, *Journal of the American Chemical Society* **2010**, *132*, 16314.
[175] E. Gultepe, J. S. Randhawa, S. Kadam, S. Yamanaka, F. M. Selaru, E. J. Shin, A. N. Kalloo, D. H. Gracias, *Advanced Materials* **2012**.
[176] E. Gultepe, S. Yamanaka, K. E. Laflin, S. Kadam, Y. Shim, A. V. Olaru, B. Limketkai, M. A. Khashab, A. N. Kalloo, D. H. Gracias, F. M. Selaru, *Gastroenterology* **2013**, *144*, 691.
[177] J. D. Rimstidt, H. L. Barnes, *Geochimica et Cosmochimica Acta* **1980**, *44*, 1683.
[178] R. K. Iler, *Journal of Colloid and Interface Science* **1973**, *43*, 399.
[179] S.-W. Hwang, H. Tao, D.-H. Kim, H. Cheng, J.-K. Song, E. Rill, M. A. Brenckle, B. Panilaitis, S. M. Won, Y.-S. Kim, Y. M. Song, K. J. Yu, A. Ameen, R. Li, Y. Su, M. Yang, D. L. Kaplan, M. R. Zakin, M. J. Slepian, Y. Huang, F. G. Omenetto, J. A. Rogers, *Science* **2012**, *337*, 1640.
[180] A. E. Hill, G. R. Hoffman, *British Journal of Applied Physics* **1967**, *18*, 13.
[181] M. Fang, D. Hu, J. Shao, *Chinese Optics Letters* **2010**, *8*, 119.
[182] H. Leplan, J. Y. Robic, Y. Pauleau, *Journal of Applied Physics* **1996**, *79*, 6926.
[183] B. Halg, "On a non-volatile memory cell based on micro-electro-mechanics", presented at *IEEE Micro Electro Mechanical Systems Workshop*, Napa Valley, CA, **1990**.
[184] M. T. Kim, *Thin Solid Films* **1996**, *283*, 12.
[185] L. B. Freund, S. Suresh, *Thin Film Materials*, Cambridge University Press, **2003**.
[186] B. Friede, M. Jansen, *Journal of Non-Crystalline Solids* **1996**, *204*, 202.
[187] K. Schulmeister, W. Mader, *Journal of Non-Crystalline Solids* **2003**, *320*, 143.
[188] S. Pandey, M. Ewing, A. Kunas, N. Nguyen, D. H. Gracias, G. Menon, *Proceedings of the National Academy of Sciences* **2011**, *108*, 19885.
[189] T. G. Leong, A. M. Zarafshar, D. H. Gracias, *Small* **2010**, *6*, 792.
[190] V. Y. Prinz, V. A. Seleznev, A. K. Gutakovsky, A. V. Chehovskiy, V. V. Preobrazhenskii, M. A. Putyato, T. A. Gavrilova, *Physica E* **2000**, *6*, 828.
[191] J. Guan, H. He, D. J. Hansford, L. J. Lee, *J. Phys. Chem. B* **2005**, *109*, 23134.
[192] H. He, J. Guan, J. L. Lee, *Journal of Controlled Release* **2006**, *110*, 339.

[193] L. Yu, G. Urban, I. Moser, G. Jobst, H. Gruber, *Polymer Bulletin* **1995**, *35*, 759.
[194] D. Duracher, F. Sauzedde, A. Elaissari, A. Perrin, C. Pichot, *Colloid & Polymer Science* **1998**, *276*, 219.
[195] D. Duracher, F. Sauzedde, A. Elaïssari, C. Pichot, L. Nabzar, *Colloid & Polymer Science* **1998**, *276*, 920.
[196] N. Bassik, B. T. Abebe, D. H. Gracias, *Langmuir* **2008**, *24*, 12158.
[197] P. Somasundaran, *Encyclopedia of Surface and Colloid Science, Volume 5*, Vol. 5, CRC Press, Boca Raton **2006**.
[198] K. Kratz, T. Hellweg, W. Eimer, *Colloids and Surfaces A: Physicochemical and Engineering Aspects* **2000**, *170*, 137.
[199] X. Liu, Z. Tong, O. Hu, *Macromolecules* **1995**, *28*, 3813.
[200] N. A. Peppas, Y. Huang, M. Morres-Lugo, J. H. Ward, J. Zhang, *Annual Review of Biomedical Engineering* **2000**, *2*, 9.
[201] B. Amsden, *Macromolecules* **1998**, *31*, 8382.
[202] L. Masaro, X. X. Zhu, *Progress in Polymer Science* **1999**, *24*, 731.
[203] N. Chronis, L. P. Lee, *Microelectromechanical Systems, Journal of* **2005**, *14*, 857.
[204] H. J. van der Linden, S. Herber, W. Olthuis, P. Bergveld, *The Analyst* **2003**, *128*, 325.
[205] R. Siegel, M. Rathbone, in *Fundamentals and Applications of Controlled Release Drug Delivery*, (Ed: J. S. e. al.), Controlled Release Society, **2012**.
[206] A. W. Basit, *Drugs* **2005**, *65*, 1991.
[207] D. Lissner, B. Siegmund, *Digestive Diseases* **2013**, *31*, 91.
[208] A. S. Cheifetz, *Journal of the American Medical Association* **2013**, *309*, 2150.
[209] P. I. Lee, C.-J. Kim, *Journal of Controlled Release* **1991**, *16*, 229.
[210] S. L. Tao, T. A. Desai, *Advanced Drug Delivery Reviews* **2003**, *55*, 315.
[211] A. Lamprecht, H. Yamamoto, H. Takeuchi, Y. Kawashima, *Journal of Controlled Release* **2005**, *104*, 337.
[212] J. J. Guan, N. Ferrell, L. J. Lee, D. J. Hansford, *Biomaterials* **2006**, *27*, 4034.
[213] L. G. J. de Leede, A. G. de Boer, E. Portzgen, *Journal of Controlled Release* **1986**, *4*, 17.
[214] J. J. Guan, H. Y. He, L. J. Lee, D. J. Hansford, *Small* **2007**, *3*, 412.
[215] C. S. Brazel, N. A. Peppas, *Journal of Controlled Release* **1996**, *39*.
[216] S. L. Tao, T. A. Desai, *Drug Discovery Today* **2005**, *10*, 909.
[217] M. Dadsetan, Z. Liu, M. Pumberger, C. V. Giraldo, T. Ruesink, L. Lu, M. J. Yaszemski, *Biomaterials* **2010**, *31*, 8051.
[218] H. D. Chirra, T. A. Desai, *Small* **2012**, *8*, 3839.
[219] D. A. Bernards, K. D. Lance, N. A. Ciaccio, T. A. Desai, *Nanoletters* **2012**, *12*, 5355.
[220] H. D. Chirra, T. A. Desai, *Advanced Drug Delivery Reviews* **2012**, *64*, 1569.
[221] L. Ionov, *Soft Matter* **2011**, *7*, 6786.
[222] T. S. Shim, S.-H. Kim, C.-J. Heo, H. C. Jeon, S.-M. Yang, *Angewandte Chemie* **2011**, *51*, 1420.
[223] G. Stoychev, S. Zakharchenko, S. Turcaud, J. Dunlop, L. Ionov, *ACS Nano* **2012**, *6*, 3925.
[224] D. H. Gracias, *Current Opinion in Chemical Engineering* **2013**, *2*, 112.

[225] Z. L. Wu, M. Moshe, J. Greener, H. Therien-Aubin, Z. Nie, E. Sharon, E. Kumacheva, *Nat Communications* **2012**, *4*, 1586.
[226] S. J. Peter, S. T. Miller, G. Zhu, A. W. Yasko, A. G. Mikos, *Journal of Biomedical Materials Research* **1998**, *41*, 1.
[227] M. D. Timmer, C. G. Ambrose, A. G. Mikos, *Biomaterials* **2003**, *2003*, 571.
[228] J. P. Fisher, M. D. Timmer, T. A. Holland, D. Dean, P. S. Engel, A. G. Mikos, *Biomacromolecules* **2003**, *4*, 1327.
[229] S. Fusco, M. S. Sakar, S. Kennedy, C. Peters, R. Bottani, F. Starsich, A. Mao, G. A. Sotiriou, S. Pané, S. E. Pratsinis, D. Mooney, B. Nelson, *Advanced Materials* **2013**.
[230] K. S. Oh, S. H. Yuk, in *Biomedical Applications of Hydrogels Handbook*, (Ed: K. P. e. al.), Springer, New York **2010**.
[231] J. P. Fisher, T. A. Holland, D. Dean, P. S. Engel, A. G. Mikos, *Journal of Biomaterials Science, Polymer Edition* **2001**, *12*, 673.
[232] J. P. Fisher, D. Dean, A. G. Mikos, *Biomaterials* **2002**, *23*, 4333.
[233] J. Choi, K. Kim, T. Kim, G. Liu, A. Bar-Shir, T. Hyeon, M. T. McMahon, J. W. M. Bulte, J. P. Fisher, A. A. Gilad, *Journal of Controlled Release* **2011**, *156*, 239.
[234] A. Haesslein, H. Ueda, M. C. Hacker, S. Jo, D. M. Ammon, R. N. Borazjani, J. F. Kunzler, J. C. Salamone, A. G. Mikos, *Journal of Controlled Release* **2006**, *114*, 251.
[235] M. O. Wang, J. M. Etheridge, J. A. Thompson, C. E. Vorwald, D. Dean, J. P. Fisher, *Biomacromolecules* **2013**, *14*, 1321.
[236] E. Gultepe, J. S. Randhawa, S. Kadam, S. Yamanaka, F. M. Selaru, E. J. Shin, A. N. Kalloo, D. H. Gracias, *Advanced Materials* **2013**, *25*, 514.
[237] E. Gultepe, S. Yamanaka, K. E. Laflin, S. Kadam, Y. Shim, A. V. Olaru, B. Limetkai, M. A. Khashab, A. N. Kalloo, D. H. Gracias, F. M. Selaru, *Gastroenterology* **2013**, *144*, 691.
[238] G. Vilar, J. Tulla-Puche, F. Albericio, *Current Drug Delivery* **2012**, *9*, 367.
[239] R. S. Langer, N. A. Peppas, *Biomaterials* **1981**, *2*, 201.
[240] R. Gurny, E. Doelker, N. A. Peppas, *Biomaterials* **1982**, *3*.
[241] R. W. Korsmeyer, R. Gurny, E. Doelker, P. Buri, N. A. Peppas, *International Journal of Pharmaceutics* **1983**, *15*, 25.
[242] S. Dash, P. N. Murthy, L. Nath, P. Chowdhury, *Acta Poloniac Pharmaceutica - Drug Research* **2010**, *67*, 217.
[243] J. Siepmann, F. Siepmann, *International Journal of Pharmaceutics* **2008**, *364*, 328.
[244] R. Shaikh, R. S. T. Raghu, G. M. James, A. D. Woolfson, R. F. Donnelly, *J Pharm Bioallied Sci.* **2011**, *3*, 89.
[245] C. Kremser, K. Albrecht, M. Greindl, C. Wolf, P. Debbage, A. Bernkop-Schnurch, *Magnetic Resonance Imaging* **2008**, *26*, 638.
[246] S. G. Penn, S. M. Norton., I. D. Walton, R. G. Freeman, G. Davis, *Proc. SPIE-IS&T Electron. Imaging* **2004**, *5310*, 337.
[247] R. Fernandes, D. H. Gracias, *Materials Today* **2009**, *12*, 14.
[248] B. J. Nelson, I. K. Kaliakatsos, J. J. Abbott, *Annual Review of Biomedical Engineering* **2010**, *12*, 55.
[249] W. R. Davis Jr., B. B. Kosicki, D. M. Boroson, D. F. Kostishack, *Lincoln Laboratory Journal* **1996**, *9*, 197.

[250] J. M. Kahn, R. H. Katz, K. S. J. Pister, in *ACM/IEEE Intl. Conf. Mobile Computing and Networking*, Seattle, WA **1999**.
[251] U. Srinivasan, D. Liepmann, R. T. Howe, *Journal of Microelectromechanical Systems* **2001**, *10*, 17.
[252] H. O. Jacobs, A. R. Tao, A. Schwartz, D. H. Gracias, G. M. Whitesides, *Science* **2002**, *296*, 323.
[253] X. Xiong, Y. Hanein, J. Fang, Y. Wang, W. Wang, D. Schwartz, B. K, *Journal of Microelectromechanical Systems* **2003**, *12*, 117.
[254] W. Zheng, H. O. Jacobs, *Applied Physics Letters* **2004**, *85*, 3635.
[255] C. J. Morris, B. A. Parviz, *J. Micromech. Microeng.* **2008**, *18*, 015022.
[256] S. B. Shetye, I. Eskinazi, D. P. Arnold, *IEEE Trans. Magn.* **2008**, *44*, 4293.
[257] G. Humpston, D. Jacobson, *Principles of Soldering.*, ASM International, Materials Park, OH **2004**.
[258] M. Jamal, N. Bassik, J.-H. Cho, C. L. Randall, D. H. Gracias, *Biomaterials* **2010**, *31*, 1683.
[259] P. Burke, C. Rutherglen, *Biomed. Microdevices* **2010**, *12*, 589.
[260] E. J. H. Robinson, T. O. Richardson, A. B. Sendova-Franks, O. Feinerman, N. R. Franks, *Behavioral Ecol. Sociobiol.* **2009**, *63*, 627.
[261] J. S. Randhawa, M. D. Keung, P. Tyagi, D. H. Gracias, *Advanced Materials* **2010**, *22*, 407.
[262] E. W. H. Jager, E. Smela, O. Inganäs, I. Lundström, *Synthetic Metals* **1999**, *102*, 1309.
[263] R. R. A. Syms, E. M. Yeatman, V. M. Bright, G. M. Whitesides, *Journal of Microelectromechanical Systems* **2003**, *12*, 387.
[264] C. L. Randall, E. Gultepe, D. H. Gracias, *Trends in Biotechnology* **2012**, *30*, 138.
[265] N. Bassik, G. M. Stern, D. H. Gracias, *Applied Physics Letters* **2009**, *95*, 091901.
[266] S. Pandey, M. Ewing, A. Kunas, N. Nguygen, D. H. Gracias, G. Menon, *Proceedings of the National Academy of Sciences* **2011**, *108*, 19885.
[267] E. Hawkes, B. An, N. M. Benbernou, H. Tanaka, S. Kim, E. D. Demaine, D. Rus, R. J. Wood, *Proceedings of the National Academy of Sciences* **2010**.
[268] J. P. Hubschman, J. L. Bourges, W. Choi, A. Mozayan, A. Tsirbas, C. J. Kim, S. D. Schwartz, *Eye* **2010**, *24*, 364.
[269] W. Small, IV, M. F. Metzger, T. S. Wilson, D. J. Maitland, *IEEE J. Quantum Electronics* **2005**, *11*, 892.
[270] C. Elbuken, L. Gui, C. L. Ren, M. Yavuz, M. B. Khamesee, *Sensors and Actuators A: Physical* **2008**, *147*, 292.
[271] Y. Liu, J. K. Boyles, J. Genzer, M. D. Dickey, *Soft Matter* **2012**, *8*, 1764.
[272] J. Ryu, M. D'Amato, X. Cui, K. N. Long, H. J. Qi, M. L. Dunn, *Applied Physics Letters* **2012**, *100*, 161908.
[273] A. J. Birnbaum, A. Pique, *Applied Physics Letters* **2011**, *98*, 134101.
[274] S. V. Ahir, A. M. Squires, A. R. Tajbakhsh, E. M. Terentjev, *Physical Review B* **2006**, *73*, 085420.
[275] L. Yang, K. Setyowati, A. Li, S. Gong, J. Chen, *Advanced Materials* **2008**, *20*, 2271.
[276] Z. H. Lim, C.-H. Sow, *Advanced Functional Materials* **2010**, *20*, 847.
[277] A. Pique, S. Mathews, A. Birnbaum, N. Charipar, *SPIE Newsroom* **2011**.

[278] H. Yamashita, N. Kodera, A. Miyagi, T. Uchihashi, D. Yamamoto, T. Ando, *Review of Scientific Instruments* **2007**, *78*, 083702.
[279] E. Merced, N. Dávila, D. Torres, R. Cabrera, F. E. Fernández, N. Sepúlveda, *Smart Materials and Structures* **2012**, *21*, 105009.
[280] J. Solem, Los Alamos National Laboratory, **1996**.
[281] F. R. Sbazo, P. E. Kladitis, "Design, Modeling and Testing of Polysilicon Optothermal Actuators for Power Scavenging Wireless Microrobots ", presented at *MEMS, NANO and Smart Systems, 2004. ICMENS 2004.* , Canada, **2004**.
[282] C. J. Morris, K. E. Laflin, W. A. Churaman, C. R. Becker, L. J. Currano, D. H. Gracias, "Initiation of nanoporous energetic silicon by optically-triggered, residual stress powered microactuators", presented at *25th IEEE International Conference on MEMS*, Paris, France, Jan. 30-Feb. 2, 2012., **2012**.
[283] T. G. Leong, B. R. Benson, E. K. Call, D. H. Gracias, *Small* **2008**, *4*, 1605.
[284] M. Bass, E. W. Van Stryland, Eds., *Handbook of Optics vol. 2 (2nd ed.)*, McGraw-Hill **1994**.
[285] M. Yim, W.-M. Shen, B. Salemi, D. Rus, M. Moll, H. Lipson, E. Klavins, G. S. Chirikjian, *Robotics & Automation Magazine, IEEE* **2007**, *14*, 43.
[286] E. T. Kisak, B. Coldren, C. A. Evans, C. Boyer, J. A. Zasadzinski, *Current Medicinal Chemistry* **2004**, *11*, 199.
[287] W. A. Churaman, L. J. Currano, J. Rajkowski, C. J.Morris, S. Bergbreiter, *Journal of Microelectromechanical Systems* **2012**, *21*, 198.
[288] K. E. Laflin, C. J. Morris, N. Bassik, M. Jamal, D. H. Gracias, *Journal of Microelectromechanical Systems* **2011**, *PP*, 1.
[289] D. S. Mottram, B. L. Wedzicha, A. T. Dodson, *Nature* **2002**, *419*, 448.
[290] World Health Organization, Geneva **2002**.
[291] M. Patenaude, T. Hoare, *ACS MacroLetters* **2012**, *1*, 409.
[292] R. M. P. da Silva, J. F. Mano, R. L. Reis, *TRENDS in Biotechnology* **2007**, *25*, 577.
[293] J. Yang, M. Yamato, K. Nishida, T. Ohki, M. Kanzaki, H. Sekine, T. Shimizu, T. Okano, *Journal of Controlled Release* **2006**, *116*, 193.
[294] M. Nakayama, T. Okano, F. M. Winnik, *Material Matters* **2010**, *5.3*, 56.
[295] A. Serres, M. Baudys, S. W. Kim, *Pharm. Res.* **1996**, *13*, 196.
[296] S. Ohya, Y. Nakayama, T. Matsuda, *Journal of Artificial Organs* **2004**, *7*, 181.

7 Appendix A: A note on the biocompatibility of pNIPAM.

Poly(N-isopropylacrylamide) or pNIPAM is a thermoresponsive polymer that undergoes a transition from hydrophilic below 32°C to hydrophobic above 32°C. With an LCST so close to body temperature, it is a natural choice as a biomaterial and has been used extensively as such in the literature. However, concerns exist over the biocompatibility of pNIPAM and its use in biomedical devices. Our literature investigation, as well as our own experiments, demonstrates that this concern is unfounded for our particular drug delivery system.

Acrylamide, the building block of pNIPAM, is found in food and cosmetics. It is created in small quantities naturally in some foods as a byproduct of the Maillard effect during high temperature baking, roasting, and frying.[289] While high concentrations have been shown to be neurotoxic and carcinogenic, a 2002 report by the Food and Agriculture Organization of the United Nations and World Health Organization determined that the small quantities found in food (0.3-0.8 μg/kg body weight) were 500-2000 times below the concentration required to cause fertility or neuropathy problems. While only limited data on the carcinogenicity of the acryamide found in food exist, these data suggest that there is no evidence of increased cancer risk due to occupational exposure from food.[290]

Although the NIPAM monomer is known to be cytotoxic, pNIPAM has been shown to be non-cytotoxic *in vitro* at biologically relevant concentrations.[291] pNIPAM has been used extensively in cell culture and tissue engineering for the creation of cell sheets.[292, 293] For this application, NIPAM is polymerized and bonded to a polystyrene tissue culture dish.

Upon cooling of the dish to below 32°C, the pNIPAM layer swells, forcing the detachment of the cell sheet.[292, 294] This technique eliminates the need for proteolytic enzymes for cell detachment which can affect cell membrane proteins and cell function. Currently, several *in vivo* demonstrations and clinical trials are underway using this technology including corneal surface reconstruction, myocardial tissue grafts, and esophageal ulcer and wound healing.[293] As an injectable hydrogel, pNIPAM cytotoxicity was evaluated on both 3T3 mouse fibroblasts and retinal pigment epithelial cells.[291] High concentrations did show slight cytotoxicity, but biologically relevant concentrations showed no adverse effects *in vitro*.

pNIPAM and pNIPAM-AAc hydrogels have also been tested as drug delivery devices and injectable scaffolds *in vivo* both in this work and in the literature. In our own theragripper deployment into a live porcine esophagus and stomach, there was no acute toxicity or inflammation observed during the course of the experiment. In another study, pNIPAM-AAc beads were loaded with human calcitonin and delivered intramuscularly to rats.[295] pNIPAM-grafted gelatin was used as an injectable, thermoresponsive scaffold in the subcutaneous tissue of rats and monitored over 12 weeks.[296] On the first day after injection, macrophages and neutrophils were observed at the injection site, but shortly thereafter the inflammation response subsided, and fibroblasts from the native tissue migrated into the scaffold. A similar study also evaluated the long term *in vivo* subcutaneous cytotoxicity and inflammatory response of pNIPAM as an injectable hydrogel in mice. As in the previous study, they also measured a small acute inflammatory response 48 hours after injection but no signs of chronic inflammation five

months after injection.[291]

The more significant barrier to pNIPAM's use as a biomaterial *in vivo* is the potential for bioaccumulation and depolymerization into its toxic monomer. There are methods of creating degradable pNIPAM and studies that demonstrate that the degradation products are also biocompatible;[291] however these methods have required more complicated chemistry than our simple photopatternablepNIPAM-AAc. Although our material is not currently enzymatically degradable, the theragrippers are not intended as permanent implants. They are designed to remain for the duration of drug delivery (approximately 1 week) and then be shed by the natural shedding of the gastrointestinal mucus. Previous experiments using the metallic microgrippers have shown that the high turnover rate of gastrointestinal mucus clears out all grippers from the lower GI tract within a period of 1 month. In this study, 1000-3000 metallic microgrippers were deployed in the esophagus and colon of three live pigs. After 35 days, the animal was euthanized and the GI tract was removed. Under magnetic resonance imaging (MRI) observation, no metallic microgrippers remained in any portion of the GI tract. We expect the polymeric theragrippers to be excreted in the same way over a similar period of time. Thus, there would be no opportunity for bioaccumulation or degradation of the theragrippers in the GI tract during the time they are in use.

8 Curriculum Vitae

Kate E. L. Malachowski
Born May 21, 1985 in Fairfax, Virginia, USA

EDUCATION

Ph.D., Chemical and Biomolecular Engineering
December 2013
Johns Hopkins University, Baltimore, MD, Advisor: Dr. David H. Gracias
Thesis title: Stimuli-Responsive Microgrippers for Biomedical and Defense Applications

B.S., Chemical Engineering, Magna Cum Laude, Virginia Tech, Blacksburg, VA
May 2008

PROFESSIONAL AND RESEARCH EXPERIENCE

The Johns Hopkins University, Baltimore, MD
2008–present
Graduate Researcher, Gracias Laboratory
- Developed thermoresponsive, autonomous microgrippers as non-invasive biopsy tools, which improve the chance of finding early stage lesions in inflammatory bowel diseases and gastrointestinal cancers
- Designed and characterized thermoresponsive all-polymeric therapeutic grippers which can be loaded with drugs such as doxorubicin and mesalamine for site specific controlled release in the GI tract
- Utilized novel materials to create single cell microgrippers as *in vitro* assay tools and biopsy tools capable of non-invasively extracting single cells from hard-to-reach areas of the body

U.S. Army Research Laboratory, Adelphi, MD
2009 – present
Guest Researcher
- Integrated RFID tags onto microgrippers for covert tagging, tracking, and locating
- Developed a low power photothermal actuation scheme for wireless, sequential folding of 2D templates into 3D devices, a step towards programmable matter and complex 3D micro-origami

Northrop Grumman Corporation, Baltimore, MD
2012-present
MEMS Scientist, Electronic Systems
- Launched an external innovation program, resulting in four new university collaborations
- Applied novel MEMS devices and nanoenergetic materials for multiple defense programs

ExxonMobil Process Research, Clinton, NJ
2008
Summer Intern
- Designed and oversaw operation of a pilot-scale hydrocracking catalyst screening study

Virginia Tech, Blacksburg, VA
2007- 2008

Undergraduate Researcher, Goldstein Laboratory
- Engineered polymeric bone scaffolds using PLGA microparticles and calcium phosphate to enhance osteoblast differentiation

The Dow Chemical Company
2005 – 2006
Engineering Research Co-op
- Improved facility safety by implementing new emergency block valve, lighting, and uninterrupted power supply procedures (Hahnville, LA)
- Ran an energy intensity analysis of four units with the Department of Energy (Seadrift, TX)
- Built, ran, and maintained gas and liquid phase pilot reactors for a catalyst screening study (Charleston, WV)

PUBLICATIONS, CONFERENCE PAPERS, AND PATENTS

K. E. Malachowski, J. Breger, H. Kwag, F.M. Selaru, M.O. Wang, J.P. Fisher, D.H. Gracias, "Theragrippers for Controlled Drug Release", under review.

K. E. Malachowski, M. Jamal, B. Polat, Q. Jin, C. Morris, D. Gracias, "Self-folding Single Cells Grippers", in preparation.

Morris, C. J., **Laflin, K. E.,** Gracias, D. J., and Dubey, M., "Wavelength-Specific Optical Actuation Apparatus For a Micormechanical Actuator Device," ARL Invention Disclosure 13-14 filed Dec. 31, 2012, Provisional Patent Application filed June 26, 2013.

E. Gultepe, S. Yamanaka, **K. E. Laflin**, S. Kadam, Y.S. Shim, A. V. Olaru, B. Limketkai, M. A. Khashab, A. N. Kalloo, D. H. Gracias, F. M. Selaru, "Biologic tissue sampling with untethered microgrippers", *Gastroenterology* 144, 4, 691-693 (2013).

K. E. Laflin, C. J. Morris, T. Muqueem, D. H. Gracias, "Laser-triggered sequential folding of microstructures", *Applied Physics Letters* 101, 131901 (2012). **Highlighted in Nature Photonics "News and Views," Dec. 2012.**

Morris, C. J., **Laflin, K. E**., Churaman, W. A., Becker, C. R., Currano, L. J., and Gracias, D. G., "Initiation of nanoporous energetic silicon by optically-triggered, residual stress powered microactuators," *Proc. 25th IEEE International Conference on MEMS,* Paris, France, Jan. 30-Feb 2, 2012, pp. 1245-48.

K. E. Laflin, C. J. Morris, N. Bassik, M. Jamal and D. H. Gracias. "Tetherless Microgrippers with Transponder Tags" *IEEE/ASME Journal of Microelectromechanical Systems (JMEMS)* 20, 2, 505-511 (2011). **Highlighted in IEEE Technology News as a top 0.5% newsworthy article.**

J. S. Randhawa, **K. E. Laflin**, N. Seelam and D. H. Gracias, "Microchemomechanical Systems" *Advanced Functional Materials* 21, 13, 2395-2410 (2011).

A. Azam, **K. Laflin**, M. Jamal, R. Fernandes and D. H. Gracias. "Self-folding micropatterned polymeric containers." *Biomedical Microdevices* 13, 1, 51-58 (2011).

Morris, C. J., **Laflin, K.,** and Gracias, D. H., "Microgripper Tags With Integrated CMOS Sensors," *International Symposium for Spectral Sensing Research (ISSSR)*, Springfield, MO, June 21-24, 2010.

Morris, C. J., **Laflin, K. E.,** Isaacson, B., Grapes, M. & Gracias, D. H., "Capillary And Magnetic Forces For Microscale Self-Assembled Systems," *Proc. Materials Research Society Spring Meeting,* vol. 1272, San Francisco, CA, April 5-9, 2010.

N. Bassik, B. Abebe, **K. Laflin** and D. H. Gracias." Photolithographically Patterned Smart Hydrogel Based Bilayer Actuators." *Polymer* 51, 6093-6098 (2010).

Popp, J.R. **K.E. Laflin**, B.J. Love, and A.S. Goldstein. "*In vitro* evaluation of osteoblastic differentiation on amorphous calcium phosphate-decorated poly(lactic-co-glycolic acid) scaffolds" *J Tissue Eng* 2011.

Popp, J.R. **K.E. Laflin**, B.J. Love, and A.S. Goldstein. "Fabrication and characterization of poly(lactic-co-glycolic acid) microsphere/amorphous calcium phosphate scaffolds" *J Tissue Eng Regen Med* 2011.

CONFERENCE PRESENATIONS AND POSTERS

"Capturing and Manipulating Single Cells in 3D with Thermo-Responsive Microgrippers." **K. Malachowski**, M. Jamal, C. Morris, D. Gracias, Biomedical Engineering Society, Seattle, WA September 2013

"Laser-Triggered Sequential Folding of Microstructures", **K. Laflin**, C. Morris, T. Muqeem, D. Gracias. MidAtlantic Micro/Nano Alliance, Gaithersburg, MD, May 2013

""Smart" Stimuli-Responsive Wireless Tools". **K. Laflin**, C. Morris, E. Gultepe, F. Selaru, D. Gracias. NSF Pan-American Advanced Studies Institute Conference on Functional, Scalable Nanomaterials, Costa Rica, August 2011.

Invited Talk: Morris, C. J., **Laflin, K.,** Gracias, D., Currano, L., Churaman, W., Polcawich, R., and Pulskamp, J., "Silicon Integration With Hinge Actuators, Nanoenergetics, and Piezoelectrics," Northrop Grumman seminar, Baltimore, MD, July 28, 2010.

AWARDS AND HONORS

Northrop Grumman/Institute for NanoBiotechnology Fellow	2009
Carl E. Heath Fellow	2008
Victoria, TX Hometown Hero	2006
Omega Chi Epsilon Chemical Engineering Honor Fraternity	2006
Virginia Tech Residence Life Student of the Year	2005
Dow Chemical Company Scholarship	2004
Boeing Company Scholarship	2004
James E. Turner Engineering Scholarship	2004
Kimberly Clark Honor Scholarship	2003
Marshall Hahn Engineering Scholarship	2003
Cady Coleman Excellence in Science Scholarship	2003